From eV to EeV: Neutrino cross sections across energy scales

Citation: Formaggio, J., and G. Zeller. "From eV to EeV: Neutrino Cross Sections Across Energy Scales." Reviews of Modern Physics 84.3 (2012): 1307–1341. © 2012 American Physical Society

As Published: http://dx.doi.org/10.1103/RevModPhys.84.1307

Publisher: American Physical Society

Persistent URL: http://hdl.handle.net/1721.1/75437

Version: Final published version: final published article, as it appeared in a journal, conference proceedings, or other formally published context

From eV to EeV: Neutrino cross sections across energy scales

J. A. Formaggio*

Laboratory for Nuclear Science Massachusetts Institute of Technology, Cambridge, Massachusetts 02139, USA

G. P. Zeller†

Fermi National Accelerator Laboratory, Batavia, Illinois 60510, USA

(published 24 September 2012)

Since its original postulation by Wolfgang Pauli in 1930, the neutrino has played a prominent role in our understanding of nuclear and particle physics. In the intervening 80 years, scientists have detected and measured neutrinos from a variety of sources, both man made and natural. Underlying all of these observations, and any inferences we may have made from them, is an understanding of how neutrinos interact with matter. Knowledge of neutrino interaction cross sections is an important and necessary ingredient in any neutrino measurement. With the advent of new precision experiments, the demands on our understanding of neutrino interactions is becoming even greater. The purpose of this article is to survey our current knowledge of neutrino cross sections across all known energy scales: from the very lowest energies to the highest that we hope to observe. The article covers a wide range of neutrino interactions including coherent scattering, neutrino capture, inverse beta decay, low-energy nuclear interactions, quasielastic scattering, resonant pion production, kaon production, deep inelastic scattering, and ultrahigh energy interactions. Strong emphasis is placed on experimental data whenever such measurements are available.

DOI: 10.1103/RevModPhys.84.1307 PACS numbers: 25.30.Pt, 13.15.+g, 14.60.Lm

CONTENTS

I. INTRODUCTION

The investigation into the basic properties of the particle known as the neutrino has been a particularly strong and active area of research within nuclear and particle physics. Research conducted over the latter half of the 20th century has revealed, for example, that neutrinos can no longer be considered as massless particles in the standard model, representing perhaps the first significant alteration to the theory. Moving into the 21st century, neutrino research continues to expand in new directions. Researchers further investigate the nature of the neutrino mass or explore whether neutrinos can help explain the matter-antimatter asymmetry of the Universe. At the heart of many of these experiments is the need for neutrinos to interact with other standard model particles. An understanding of these basic interaction cross sections is often an understated but truly essential element of any experimental neutrino program.

The known reactions of neutrinos with matter fall completely within the purview of the standard model of particle physics. The model of electroweak interactions govern what those reactions should be, with radiative corrections that can be

*josephf@mit.edu
†gzeller@fnal.gov

accurately calculated to many orders. As such, our goal in this review is essentially already complete: we would simply write down the electroweak Lagrangian and we would be finished. Of course, in practice this is very far from the truth. As with many other disciplines, many factors compound our simple description, including unclear initial-state conditions, subtle-but-important nuclear corrections, final-state interactions, and other effects. One quickly finds that theoretical approximations which work well in one particular energy regime completely break down elsewhere. Even the language used in describing certain processes in one context may seem completely foreign in another. Previous neutrino experiments could avoid this issue by virtue of the energy range in which they operated; now, however, more experiments find themselves "crossing boundaries" between different energy regimes. Thus, the need for understanding neutrino cross sections across many decades of energy is becoming more imperative. To summarize our current collective understanding, this work provides a review of neutrino cross sections across all explored energy scales. The range of energies covered, as well as their relevance to various neutrino sources, is highlighted in Fig. 1. We first establish the formalism of neutrino interactions by considering the simplest case of neutrino-electron scattering. Our focus will then shift to neutrino interaction cross sections at low (1–100 MeV), intermediate (0.1–20 GeV), high (20–500 GeV), and ultrahigh (0.5 TeV–1 EeV) energies, emphasizing our current theoretical and experimental understanding of the processes involved. Though it may be tempting to interpret these delineations as hard and absolute, they are only approximate in nature, meant as a guide for the reader.

II. A SIMPLE CASE: NEUTRINO-LEPTON SCATTERING

A. Formalism: Kinematics

We begin with the simplest of neutrino interactions, neutrino-lepton scattering. As a purely leptonic interaction, neutrino-lepton scattering allows us to establish the formalism and terminology used through the paper, without introducing some of the complexity that often accompanies neutrino-nuclear scattering. The general form of the two-body scattering process is governed by the dynamics of the process encoded in the matrix elements and the phase space available in the interaction. Figure 2 shows the tree-level diagram of a neutrino-lepton charged current interaction, known as inverse muon decay. A muon neutrino with four-momentum p_ν (aligned along the z direction) scatters in this example with an electron with four-momentum p_e, which is at rest in the laboratory frame. This produces an outgoing muon with four-momentum k_μ and a scattered electron neutrino with four-momentum k_e. In the laboratory frame, the components of these quantities can be written as

$$p_\nu = (E_\nu, \vec{p}_\nu), \qquad k_\mu = (E_\mu, \vec{k}_\mu),$$
$$p_e = (m_e, 0), \qquad k_e = (E_e, \vec{k}_e).$$

Here we use the convention of the zeroth component corresponding to the energy portion of the energy-momentum vector, with the usual energy-momentum relation $E_i^2 = |\vec{k}|_i^2 + m_i^2$. From these four-vector quantities, it is often useful to construct new variables which are invariant under Lorentz transformations:

$$s = (p_\nu + p_e)^2 \qquad \text{(center of mass energy)},$$
$$Q^2 = -q^2 = (p_\nu - k_\mu)^2 \qquad \text{(4-momentum transfer)},$$
$$y = \frac{p_e \cdot q}{p_e \cdot p_\nu} \qquad \text{(inelasticity)}.$$

In the case of two-body collisions between an incoming neutrino and a (stationary) target lepton, the cross section is given in general by ($\hbar = c = 1$) (Berestetskii, Lifshitz, and Pitaevski, 1974),

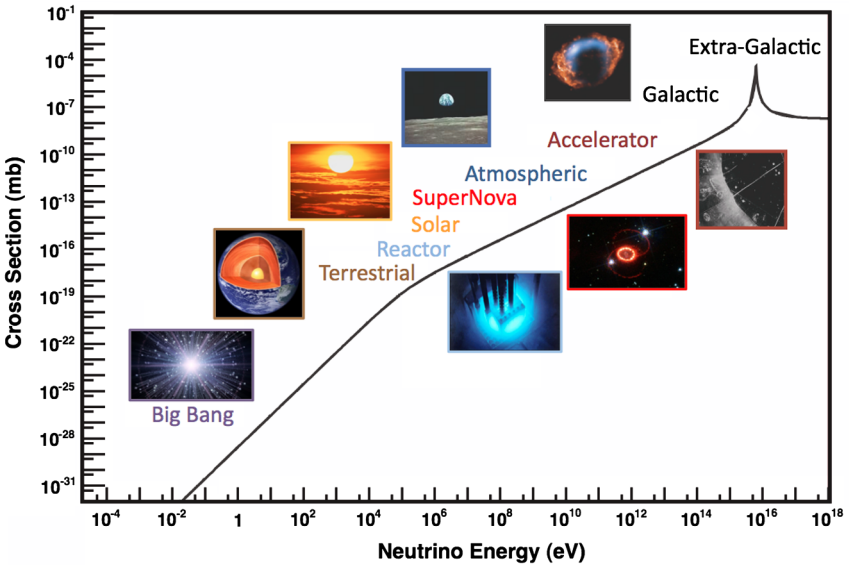

FIG. 1 (color online). Representative example of various neutrino sources across decades of energy. The electroweak cross section for $\bar{\nu}_e e^- \to \bar{\nu}_e e^-$ scattering on free electrons as a function of neutrino energy (for a massless neutrino) is shown for comparison. The peak at 10^{16} eV is due to the W^- resonance, which we discuss in greater detail in Sec. VII.

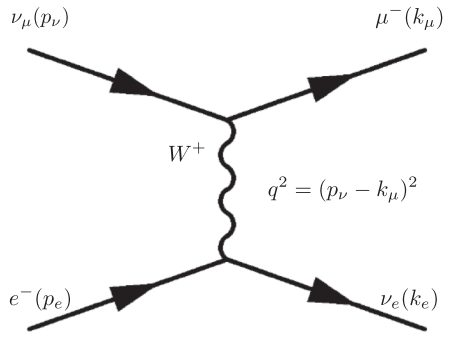

FIG. 2. Diagram of two-body scattering between an incoming muon neutrino with four-momentum p_ν and an electron at rest with four-momentum p_e. See text for details.

$$\frac{d\sigma}{dq^2} = \frac{1}{16\pi}\frac{|\mathcal{M}^2|}{[s-(m_e+m_\nu)^2][s-(m_e-m_\nu)^2]} \tag{1}$$

which, in the context of very small neutrino masses, simplifies to

$$\frac{d\sigma}{dq^2} = \frac{1}{16\pi}\frac{|\mathcal{M}^2|}{(s-m_e^2)^2}. \tag{2}$$

Here $\mathcal{M}$ is the matrix element associated with our particular interaction (Fig. 2). In the laboratory frame, it is always possible to express the cross section in alternative ways by making use of the appropriate Jacobian. For example, to determine the cross section as a function of the muon's scattering angle θ_μ, the Jacobian is given by

$$\frac{dq^2}{d\cos\theta_\mu} = 2|\vec{p}_\nu||\vec{k}_\mu|, \tag{3}$$

while the Jacobian written in terms of the fraction of the neutrino energy imparted to the outgoing lepton energy (y) is given by

$$\frac{dq^2}{dy} = 2m_e E_\nu. \tag{4}$$

Pending on what one is interested in studying, the differential cross sections can be recast to highlight a particular dependence or behavior.

B. Formalism: Matrix elements

The full description of the interaction is encoded within the matrix element $\mathcal{M}$. The standard model readily provides a prescription to describe neutrino interactions via the leptonic charged current and neutral current in the weak interaction Lagrangian. Within the framework of the standard model, a variety of neutrino interactions are readily described (Weinberg, 1967). These interactions all fall within the context of the general gauge theory of $\mathrm{SU}(2)_L \times \mathrm{U}(1)_Y$. This divides the types of possible interactions for neutrinos into three broad categories. The first is mediated by the exchange of a charged W boson, otherwise known as a charged current (CC) exchange. The leptonic charged weak current j_W^μ is given by the form

$$j_W^\mu = 2\sum_{\alpha=e,\mu,\tau} \bar{\nu}_{L,\alpha}\gamma^\mu l_{\alpha L}. \tag{5}$$

The second type of interaction, known as the neutral-current (NC) exchange, is similar in character to the charged current case. The leptonic neutral-current term, j_Z^μ, describes the exchange of the neutral boson, Z^0,

$$j_Z^\mu = 2\sum_{\alpha=e,\mu,\tau} g_L^\nu \bar{\nu}_{\alpha L}\gamma^\mu \nu_{\alpha L} + g_L^f \bar{l}_{\alpha L}\gamma^\mu l_{\alpha L} + g_R^f \bar{l}_{\alpha R}\gamma^\mu l_{\alpha R}. \tag{6}$$

Here $\nu_{\alpha L(R)}$ and $l_{\alpha L(R)}$ correspond to the left (right) neutral and charged leptonic fields, while g_L^ν, g_L^f, and g_R^f represent the fermion left- and right-handed couplings (for a list of these values, see Table I). Though the charged leptonic fields are of a definite mass eigenstate, this is not necessarily so for the neutrino fields, giving rise to the well-known phenomena of neutrino oscillations.

Historically, the neutrino-lepton charged current and neutral-current interactions have been used to study the nature of the weak force in great detail. We now return to the case of calculating the charged and neutral-current reactions. These previously defined components enter directly into the Lagrangian via their coupling to the heavy gauge bosons, $W^\pm$ and Z^0,

$$\mathcal{L}_{\mathrm{CC}} = -\frac{g}{2\sqrt{2}}(j_W^\mu W_\mu + j_W^{\mu,\dagger} W_\mu^\dagger), \tag{7}$$

$$\mathcal{L}_{\mathrm{NC}} = -\frac{g}{2\cos\theta_W} j_Z^\mu Z_\mu. \tag{8}$$

Here W_μ and Z_μ represent the heavy gauge boson field, g is the coupling constant while θ_W is the weak mixing angle. It is possible to represent these exchanges with the use of Feynman diagrams, as is shown in Fig. 3. Using this formalism, it is possible to articulate all neutrino interactions ('t Hooft, 1971) within this simple framework.

We begin by looking at one of the simplest manifestations of the above formalism, where the reaction is a pure charged current interaction

$$\nu_l + e^- \rightarrow l^- + \nu_e \qquad (l = \mu \quad \text{or} \quad \tau). \tag{9}$$

The corresponding tree-level amplitude can be calculated from the above expressions. In the case of $\nu_l + e$ (sometimes known as inverse muon or inverse tau decays) one finds

$$\mathcal{M}_{\mathrm{CC}} = -\frac{G_F}{\sqrt{2}}\{[\bar{l}\gamma^\mu(1-\gamma^5)\nu_l][\bar{\nu}_e\gamma_\mu(1-\gamma^5)e]\}. \tag{10}$$

TABLE I. Values for the g_V (vector), g_A (axial), g_L (left), and g_R (right) coupling constants for the known fermion fields.

Fermion	g_L^f	g_R^f	g_V^f	g_A^f
ν_e, ν_μ, ν_τ	$+\frac{1}{2}$	0	$+\frac{1}{2}$	$+\frac{1}{2}$
e, μ, τ	$-\frac{1}{2}+\sin^2\theta_W$	$+\sin^2\theta_W$	$-\frac{1}{2}+2\sin^2\theta_W$	$-\frac{1}{2}$
u, c, t	$+\frac{1}{2}-\frac{2}{3}\sin^2\theta_W$	$-\frac{2}{3}\sin^2\theta_W$	$+\frac{1}{2}-\frac{4}{3}\sin^2\theta_W$	$+\frac{1}{2}$
d, s, b	$-\frac{1}{2}+\frac{1}{3}\sin^2\theta_W$	$+\frac{1}{3}\sin^2\theta_W$	$-\frac{1}{2}+\frac{2}{3}\sin^2\theta_W$	$-\frac{1}{2}$

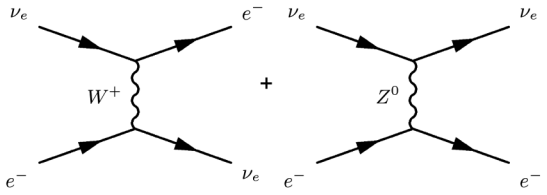

FIG. 3. Feynman tree-level diagram for charged and neutral-current components of $\nu_e + e^- \rightarrow \nu_e + e^-$ scattering.

Here, and in all future cases unless specified, we assume that the four-momentum of the intermediate boson is much smaller than its mass (i.e., $|q^2| \ll M_{W,Z}^2$) such that propagator effects can be ignored. In this approximation, the coupling strength is then dictated primarily by the Fermi constant G_F,

$$G_F = \frac{g^2}{4\sqrt{2}M_W^2} = 1.1663\,788(7) \times 10^{-5}\ \text{GeV}^{-2}. \quad (11)$$

By summing over all polarization and spin states, and integrating over all unobserved momenta, one attains the differential cross section with respect to the fractional energy imparted to the outgoing lepton,

$$\frac{d\sigma(\nu_l e \rightarrow \nu_e l)}{dy} = \frac{2m_e G_F^2 E_\nu}{\pi}\left(1 - \frac{m_l^2 - m_e^2}{2m_e E_\nu}\right), \quad (12)$$

where E_ν is the energy of the incident neutrino and m_e and m_l are the masses of the electron and outgoing lepton, respectively. The dimensionless inelasticity parameter y reflects the kinetic energy of the outgoing lepton, which in this particular example is $y = [E_l - (m_l^2 + m_e^2)/2m_e]/E_\nu$. The limits of y are such that

$$0 \le y \le y_{\max} = 1 - \frac{m_l^2}{2m_e E_\nu + m_e^2}. \quad (13)$$

Note that in this derivation, we have neglected the contribution from neutrino masses, which in this context is too small to be observed kinematically. The above cross section has a threshold energy imposed by the kinematics of the system, $E_\nu \ge (m_l^2 - m_e^2)/2m_e$.

In the case where $E_\nu \gg E_{\text{thresh}}$, integration of the above expression yields a simple expression for the total neutrino cross section as a function of neutrino energy,

$$\sigma \simeq \frac{2m_e G_F^2 E_\nu}{\pi} = \frac{G_F^2 s}{\pi}, \quad (14)$$

where s is the center-of-mass energy of the collision. Note that the neutrino cross section grows linearly with energy.

Because of the different available spin states, the equivalent expression for the inverse lepton decay of antineutrinos,

$$\bar{\nu}_e + e \rightarrow \bar{\nu}_l + l \qquad (l = \mu \quad \text{or} \quad \tau), \quad (15)$$

has a different dependence on y than its neutrino counterpart, although the matrix elements are equivalent

$$\frac{d\sigma(\bar{\nu}_e e \rightarrow \bar{\nu}_l l)}{dy} = \frac{2m_e G_F^2 E_\nu}{\pi} \times \left((1-y)^2 - \frac{(m_l^2 - m_e^2)(1-y)}{2m_e E_\nu}\right). \quad (16)$$

Upon integration, the total antineutrino cross section is approximately a factor of 3 lower than the neutrino cross section. The suppression comes entirely from helicity considerations.

Having just completed a charged current example, we now turn our attention to a pure neutral current exchange, such as witnessed in the reaction

$$\bar{\nu}_l + e \rightarrow \bar{\nu}_l + e \qquad (l = \mu \quad \text{or} \quad \tau). \quad (17)$$

In the instance of a pure neutral-current interaction, we are no longer at liberty to ignore the left- and right-handed leptonic couplings. As a result, one obtains a more complex expression for the relevant matrix element [for a review, see Adams *et al.* (2009)]

$$\mathcal{M}_{\text{NC}} = -\sqrt{2}G_F\{[\bar{\nu}_l \gamma^\mu (g_V^\nu - g_A^\nu \gamma^5)\nu_l] \times [\bar{e}\gamma_\mu (g_V^f - g_A^f \gamma^5)e]\}. \quad (18)$$

We have expressed the strength of the coupling in terms of the vector and axial-vector coupling constants (g_V and g_A, respectively). An equivalent formulation can be constructed using left- and right-handed couplings

$$\mathcal{M}_{\text{NC}} = -\sqrt{2}G_F\{[g_L^\nu \bar{\nu}_l \gamma^\mu (1-\gamma^5)\nu_l + g_R^\nu \bar{\nu}_l \gamma^\mu (1+\gamma^5)\nu_l] \times \{[g_L^f \bar{e}\gamma^\mu (1-\gamma^5)e + g_R^f \bar{e}\gamma^\mu (1+\gamma^5)e]\}. \quad (19)$$

The relation between the coupling constants are dictated by the standard model,

$$g_L^\nu = \sqrt{\rho}(+\tfrac{1}{2}), \qquad g_R^\nu = 0,$$
$$g_L^f = \sqrt{\rho}(I_3^f - Q^f \sin^2\theta_W), \qquad g_R^f = \sqrt{\rho}(-Q^f \sin^2\theta_W),$$

or, equivalently,

$$g_V^\nu = g_L^\nu + g_R^\nu = \sqrt{\rho}(+\tfrac{1}{2}),$$
$$g_A^\nu = g_L^\nu - g_R^\nu = \sqrt{\rho}(+\tfrac{1}{2}),$$
$$g_V^f = g_L^f + g_R^f = \sqrt{\rho}(I_3^f - 2Q^f \sin^2\theta_W),$$
$$g_A^f = g_L^f - g_R^f = \sqrt{\rho}(I_3^f).$$

Here I_3^f and Q^f are the weak isospin and electromagnetic charge of the target lepton, ρ is the relative coupling strength between charged and neutral-current interaction (at tree level, $\rho \equiv 1$), and θ_W is the Weinberg mixing angle. The standard model defines a relation between the electroweak couplings and gauge boson masses M_W and M_Z

$$\sin^2\theta_W \equiv 1 - \frac{M_W^2}{M_Z^2}. \quad (20)$$

In the observable cross section for the neutral-current reactions highlighted above, we find that they are directly sensitive to the left- and right-handed couplings. In the literature, the cross section is often expressed in terms of their vector and axial-vector currents,

$$g_V \equiv (2g_L^\nu g_V^f),$$
$$g_A \equiv (2g_L^\nu g_A^f),$$
$$\frac{d\sigma(\nu_l e \to \nu_l e)}{dy} = \frac{m_e G_F^2 E_\nu}{2\pi}\left((g_V + g_A)^2 + (g_V - g_A)^2 \times (1-y)^2 - (g_V^2 - g_A^2)\frac{m_e y}{E_\nu}\right),$$
$$\frac{d\sigma(\bar\nu_l e \to \bar\nu_l e)}{dy} = \frac{m_e G_F^2 E_\nu}{2\pi}\left((g_V - g_A)^2 + (g_V + g_A)^2 \times (1-y)^2 - (g_V^2 - g_A^2)\frac{m_e y}{E_\nu}\right).$$

Though we have limited ourselves to discussing neutrino-lepton scattering, the rules governing the coupling strengths are predetermined by the standard model and can be used to describe neutrino-quark interactions as well. A full list of the different possible coupling strengths for the known fermion fields is shown in Table I. A more in-depth discussion of these topics can be found in a variety of introductory textbooks. We highlight the work of Giunti and Kim (2007) as an excellent in-depth resource for the interested reader.

As such, neutrino-electron scattering is a powerful probe of the nature of the weak interaction, both in terms of the total cross section as well as its energy dependence (Marciano and Parsa, 2003). We will briefly examine the experimental tests of these reactions in the next section.

Before leaving neutrino-lepton interactions completely, we turn our attention to the last possible reaction archetype, where the charged current and neutral-current amplitudes interfere with one another. Such a combined exchange is realized in $\nu_e + e \to \nu_e + e$ scattering (see Fig. 3). The interference term comes into play by shifting $g_V^f \to g_V^f + \frac{1}{2}$ and $g_A^f \to g_A^f + \frac{1}{2}$.

One remarkable feature of neutrino-electron scattering is that it is highly directional in nature. The outgoing electron is emitted at very small angles with respect to the incoming neutrino direction. A simple kinematic argument shows that indeed

$$E_e \theta_e^2 \le 2m_e. \tag{21}$$

This remarkable feature has been exploited extensively in various neutrino experiments, particularly for solar neutrino detection. The Kamiokande neutrino experiment was the first to use this reaction to reconstruct ^{8}B neutrino events from the Sun and point back to the source. The Super-Kamiokande experiment later expanded the technique, creating a photograph of the Sun using neutrinos (Fukuda *et al.*, 1998).[1] The technique was later used by other solar experiments, such as the Sudbury Neutrino Observatory (SNO) (Ahmad *et al.*, 2001, 2002a, 2002b) and Borexino (Alimonti *et al.*, 2002; Arpesella *et al.*, 2008).

C. Experimental tests of electroweak theory

Neutrino-lepton interactions have played a pivotal role in our understanding of the working of the electroweak force and the standard model as a whole. Consider as an example the first observation of the reaction $\bar\nu_\mu + e^- \to \bar\nu_\mu + e^-$ made with the CERN bubble chamber neutrino experiment, Gargamelle (Hasert *et al.*, 1973); see Fig. 4. This observation, in conjunction with the observation of neutral-current deep inelastic scattering (Hasert *et al.*, 1973; Benvenuti *et al.*, 1974), confirmed the existence of weak neutral currents and helped solidify the $SU_L(2) \times U(1)_Y$ structure of the standard model (Weinberg, 1967; 't Hooft, 1971). The very observation of the phenomena made a profound impact on the field of particle physics.

Subsequent experiments further utilized the information from the observed rates of neutral-current reactions as a gauge for measuring $\sin^2\theta_W$ directly. Neutrino-lepton scattering is a particularly sensitive probe in this regard because to first order (and even to further orders of α, see Sec. II.D), the cross sections depend only on one parameter, $\sin^2\theta_W$.

Various experimental methods have been employed to measure neutrino-lepton scattering. Among the first included the observation of $\bar\nu_e + e^- \to e^- + \bar\nu_e$ scattering by Reines, Gurr, and Sobel (1976) at the Savannah River Plant reactor complex. Making use of the intense $\bar\nu_e$ flux produced in reactors, a $\pm 20\%$ measurement of the weak mixing angle was extracted. A more recent result from the Taiwan EXperiment On Neu-trinO (TEXANO) experiment (Deniz and Wong, 2008; Deniz *et al.*, 2010) also utilizes reactor antineutrinos as their source. There exists an inherent difficulty in extracting these events, as they are often masked by large low-energy backgrounds, particularly those derived from uranium and thorium decays.

The majority of the recent precision tests have been carried out using high-energy neutrino beams. Experiments such as Gargamelle (Hasert *et al.*, 1973), Brookhaven's Alternating

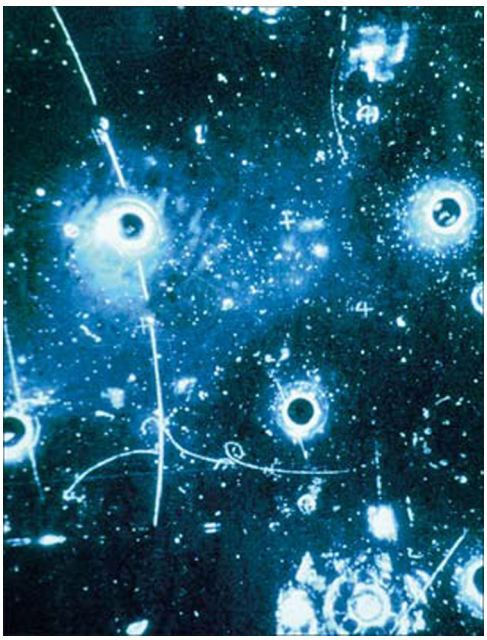

FIG. 4 (color online). The first candidate leptonic neutral-current event from the Gargamelle CERN experiment. An incoming muon-antineutrino knocks an electron forwards (towards the left), creating a characteristic electronic shower with electron-positron pairs. Photograph from CERN.

[1] The fact that such a picture was taken underground during both day and night is also quite remarkable.

TABLE II. The integrated cross section for neutrino-lepton scattering interactions. Corrections due to leptonic masses and radiative correlations are ignored. Cross sections are compared to the asymptotic cross section $\sigma_0 = G_F^2 s/\pi$. Listed are also the experiments which have measured the given reaction, including Gargamelle (Hasert *et al.*, 1973), the Savannah River Plant (Reines, Gurr, and Sobel, 1976), Brookhaven National Laboratory (BNL) (Ahrens *et al.*, 1983; Abe *et al.*, 1989; Ahrens *et al.*, 1990), LAMPF (Allen *et al.*, 1993), LSND (Auerbach *et al.*, 2001), CCFR (Mishra *et al.*, 1990), CHARM (Vilain *et al.*, 1995a; Vilain *et al.*, 1995b), NuTeV (Formaggio *et al.*, 2001), and TEXONO (Deniz and Wong, 2008).

Reaction	Type	$\sigma(E_\nu \gg E_{\text{thresh}})/\sigma_0$	Experimental probes
$\nu_e e^- \to \nu_e e^-$	CC and NC	$\frac{1}{4} + \sin^2\theta_W + \frac{4}{3}\sin^4\theta_W$	CHARM, LAMPF, LSND
$\bar{\nu}_e e^- \to \bar{\nu}_e e^-$	CC and NC	$\frac{1}{12} + \frac{1}{3}\sin^2\theta_W + \frac{4}{3}\sin^4\theta_W$	CHARM, TEXONO, Savannah River
$\bar{\nu}_e e^- \to \bar{\nu}_\mu \mu^-$	CC	$\frac{1}{3}$	
$\nu_\mu e^- \to \nu_e \mu^-$	CC	1	CHARM, CCFR, NuTeV
$\nu_\mu e^- \to \nu_\mu e^-$	NC	$\frac{1}{4} - \sin^2\theta_W + \frac{4}{3}\sin^4\theta_W$	CHARM, LAMPF, LSND, BNL
$\bar{\nu}_\mu e^- \to \bar{\nu}_\mu e^-$	NC	$\frac{1}{12} - \frac{1}{3}\sin^2\theta_W + \frac{4}{3}\sin^4\theta_W$	Gargamelle, BNL

Gradient Synchrotron (AGS) source (Ahrens *et al.*, 1983, 1990; Abe *et al.*, 1989), CERN HAmburg Rome Moscow (CHARM-II) (Vilain *et al.*, 1995a, 1995b), Chicago-Columbia-Fermilab-Rochester (CCFR) (Mishra *et al.*, 1990), and NuTeV (Formaggio *et al.*, 2001) fall within this category. Often these experiments exploit the rise in cross section with energy to increase the sample size collected for analysis. Stopped pion beams have also been used for these electroweak tests at the Los Alamos National Laboratory in the Los Alamos Meson Physics Facility (LAMPF) (Allen *et al.*, 1993) and Liquid Scintillator Neutrino Detector (LSND) (Auerbach *et al.*, 2001) experiments. Table II provides a summary of the types of measurements made using pure neutrino-lepton scattering.

D. Radiative corrections and G_F

Upon inspection of the cross section formalisms discussed above, it is clear that, with the exception of ratios, one is critically dependent on certain fundamental constants, such as the strength of the weak coupling constant G_F. Ideally, one wants to separate the dependence on the weak mixing angle from the Fermi constant strength. Fortunately, measurements of the muon lifetime provides such a possibility, as it is inversely proportional to the coupling strength G_F and the muon mass m_μ,

$$(\tau_\mu)^{-1} = \frac{G_F^2 m_\mu^5}{192\pi^3} f(\rho)\left(1 + \frac{3}{5}\frac{m_\mu^2}{M_W^2}\right)[1 + \Delta(\alpha)]. \tag{22}$$

In the above expression, $f(\rho)$ is a phase factor, the m_μ^2/M_W^2 factor encapsulates the W-boson propagator, and $\Delta(\alpha)$ encodes the QED radiative field corrections. For completeness, we list these correction factors:

$$f(\rho) = 1 - 8\rho + 8\rho^3 - \rho^4 - 12\rho^2 \ln\rho \simeq 0.999\,813, \tag{23}$$

$$\Delta = \alpha\left(\frac{25}{8} - \frac{\pi^2}{2} - (9 + 4\pi^2 + 12\ln\rho)\rho + 16\pi^2\rho^{3/2} + \mathcal{O}(\rho^2)\right) + \mathcal{O}(\alpha^2) + \ldots, \tag{24}$$

where $\rho = (m_e/m_\mu)^2$ and α is the fine structure constant. Radiative QED corrections have been calculated to second order and higher in electroweak theory paving the way to precision electroweak tests of the standard model. The best measurement of the muon lifetime to date has been made by the MuLan experiment (Webber *et al.*, 2011), yielding a value for G_F of $1.166\,378\,8(7) \times 10^{-5}$ GeV^{-2}, a precision of 0.6 ppm.

At tree level, knowing G_F (and α and M_Z) it is possible to exactly predict the value of $\sin^2\theta_W$ and test this prediction against the relevant cross section measurements. However, once one introduces one-loop radiative contributions, dependencies on the top and Higgs masses are also introduced. The size of these corrections depends partially on the choice of the normalization scheme. The two commonly used renormalization schemes include the Sirlin on-shell model (Sirlin, 1980) and the modified minimal subtraction scheme (Marciano and Sirlin, 1981). In the latter method, the Weinberg angle is defined by M_W and M_Z at some arbitrary renormalized mass scale μ, which is typically set to the electroweak scale M_Z

$$\sin^2\theta_W^{\bar{M}S} = 1 - \frac{M_W(\mu)^2}{M_Z(\mu)^2}. \tag{25}$$

Such radiative corrections, although small, often need to be accounted for in order to properly predict the $\sin^2\theta_W$ value. Theoretical compilation of such radiative effects can be found in a variety of papers [see, for example, Marciano and Parsa (2003)].

III. THRESHOLDLESS PROCESSES: $E_\nu \sim$ 0–1 MeV

Having established the formalism of basic neutrino interactions, we turn our attention toward describing neutrino interactions across the various energy scales. The first step in our journey involves *thresholdless* interactions, which can be initiated when the neutrino has essentially zero momentum. Such processes include coherent scattering and neutrino capture.[2]

A. Coherent scattering

Coherent scattering involves the neutral-current exchange where a neutrino interacts *coherently* with the nucleus,

[2]Technically, neutrino elastic scattering off of free electrons also falls within this definition, as discussed earlier in this paper.

$$\nu + A_N^Z \rightarrow \nu + A_N^{*Z}. \tag{26}$$

Shortly after the discovery of neutral-current neutrino reactions, Freedman, Schramm, and Tubbs pointed out that neutrino-nucleus interactions should also exist (Freedman, Schramm, and Tubbs, 1977). Furthermore, one could take advantage of the fact that at low energies the cross section should be coherent across all of the nucleons present in the nucleus. As a result, the cross section grows as the square of the atomic number A^2. Such an enhancement is possible if the momentum transfer of the reaction is much smaller than the inverse of the target size. Letting Q represent the momentum transfer and R the nuclear radius, the coherence condition is satisfied when $QR \ll 1$. Under these conditions, the relevant phases have little effect, allowing the scaling to grow as A^2.

Given a recoil kinetic energy T and an incoming neutrino energy E_ν, the differential cross section can be written compactly as the following:

$$\frac{d\sigma}{dT} = \frac{G_F^2}{4\pi} Q_W^2 M_A \left(1 - \frac{M_A T}{2E_\nu^2}\right) F(Q^2)^2, \tag{27}$$

where M_A is the target mass ($M_A = AM_{\text{nucleon}}$), $F(Q^2)$ is the nucleon form factor, and Q_W is the weak current term

$$Q_W = N - Z(1 - 4\sin^2\theta_W). \tag{28}$$

The cross section essentially scales quadratically with neutron (N) and proton (Z) number; the latter highly suppressed due to the $1 - 4\sin^2\theta_W \simeq 0$ term. The form factor $F(Q^2)$ encodes the coherence across the nucleus and drops quickly to zero as QR becomes large.

Despite the strong coherent enhancement enjoyed by this process, this particular interaction has yet to be detected experimentally. Part of the obstacle stems from the extremely small energies of the emitted recoil. The maximum recoil energy from such an interaction is limited by the kinematics of the elastic collision,

$$T_{\max} = \frac{E_\nu}{1 + M_A/2E_\nu}, \tag{29}$$

similar to that of any elastic scatter where the mass of the incoming particle is negligible. Several experiments have been proposed to detect this interaction, often taking advantage of advances in recoil detection typically utilized by dark matter experiments (Scholberg, 2006; Formaggio, Figueroa-Feliciano, and Anderson, 2012). The interaction has also been proposed as a possible mechanism for cosmic relic neutrinos, due to its nonzero cross section at zero momentum. However, the G_F^2 suppression makes detection beyond the reach of any realizable experiment.

B. Neutrino capture on radioactive nuclei

Neutrino capture on radioactive nuclei, sometimes referred to as *enhanced* or *stimulated* beta decay emission, constitutes another thresholdless mechanism in our library of possible neutrino interactions. The process is similar to that of ordinary beta decay

$$A_N^Z \rightarrow A_{N-1}^{Z+1} + e^- + \bar{\nu}_e, \tag{30}$$

except the neutrino is interacting with the target nucleus

$$\nu_e + A_N^Z \rightarrow e^- + A_{N-1}^{Z+1}. \tag{31}$$

This reaction has the same observable final states as its beta decay counterpart. What sets this reaction apart from other neutrino interactions is that the process is exothermic and hence no energy is required to initiate the reaction.[3] The cross section amplitude is directly related to that of beta decay. Using the formalism of Beacom and Vogel (1999), the cross section can be written as

$$\frac{d\sigma}{d\cos\theta} = \frac{G_F^2 |V_{ud}|^2 F(Z_f, E_e)}{2\pi\beta_\nu} E_e p_e f_V^2(0) \Big[(1 + \beta_e\beta_\nu\cos\theta) + 3\lambda^2 \left(1 - \frac{1}{3}\beta_e\beta_\nu\cos\theta\right)\Big], \tag{32}$$

where β_e and β_ν are the electron and neutrino velocities, respectively, E_e, p_e, and $\cos\theta$ are the electron energy, momentum, and scattering angle, λ^2 is the axial-to-vector coupling ratio, and $|V_{ud}|^2$ is the Cabbibo angle. The Fermi function $F(Z_f, E)$ encapsulates the effects of the Coulomb interaction for a given lepton energy E_e and final-state proton number Z_f. We discuss the coupling strengths $f_V(0)$ and λ^2 later.

In Eq. (32), we no longer assume that $\beta_\nu \rightarrow c$. If the neutrino flux is proportional to the neutrino velocity, then the product of the cross section and the flux results in a finite number of observable events. If the neutrino and the nucleus each possess negligible energy and momentum, the final-state electron is ejected as a monoenergetic particle whose energy is above the end-point energy of the reaction.

The interaction cross section of very low-energy neutrinos was first suggested by Weinberg (1962). Recently, this process has attracted particular interest thanks to the work by Cocco, Mangano, and Messina (2007), where they considered the process as a means to detect cosmological neutrinos. The reaction has received attention partially due to the advancement of beta decay experiments in extending the reach on neutrino mass scales. The mechanism, like its coherent counterpart, remains to be observed.

IV. LOW-ENERGY NUCLEAR PROCESSES: $E_\nu \sim$ 1–100 MeV

As the energy of the neutrino increases, it is possible to probe the target nucleus at smaller and smaller length scales. Whereas coherent scattering only allows one to "see" the nucleus as a single coherent structure, higher energies allow one to access nucleons individually. These low-energy interactions have the same fundamental characteristics as those of lepton scattering, though the manner in which they are gauged and calibrated is very different. And, unlike the thresholdless scattering mechanisms discussed previously, these low-energy nuclear processes have been studied extensively in neutrino experiments.

[3] In principle, any elastic interaction on a free target has a finite cross section at zero momentum, but such interactions would be impossible to discern due to the extremely small transfer of momentum.

TABLE III. Neutron decay parameters contributing to Eq. (36). Values extracted from Nico and Snow (2005) and Nakamura, K. *et al.* (2010).

Constant	Expression	Numerical value	Comment
λ	$\lvert\frac{g_A}{g_V}\rvert e^{i\phi}$	-1.2694 ± 0.0028	Axial and vector coupling ratio
a	$\frac{1-\lvert\lambda\rvert^2}{1+3\lvert\lambda\rvert^2}$	-0.103 ± 0.004	Electron-antineutrino asymmetry
b	0	0	Fietz interference
A	$-2\frac{\lvert\lambda\rvert^2+\lvert\lambda\rvert\cos\phi}{1+3\lvert\lambda\rvert^2}$	-0.1173 ± 0.0013	Spin-electron asymmetry
B	$+2\frac{\lvert\lambda\rvert^2-\lvert\lambda\rvert\cos\phi}{1+3\lvert\lambda\rvert^2}$	0.9807 ± 0.0030	Spin-antineutrino asymmetry
D	$2\frac{\lvert\lambda\rvert\sin\phi}{1+3\lvert\lambda\rvert^2}$	$(-4 \pm 6) \times 10^{-4}$	T-odd triple product
$f(1+\delta_R)$		1.71480 ± 0.000002	Theoretical phase space factor
τ_n	$[\frac{m_e^5}{2\pi^3} f_R G_F^2 \lvert V_{ud}\rvert^2(1+3\lambda^2)]^{-1}$	(885.7 ± 0.8) s	Neutron lifetime

A. Inverse beta decay

The simplest nuclear interaction that we can study is antineutrino-proton scattering, otherwise known as inverse beta decay

$$\bar{\nu}_e + p \rightarrow e^+ + n. \tag{33}$$

Inverse beta decay represents one of the earliest reactions to be studied, both theoretically (Bethe and Peierls, 1934) and experimentally (Reines, Gurr, and Sobel, 1976). This reaction is typically measured using neutrinos produced from fission in nuclear reactors. The typical neutrino energies used to probe this process range from threshold[4] ($E_\nu \geq 1.806$ MeV) to about 10 MeV. As this reaction plays an important role in understanding supernova explosion mechanisms, its relevance at slightly higher energies (10–20 MeV) is also of importance. In this paper, we follow the formalism of Beacom and Vogel (1999), who expand the cross section on the proton to first order in nucleon mass in order to study the cross section's angular dependence. In this approximation, all relevant form factors approach their zero-momentum values. The relevant matrix element is given by

$$\mathcal{M} = \frac{G_F V_{ud}}{\sqrt{2}}\Big[\langle \bar{n}|\Big(\gamma_\mu f_V(0) - \gamma_\mu\gamma^5 f_A(0) - \frac{i f_P(0)}{2M_n}\sigma_{\mu\nu}q^\nu\Big)|p\rangle\langle\bar{\nu}_e|\gamma^\mu(1-\gamma^5)|e\rangle\Big]. \tag{34}$$

In the above equation, f_V, f_A, and f_P are nuclear vector, axial vector, and Pauli (weak magnetism) form factors evaluated at zero-momentum transfer (for greater detail on the form factor behavior, see Sec. IV.D). To first order, the differential cross section can therefore be written as

$$\frac{d\sigma(\bar{\nu}_e p \rightarrow e^+ n)}{d\cos\theta} = \frac{G_F^2\lvert V_{ud}\rvert^2 E_e p_e}{2\pi}\Big[f_V^2(0)(1+\beta_e\cos\theta) + 3f_A^2(0)\Big(1-\frac{\beta_e}{3}\cos\theta\Big)\Big], \tag{35}$$

where E_e, p_e, β_e, and $\cos\theta$ refer to the electron's energy, momentum, velocity, and scattering angle, respectively.

[4]The neutrino energy threshold E_ν^{thresh} in the laboratory frame is defined by $[(m_n+m_e)^2 - m_p^2]/2m_p$.

A few properties in Eq. (35) immediately attract our attention. First and foremost is that the cross section neatly divides into two distinct "components"; a vectorlike component, called the Fermi transition, and an axial-vectorlike component, referred to as Gamow-Teller. We talk more about Fermi and Gamow-Teller transitions later.

A second striking feature is its angular dependence. The vector portion has a clear $1+\beta_e\cos\theta$ dependence, while the axial portion has a $1-(\beta_e/3)\cos\theta$ behavior, at least to first order in the nucleon mass. The overall angular effect is weakly backward scattered for antineutrino-proton interactions, showing that the vector and axial-vector terms both contribute at equivalent amplitudes. This is less so for cases where the interaction is almost purely Gamow-Teller in nature, such as νd reactions. In such reactions, the backwards direction is more prominent. Such angular distributions have been posited as an experimental tag for supernova detection (Beacom, Farr, and Vogel, 2002).

The final aspect of the cross section that is worthy to note is that it has a near one-to-one correspondence with the beta decay of the neutron. We explore this property in greater detail in the next section.

B. Beta decay and its role in cross section calibration

The weak interaction governs both the processes of decay and scattering amplitudes. It goes to show that, especially for simple systems, the two are intimately intertwined, often allowing one process to provide robust predictions for the other. The most obvious nuclear target where this takes place is in the beta decay of the neutron. In much the same way as muon decay provided a calibration of the Fermi coupling constant for purely leptonic interactions (Sec. II.D), neutron beta decay allows one to make a prediction of the inverse beta decay cross section from experimental considerations alone.

For the case of neutron beta decay, the double differential decay width at tree level is given by (Nico and Snow, 2005)

$$\frac{d^3\Gamma}{dE_e d\Omega_e d\Omega_\nu} = G_F^2\lvert V_{ud}\rvert^2(1+3\lambda^2)\lvert\vec{p}_e\rvert(T_e+m_e) \times (E_0-T_e)^2\Big[1 + a\frac{\vec{p}_e\cdot\vec{p}_\nu}{T_e E_\nu} + b\frac{m_e}{T_e} + \vec{\sigma}_n\cdot\Big(A\frac{\vec{p}_e}{T_e} + B\frac{\vec{p}_\nu}{E_\nu} + D\frac{\vec{p}_e\times\vec{p}_\nu}{T_e E_\nu}\Big)\Big].$$

Here $\vec{p}_e$ and $\vec{p}_\nu$ are the electron and neutrino momenta, T_e is the electron's kinetic energy, E_ν is the outgoing antineutrino energy, E_0 is the end-point energy for beta decay, and σ_n is the neutron spin. The definitions of the other various constants are listed in Table III.

Integrating over the allowed phase space provides a direct measure of the energy-independent portion of the inverse beta decay cross section, including internal radiative corrections. That is, Eq. (35) can also be written as

$$\frac{d\sigma(\bar{\nu}_e p \to e^+ n)}{d\cos\theta} = \frac{2\pi^2}{2m_e^5 f(1+\delta_R)\tau_n} E_e p_e \Big[(1+\beta_e \cos\theta) + 3\lambda^2 \Big(1 - \frac{\beta_e}{3}\cos\theta\Big)\Big]. \tag{36}$$

The term $f(1+\delta_R)$ is a phase space factor that includes several inner radiative corrections. Additional radiative corrections and effects due to finite momentum transfer have been evaluated. From a theoretical standpoint, therefore, the inverse beta decay cross section is well predicted, with uncertainties around $\pm 0.5\%$.[5]

The ability for measured beta decay rates to assist in the evaluation of neutrino cross sections is not limited solely to inverse beta decay. Beta decay transitions also play a pivotal role in the evaluation of neutrino cross sections for a variety of other target nuclei. Nuclei which relate back to superallowed nuclear transitions stand as one excellent example. Isotopes that undergo superallowed Fermi transitions ($0^+ \to 0^+$) provide the best test of the conserved vector current (CVC) hypothesis (Gerstein and Zeldovich, 1956; Feynman and Gell-Mann, 1958) and, if one includes measurements of the muon lifetime, the most accurate measurements of the quark mixing matrix element of the Cabibbo-Kobayashi-Maskawa matrix V_{ud} (Hardy and Towner, 1999). Typically, the value for V_{ud} can be extracted by looking at the combination of the statistical rate function ($\mathcal{F}$) and the partial half-life (t) of a given superallowed transition. Because the axial current cannot contribute in lowest order to transitions between spin-0 states, the experimental $\mathcal{F}t$ value is related directly to the vector coupling constant. For an isospin-1 multiplet, one obtains

$$|V_{ud}|^2 = \frac{K}{2G_F^2(1+\Delta_R)\mathcal{F}t}, \tag{37}$$

where Δ_R are the nucleus-independent radiative corrections in $0^+ \to 0^+$ transitions and K is defined as $K \equiv 2\pi^3 \ln 2/m_e^5 = (8120.271 \pm 0.012) \times 10^{-10}$ GeV^{-4} s. The $\mathcal{F}t$ value from various transitions are very precisely measured (down to the 0.1% level) to be 3072.3 ± 2.0, while the radiative corrections enter at the 2.4% level (Towner, 1998). The process is not directly relatable to that of inverse beta decay because of the lack of the axial form factor, but it provides a strong constraint on the validity of the CVC hypothesis.

Even excluding neutron decay and superallowed transitions, beta decay measurements also play an important role in the calculation of low-energy cross sections simply because they represent a readily measurable analog to their neutrino interaction counterpart. For example, the β^+ decay from ^{12}N to the ground state of ^{12}C is often used to calibrate calculations of the exclusive cross section of $^{12}\mathrm{C}(\nu_e, e^-)^{12}\mathrm{N}$ (Fukugita, Kohyama, and Kubodera, 1988). In the case of deuterium targets, the decay width of tritium beta decay provides an extremely strong constraint on the νd cross section (Nakamura *et al.*, 2001). Finally, though not least, both allowed and forbidden $\beta^\pm$ decays often allow a direct measure of the Gamow-Teller contribution to the total cross section. Comparisons of neutrino reactions on ^{37}Cl and the decay process $^{37}\mathrm{Ca}(\beta^+)^{37}\mathrm{K}$ are prime example of this last constraint technique (Aufderheide *et al.*, 1994).

C. Theoretical calculations of neutrino-deuterium cross sections

Next to hydrogen, no nuclear target is better understood than deuterium. Neutrino-deuterium scattering plays an important role in experimental physics, as heavy water (D_2O) was the primary target of SNO (Ahmad *et al.*, 2001, 2002a, 2002b, 2004; Aharmin *et al.*, 2005, 2007, 2008). The SNO experiment is able to simultaneously measure the electron and nonelectron component of the solar neutrino spectrum by comparing the charged current and neutral-current neutrino reactions on deuterium

$$\nu_e + d \to e^- + p + p \qquad \text{(charged current)}, \tag{38}$$

$$\nu_x + d \to \nu_x + n + p \qquad \text{(neutral current)}. \tag{39}$$

Results from the experiment allowed confirmation of the flavor-changing signature of neutrino oscillations and verification of the Mikheyev-Smirnov-Wolfenstein mechanism (Wolfenstein, 1978; Mikheyev and Smirnov, 1989).

Deuterium with its extremely small binding energy ($E_{\mathrm{bind}} \simeq 2.2$ MeV) has no bound final state after scattering. There exist two prominent methods for calculating such cross sections. The first method, sometimes referred to in the literature as the elementary-particle treatment (EPT) or at times the standard nuclear physics approach, was first introduced by Fujii and Yamaguchi (1964) and Kim and Primakoff (1965). The technique treats the relevant nuclei as fundamental particles with assigned quantum numbers. A transition matrix element for a given process is parametrized in terms of the nuclear form factors solely based on the transformation properties of the nuclear states, which in turn are constrained from complementary experimental data. Such a technique provides a robust method for calculating νd scattering. Typically one divides the problem into two parts; the one-body impulse approximation terms and two-body exchange currents acting on the appropriate nuclear wave functions. In general, the calculation of these two-body currents presents the most difficulty in terms of verification. However, data gathered from $n + p \to d + \gamma$ scattering provide one means of constraining any terms which may arise in νd scattering. An additional means of verification, as discussed previously, involves the reproduction of the experimental tritium beta decay width, which is very precisely measured.

An alternative approach to such calculations has recently emerged on the theoretical scene based on effective field theory (EFT) which has proven to be particularly powerful

[5]Some caution should be taken, as currently the most accurate value for the neutron lifetime is 6.5σ away from the PDG average value (Serebrov *et al.*, 2005).

in the calculations of νd scattering (Butler and Chen, 2000; Butler, Chen, and Kong, 2001). EFT techniques make use of the gap between the long-wavelength and short-range properties of nuclear interactions. Calculations separate the long-wavelength behavior of the interaction, which can be readily calculated, while absorbing the omitted degrees of freedom into effective operators which are expanded in powers of some cutoff momentum. Such effective operators can then be related directly to some observable or constraint that fixes the expansion. In the case of νd scattering, the expansion is often carried out as an expansion of the pion mass q/m_π. EFT separates the two-body current process such that it is dependent on one single parameter, referred to in the literature as $L_{1,A}$. This low-energy constant can be experimentally constrained, and in doing so provides an overall regularization for the entire cross section. Comparisons between these two different methods agree to within 1%–2% for energies relevant for solar neutrinos (< 20 MeV) (Nakamura *et al.*, 2001; Mosconi, Ricci, and Truhlik, 2006; Mosconi *et al.*, 2007). In general, the EFT approach has been extremely successful in providing a solid prediction of the deuterium cross section, and central to the reduction in the theoretical uncertainties associated with the reaction (Adelberger *et al.*, 2010). Given the precision of such cross sections, one must often include radiative corrections (Towner, 1998; Beacom and Parke, 2001; Kurylov, Ramsey-Musolf, and Vogel, 2002).

D. Other nuclear targets

So far we have only discussed the most simple of reactions; that is, scattering of antineutrinos off of free protons and scattering of neutrinos off of deuterium, both of which do not readily involve any bound states. In such circumstances, the uncertainties involved are small and well understood. But what happens when we expand our arsenal and attempt to evaluate more complex nuclei or nuclei at higher momenta transfer? The specific technique used depends in part on the type of problem that one is attempting to solve, but it usually falls in one of three main categories:

(1) For the very lowest energies, one must consider the exclusive scattering to particular nuclear bound states and provide an appropriate description of the nuclear response and correlations among nucleons. The shell model is often invoked here, given its success in describing Fermi and Gamow-Teller amplitudes (Caurier *et al.*, 2005).

(2) At higher energies, enumeration of all states becomes difficult and cumbersome. However, at this stage one can begin to look at the *collective* excitation of the nucleus. Several theoretical tools, such as the random phase approximation (RPA) (Auerbach and Klein, 1983) and extensions of the theory, including continuous random phase approximation (CRPA) (Kolbe, Langanke, and Vogel, 1999), and quasiparticle random phase approximation (QRPA) (Volpe *et al.*, 2000), have been developed along this strategy.

(3) Beyond a certain energy scale, it is possible to begin describing the nucleus in terms of individual, quasifree nucleons. Techniques in this regime are discussed later in the text.

We first turn our attention to the nature of the matrix elements which describe the cross section amplitudes of the reaction under study. In almost all cases, we wish to determine the amplitude of the matrix element that allows us to transition from some initial state i (with initial spin J_i) to some final state f (with final spin J_f). For a charged current interaction of the type $\nu_e + A_N^Z \rightarrow e^- + A_{N-1}^{*Z+1}$, the cross section can be written in terms of a very general expression

$$\frac{d\sigma}{d\cos\theta} = \frac{E_e p_e}{2\pi} \sum_i \frac{1}{(2J_i+1)} \left[\sum_{M_i, M_f} |\langle f|\hat{H}_W|i\rangle|^2 \right], \tag{40}$$

where E_e, p_e, and $\cos\theta$ are the outgoing electron energy, momentum, and scattering angle, respectively, and J_i is the total spin of the target nucleus. The sum is carried over all the accessible spins of the initial and final states. The term in brackets encapsulates the elements due to the hadronic-lepton interaction. A Fourier transform of the above expression allows one to express the matrix elements of the Hamiltonian in terms of the four-momenta of the initial and final states of the reaction. The Hamiltonian which governs the strength of the interaction is given by the product of the hadronic current $H(\vec{x})$ and the leptonic current $J(\vec{x})$

$$\mathcal{H}_W^{\mathrm{CC}} = \frac{G_F V_{ud}}{\sqrt{2}} \int [J^{\mathrm{CC},\mu}(\vec{x}) H_\mu^{\mathrm{CC}}(\vec{x}) + \mathrm{H.c.}] d\vec{x},$$

$$\mathcal{H}_W^{\mathrm{NC}} = \frac{G_F}{\sqrt{2}} \int [J^{\mathrm{NC},\mu}(\vec{x}) H_\mu^{\mathrm{NC}}(\vec{x}) + \mathrm{H.c.}] d\vec{x},$$

where

$$H_\mu^{\mathrm{CC}}(\vec{x}) = V_\mu^{\pm}(\vec{x}) + A_\mu^{\pm}(\vec{x}),$$

$$H_\mu^{\mathrm{NC}}(\vec{x}) = (1 - 2\sin^2\theta_W) V_\mu^0(\vec{x}) + A_\mu^0(\vec{x}) - 2\sin^2\theta_W V_\mu^s.$$

We concentrate on the charged current reaction first. In the above expression, the $V^{\pm}$ and $A^{\pm}$ components denote the vector and axial-vector currents, respectively. The $\pm$ and 0 index notation denotes the three components of the isospin raising (lowering) currents for the neutrino (or antineutrino) reaction. The final ingredient V^s denotes the isoscalar current. For the case of the impulse approximation, it is possible to write down a general representation of the hadronic weak current in terms of the relevant spin contributions

$$\langle f|V_\mu^a(q^2)|i\rangle = \bar{u}(p') \frac{\tau^a}{2} \left[F_1(q^2)\gamma_\mu + i\frac{F_2(q^2)}{2m_n}\sigma_{\mu\nu}q^\nu + i\frac{q_\mu}{M_N}F_S(q^2) \right] u(p),$$

$$\langle f|A_\mu^a(q^2)|i\rangle = \bar{u}(p') \frac{\tau^a}{2} \left[F_A(q^2)\gamma_\mu\gamma_5 + \frac{F_P}{M_N}(q^2)q_\mu\gamma_5 + \frac{F_T}{M_N}(q^2)\sigma_{\mu\nu}q^\nu\gamma_5 \right] u(p).$$

Here τ^a is indexed as $a = \pm, 0$, $\sigma_{\mu\nu}$ are the spin matrices, $\bar{u}(p')$ and $u(p)$ are the Dirac spinors for the target and final-state nucleon, M_N is the (averaged) nucleon mass, and $F_{[S,1,A,2,P,T]}(q^2)$ correspond to the scalar, Dirac, axial vector, Pauli, pseudoscalar, and tensor weak form factors, respectively. The invariance of the strong interaction under isospin simplifies the picture for the charged current interaction, as both the scalar and tensor components are zero

$$F_S(q^2) = F_T(q^2) \equiv 0. \tag{41}$$

In order to proceed further, one needs to make some link between the form factors probed by weak interactions and those from pure electromagnetic interactions. Fortunately, the CVC hypothesis allows us to do just that:

$$F_1(q^2) = F_1^p(q^2) - F_1^n(q^2),$$
$$F_2(q^2) = F_2^p(q^2) - F_2^n(q^2).$$

Here $F_1^{n,p}$ and $F_2^{n,p}$ are known in the literature as the electromagnetic Dirac and Pauli form factors of the proton and neutron, respectively. In the limit of zero-momentum transfer, the Dirac form factors reduce to the charge of the nucleon, while the Pauli form factors reduce to the nucleon's magnetic moments

$$F_1^N(0) = q_N = \begin{cases} 1 & \text{if proton,} \\ 0 & \text{if neutron,} \end{cases}$$

$$F_2^N(0) = \begin{cases} \frac{\mu_p}{\mu_N} - 1 & \text{if proton,} \\ \frac{\mu_n}{\mu_N} & \text{if neutron.} \end{cases}$$

Here q_N is the nucleon charge, μ_N is the nuclear magneton, and $\mu_{p,n}$ are the proton and neutron magnetic form factors.

To ascertain the q^2 dependence of these form factors, it is common to use the Sachs electric and magnetic form factors and relate them back to F_1^N and F_2^N,

$$G_E^N(q^2) = F_1^N(q^2) - \eta F_2^N(q^2),$$
$$G_M^N(q^2) = F_1^N(q^2) + F_2^N(q^2),$$

with $\eta \equiv -q^2/4M_N$ and

$$G_E^p(q^2) = G_D(q^2), \qquad G_E^n(q^2) = 0,$$
$$G_M^p(q^2) = \frac{\mu_p}{\mu_N} G_D(q^2), \qquad G_M^n(q^2) = \frac{\mu_n}{\mu_N} G_D(q^2).$$

Here $G_D(q^2)$ is a dipole function determined by the charge radius of the nucleon. Empirically, the dipole term can be written as

$$G_D(q^2) = \left(1 - \frac{q^2}{m_V^2}\right)^{-1}, \tag{42}$$

where $m_V \simeq 0.84$ MeV.

We now turn our attention to the axial portion of the current, where the terms $F_A(q^2)$ and $F_P(q^2)$ play a role. For $F_A(q^2)$, one also often assumes a dipolelike behavior, but with a different coupling and axial mass term (m_A)

$$F_A(q^2) = -g_A G_A(q^2), \qquad G_A(q^2) = \frac{1}{(1 - q^2/m_A^2)^2}.$$

The Goldberger-Treiman relation allows one to also relate the pseudoscalar contribution in terms of the axial term as well; typically

$$F_P(q^2) = \frac{2M_N^2}{m_\pi^2 - q^2} F_A(q^2),$$

where m_π is the pion mass. In the limit that the momentum exchange is small (such as in neutron decay or inverse beta decay), the form factors reduce to the constants defined previously in this section

$$f_V(0) \equiv F_1(0) = 1,$$
$$f_P(0) \equiv F_2(0) = \frac{\mu_p - \mu_n}{\mu_N} - 1 \simeq 3.706,$$
$$f_A(0) \equiv F_A(0) = -g_A,$$

with $\lambda \equiv f_A(0)/f_V(0) \equiv -1.2694 \pm 0.0028$, as before (Nakamura, K. *et al.*, 2010).

The above represents an approach that works quite well when the final states are simple, for example, when one is dealing with a few-nucleon system with no strong bound states or when the momentum exchange is very high (see the next section on quasielastic interactions).

Seminal articles on neutrino (and electron) scattering can be found in earlier review articles by Donnelly *et al.* (1974), Donnelly and Walecka (1975), Donnelly and Peccei (1979), and Peccei and Donnelly (1979). Peccei and Donnelly equate the relevant form factors to those measured in (e, e') scattering (Drell and Walecka, 1964; de Forest Jr. and Walecka, 1966), removing some of the model dependence and q^2 restrictions prevalent in certain techniques. This approach is not entirely model independent, as certain axial form factors are not completely accessible via electron scattering. This technique has been expanded in describing neutrino scattering at much higher energy scales (Amaro *et al.*, 2005, 2007) with the recent realization that added nuclear effects come into play (Amaro *et al.*, 2011b).

E. Estimating fermi and Gamow-Teller strengths

For very small momentum transfers, the relevant impact of these various form factors take a back seat to the individual final states accessible to the system. Under this scheme, it is customary to divide into two general groupings: the Fermi transitions [associated with $f_V(0)$] and the Gamow-Teller transitions [associated with $f_A(0)$]. In doing so, the cross section can be rewritten as

$$\frac{d\sigma}{d\cos\theta} \simeq \frac{G_F^2 |V_{ud}|^2 F(Z_f, E_e) E_e p_e}{2\pi} \Big(f_F(q^2) |M_F|^2 + f_{GT}(q^2) \frac{1}{3} |M_{GT}|^2 + \text{interference terms} \Big), \tag{43}$$

where

$$|M_F|^2 = \frac{1}{2J_i + 1} \sum_{M_f, M_i} \left| \langle J_f, M_f | \sum_{k=1}^{A} \tau_\pm(k) e^{iq\cdot r_k} | J_i, M_i \rangle \right|^2, \tag{44}$$

$$|M_{GT}|^2 = \frac{1}{2J_i + 1} \times \sum_{M_f, M_i} \left| \langle J_f, M_f | \sum_{k=1}^{A} \tau_\pm(k) \sigma(k) e^{iq\cdot r_k} | J_i, M_i \rangle \right|^2. \tag{45}$$

We note that we have altered our notation slightly to denote explicit summation over individual accessible nuclear states. Equations (44) and (45) show explicitly the summation across

both initial ($|J_i, M_i\rangle$) and final ($|J_f, M_f\rangle$) spin states. In general, the terms associated with the Fermi transitions $f_F(q^2)$ and the Gamow-Teller transitions $f_{\rm GT}(q^2)$ are nontrivial combinations of the various form factors described previously [see also Kuramoto *et al.*, (1990)]. However, as one approaches zero momentum, we can immediately connect the relevant Fermi and Gamow-Teller amplitudes directly to β decay

$$M_\beta = f_V(0)^2|M_F|^2 + f_A(0)^2\tfrac{1}{3}|M_{\rm GT}|^2, \tag{46}$$

$$|M_F|^2 = \frac{1}{2J_i+1}\sum_{M_f,M_i}\left|\langle J_f, M_f|\sum_{k=1}^{A}\tau_\pm(k)|J_i, M_i\rangle\right|^2, \tag{47}$$

$$|M_{\rm GT}|^2 = \frac{1}{2J_i+1}\sum_{M_f,M_i}\left|\langle J_f, M_f|\sum_{k=1}^{A}\tau_\pm(k)\sigma(k)|J_i, M_i\rangle\right|^2, \tag{48}$$

and

$$\mathcal{F}t = \frac{2\pi^3\ln 2}{G_F^2|V_{ud}|^2 m_e^5 M_\beta}. \tag{49}$$

Hence, in the most simplistic model, the total charged current cross section can be calculated directly from evaluating the appropriate β decay reaction and correcting for the spin of the system

$$\sigma = \frac{2\pi^2\ln 2}{m_e^5\mathcal{F}t}p_e E_e F(E_e, Z_{\rm f})\frac{2J_f+1}{2J_i+1}. \tag{50}$$

Further information on the relevant coefficients can also be obtained by studying muon capture on the nucleus of interest (Luyten, Rood, and Tolhoek, 1963; Nguyen, 1975; Ricci and Truhlik, 2010), or by imposing sum rules on the total strength of the interaction.[6]

Another extremely powerful technique in helping discern the contributions to the neutrino cross section, particularly for Gamow-Teller transitions, has been through (p, n) scattering. Unlike its β decay counterpart, (p, n) scattering does not suffer from being limited to a particular momentum band; in principle, a wider band is accessible via this channel. Since the processes involved for (p, n) scattering are essentially the same as those for the weak interaction in general, one can obtain an empirical evaluation of the Fermi and Gamow-Teller strengths for a given nucleus. This is particularly relevant for (p, n) reactions at high incident energies and forward angles, where the direct reaction mechanism dominates. The use of (p, n) reactions is particularly favorable for studying weak interaction matrix elements for a number of reasons. The reaction is naturally spin selective and spin sensitive over a wide range of beam energies. Furthermore, small angle scattering is relatively easy to prove experimentally. This approach was first explored empirically by Goodman and others (Goodman *et al.*, 1980; Watson *et al.*, 1985) and later expanded in a seminal paper by Taddeucci *et al.* (1987). Provided that (p, n) forward scattering data on a particular nucleus are available, one can reduce the uncertainties on the corresponding neutrino cross section considerably. Data on (p, n) scattering have been taken for a variety of nuclear targets, with particular focus on isotopes relevant for solar neutrino physics and stellar astrophysics. An example of the latter would be the treatment of the neutrino cross section at low energies for ^{71}Ga (Haxton, 1998).

[6]Examples of known sum rules to this effect include the Ikeda sum rule for the Gamow-Teller strength (Ikeda, 1964)

$$\sum_i M_{\rm GT}^2(Z\to Z+1)_i - M_{\rm GT}^2(Z\to Z-1)_i = 3(N-Z).$$

.

F. Experimental tests of low-energy cross sections on nuclei

Low-energy neutrino cross sections feature prominently in a variety of model-building scenarios. Precise knowledge of the inclusive and differential cross section feeds into reactor neutrino analysis, supernova modeling, neutrino oscillation tests, and countless others. Yet, the number of direct experimental tests of these cross sections is remarkably few. We describe some examples next.

1. Hydrogen

Inverse beta decay holds a special place for experimental neutrino physics, as it is via this channel that neutrinos were first detected (Cowan *et al.*, 1956; Navarro, 2006). Currently, the technique of tagging inverse beta decay is prevalently used in the field for the identification and study of neutrino interactions. Inverse beta decay and neutrino absorption are still, after 60 years, the main reaction channels used for detecting reactor and solar neutrinos. Within the context of studying neutrino cross sections, however, the experimental data are somewhat limited. Most studies of neutrino interactions on protons (hydrogen) come from reactor experiments, whereby neutrinos are produced from the fission of ^{235}U, ^{239}Pu, ^{241}Pu, and ^{238}U. These experiments include Institut Laue-Langevin (ILL)-Grenoble (Kwon *et al.*, 1981; Hoummada *et al.*, 1995),[7] Gösgen (Zacek *et al.*, 1986), ROVNO (Kuvshinnikov *et al.*, 1991), Krasnoyarsk (Vidyakin *et al.*, 1987), and Bugey (Declais *et al.*, 1994; Achkar *et al.*, 1995), the latter of which had the most precise determination of the cross section. In almost all cases, the knowledge of the neutrino flux contributes the largest uncertainty. A tabulation of extracted cross sections compared to theoretical predictions is shown in Table IV. We currently omit measurements from Palo Verde (Boehm *et al.*, 2001), CHOOZ (Apollonio *et al.*, 2003), and KamLAND (Gando *et al.*, 2011), as such measurements were performed at a distance greater than 100 m from the reactor core. Such distances are much more sensitive to oscillation phenomena. Also, the level of statistical precision from this latter set of experiments is lower than that from the Bugey reactor.

Because most experimental tests of inverse beta decay involve neutrinos produced from reactor sources, the conversion from the fission decays of ^{235}U, ^{239}Pu, ^{239}U, and ^{241}Pu to neutrino fluxes is extremely important. Most predictions rely on the calculations made by Schreckenbach *et al.* (1985).

[7]The ILL experiment revised their original 1986 measurement due to better estimates of power consumption and neutron lifetime.

TABLE IV. Measured inverse β decay cross sections from short-baseline (< 100 m) reactor experiments. Data are taken from ILL-Grenoble (Kwon *et al.*, 1981; Hoummada *et al.*, 1995), Gösgen (Zacek *et al.*, 1986), ROVNO (Kuvshinnikov *et al.*, 1991), Krasnoyarsk (Vidyakin *et al.*, 1987), and Bugey (Declais *et al.*, 1994; Achkar *et al.*, 1995). Theoretical predictions include original estimates and (in parenthesis) the recalculated predictions from (Mention *et al.*, 2011).

Experiment	Fuel composition ^{235}U	^{239}Pu	^{239}U	^{241}Pu	Distance (m)	$\sigma_{\text{exp}}/\sigma_{\text{theo}}$
ILL (Kwon *et al.*, 1981; Hoummada *et al.*, 1995)	93%	···	···	···	9	0.800(0.832) ± 0.028 ± 0.071
Bugey (Declais *et al.*, 1994) 94	53.8%	32.8%	7.8%	5.6%	15	0.987(0.943) ± 0.014 ± 0.027
Bugey (Achkar *et al.*, 1995) 95	53.8%	32.8%	7.8%	5.6%	15	0.988(0.943) ± 0.037 ± 0.044
Bugey (Achkar *et al.*, 1995) 95	53.8%	32.8%	7.8%	5.6%	40	0.994(0.948) ± 0.010 ± 0.045
Bugey (Achkar *et al.*, 1995) 95	53.8%	32.8%	7.8%	5.6%	95	0.915(0.873) ± 0.10 ± 0.041
Gösgen (Zacek *et al.*, 1986) I	61.9%	27.2%	6.7%	4.2%	37.9	1.018(0.971) ± 0.017 ± 0.06
Gösgen (Zacek *et al.*, 1986) II	58.4%	29.8%	6.8%	5.0%	45.9	1.045(0.997) ± 0.019 ± 0.06
Gösgen (Zacek *et al.*, 1986) III	54.3%	32.9%	7.0%	5.8%	64.7	0.975(0.930) ± 0.033 ± 0.06
ROVNO (Kuvshinnikov *et al.*, 1991)	61.4%	27.5%	3.1%	7.4%	18	0.985(0.940) ± 0.028 ± 0.027
Krasnoyarsk (Vidyakin *et al.*, 1987) I	99%	···	···	···	33	1.013(0.944) ± 0.051
Krasnoyarsk (Vidyakin *et al.*, 1987) II	99%	···	···	···	57	0.989(0.954) ± 0.041
Krasnoyarsk (Vidyakin *et al.*, 1987) III	99%	···	···	···	33	1.031(0.960) ± 0.20

Recently, a new calculation of the antineutrino spectrum has emerged which incorporates a more comprehensive model of fission production (Mueller *et al.*, 2011). The new method, which is well constrained by the accompanying electron spectrum measured from fission, has the effect that it systematically raises the expected antineutrino flux from reactors (Mention *et al.*, 2011), providing some tension between the data and theoretical predictions. The new calculation is still under evaluation. In our review, we list both the shifted and unshifted cross section ratios (see Table IV and Fig. 5).

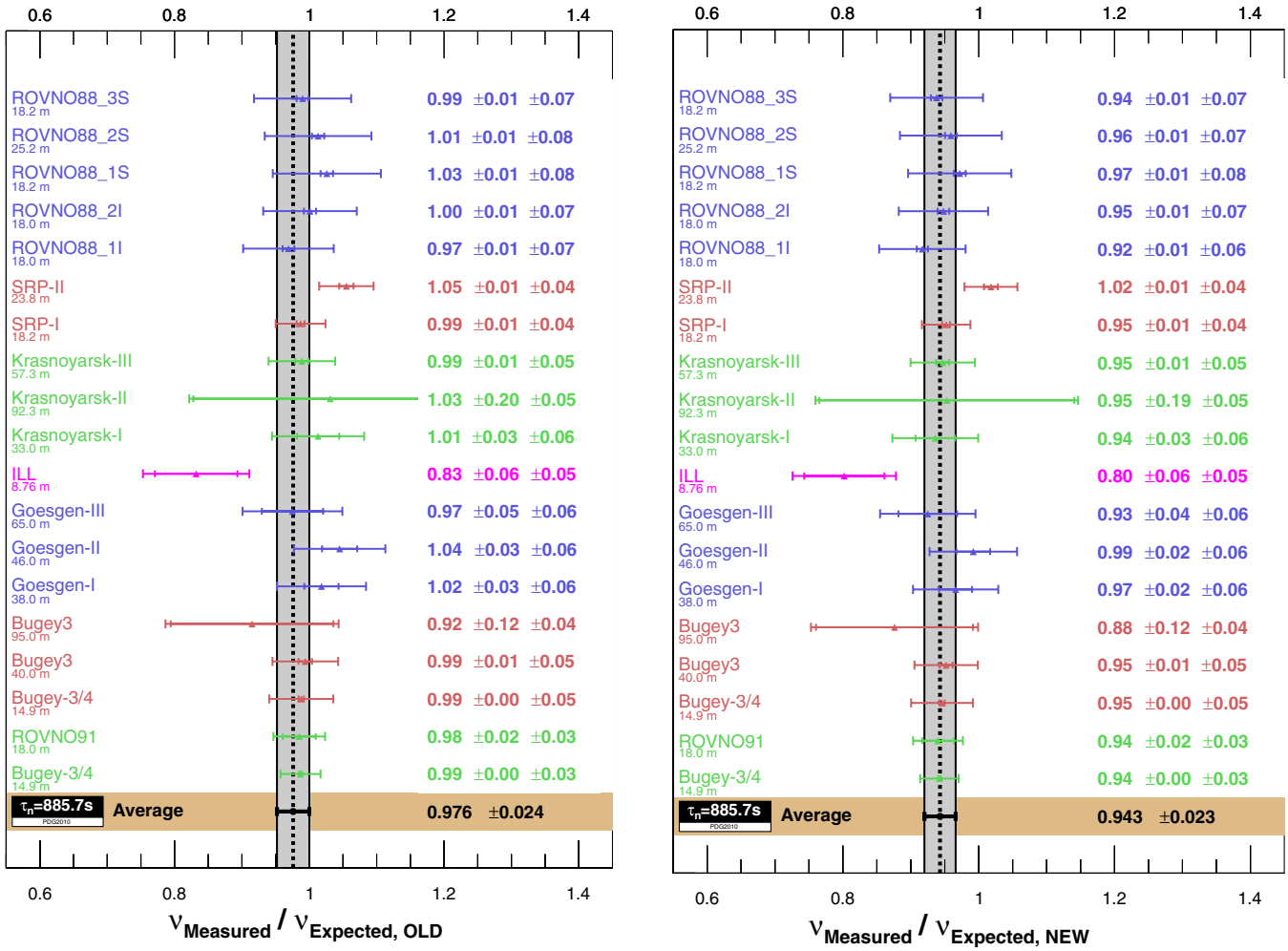

FIG. 5 (color online). Compilation of world reactor data for neutrino inverse beta decay processes for distances ≤ 100 m based on former (left) and new (right) theoretical flux predictions. The error on the neutron lifetime is shown for comparison. From Mention *et al.*, 2011.

TABLE V. Measured charged current ($\bar{\nu}_e$CC) and neutral-current ($\bar{\nu}_e$NC) neutrino cross sections on deuterium from short-baseline (< 100 m) reactor experiments. Data are taken from Savannah River (Pasierb *et al.*, 1979), ROVNO (Vershinsky *et al.*, 1991), Krasnoyarsk (Riley *et al.*, 1999; Kozlov *et al.*, 2000), and Bugey (Riley *et al.*, 1999). The comparison with theory is from Kozlov *et al.* (2000).

Experiment	Measurement	$\sigma_{\text{fission}}(10^{-44}$ cm^2/fission)	$\sigma_{\text{exp}}/\sigma_{\text{theory}}$
Savannah River (Pasierb *et al.*, 1979)	$\bar{\nu}_e$CC	1.5 ± 0.4	0.7 ± 0.2
ROVNO (Vershinsky *et al.*, 1991)	$\bar{\nu}_e$CC	1.17 ± 0.16	1.08 ± 0.19
Krasnoyarsk (Kozlov *et al.*, 2000)	$\bar{\nu}_e$CC	1.05 ± 0.12	0.98 ± 0.18
Bugey (Riley *et al.*, 1999)	$\bar{\nu}_e$CC	0.95 ± 0.20	0.97 ± 0.20
Savannah River (Pasierb *et al.*, 1979)	$\bar{\nu}_e$NC	3.8 ± 0.9	0.8 ± 0.2
ROVNO (Vershinsky *et al.*, 1991)	$\bar{\nu}_e$NC	2.71 ± 0.47	0.92 ± 0.18
Krasnoyarsk (Kozlov *et al.*, 2000)	$\bar{\nu}_e$NC	3.09 ± 0.30	0.95 ± 0.33
Bugey (Riley *et al.*, 1999)	$\bar{\nu}_e$NC	3.15 ± 0.40	1.01 ± 0.13

2. Deuterium

Direct tests of low-energy neutrino interactions on deuterium are of particular importance for both solar processes and solar oscillation probes. The Sudbury Neutrino Observatory stands as the main example, as it uses heavy water as its main target to study charged current and neutral-current interactions from the production of neutrinos from ^{8}B in the solar core. The Clinton P. Anderson Meson Physics Facility (LAMPF) at Los Alamos made the only direct measurement of the reaction $\nu_e d \rightarrow e^- pp$ using neutrinos produced from a source of stopped μ^+ decays from stopped pions created at their 720 MeV proton beam stop (Willis *et al.*, 1980). The cross section is averaged over the Michel muon decay spectrum. Their reported measurement of $\langle \sigma_\nu \rangle = (0.52 \pm 0.18) \times 10^{-40}$ cm^2 is in good agreement with theoretical predictions.

Direct cross section measurements on deuterium targets have also been carried out using antineutrinos produced in nuclear reactors. Reactor experiments, including Savannah River (Reines, Gurr, and Sobel, 1976), ROVNO (Vershinsky *et al.*, 1991), Krasnoyarsk (Kozlov *et al.*, 2000), and Bugey Riley *et al.* (1999), have reported cross sections per fission for both charged current ($\bar{\nu}_e d \rightarrow e^+ nn$) and neutral-current ($\bar{\nu}_e d \rightarrow \bar{\nu}_e pn$) reactions (see Table V).

Given the ever-increasing precision gained by large scale solar experiments, however, there has been greater urgency to improve upon the $\pm 20\%$ accuracy on the cross section amplitude achieved by direct beam measurements. Indirect constraints on the $\nu_e d$ cross section have therefore emerged, particularly within the context of effective field theory. As discussed in the previous section, the main uncertainty in the neutrino-deuterium cross section can be encapsulated in a single common isovector axial two-body current parameter $L_{1,A}$. Constraints on $L_{1,A}$ come from a variety of experimental probes. There are direct extractions, such as from solar neutrino experiments and reactor measurements, as highlighted above. Constraints can also be extracted from the lifetime of tritium beta decay, muon capture on deuterium, and helio-seismology. These methods were recently summarized by Butler, Chen, and Vogel (2002) and are reproduced in Table VI.

Deuterium represents one of those rare instances where the theoretical predictions are on a more solid footing than even the experimental constraints. This robustness has translated into direct improvement on the interpretation of collected neutrino data, particularly for solar oscillation phenomena. As we proceed to other nuclear targets, one immediately appreciates the rarity of this state.

3. Additional nuclear targets

The other main nuclear isotope studied in detail is ^{12}C. There are a number of neutrino interactions on ^{12}C that have been investigated experimentally

$$\nu_{e,\mu} + {}^{12}\text{C}_{\text{g.s.}} \rightarrow (e^-, \mu^-) + {}^{12}\text{N}_{\text{g.s.}} \quad \text{(exclusive charged current)}, \tag{51}$$

$$\nu_{e,\mu} + {}^{12}\text{C}_{\text{g.s.}} \rightarrow (e^-, \mu^-) + {}^{12}\text{N}^* \quad \text{(inclusive charged current)}, \tag{52}$$

$$\nu + {}^{12}\text{C}_{\text{g.s.}} \rightarrow \nu + {}^{12}\text{C}^* \qquad \text{(neutral current)}. \tag{53}$$

Reaction (51) is a uniquely clean test case for both theory and experiment. The spin parity of the ground state of ^{12}C is $J^\pi = 0^+, T = 0$, while for the final state it is $J^\pi = 1^+, T = 1$. As such, there exists both an isospin and spin flip in the interaction, the former involving the isovector components of the reaction, while the latter invoking the axial-vector components. Therefore, both vector and axial-vector components contribute strongly to the interaction. The isovector components are well constrained by electron scattering data. Since the final state of the nucleus is also well defined, the axial form factors can be equally constrained by looking at the β decay of ^{12}N, as well as the muon capture on ^{12}C. Although these constraints occur at a specific momentum transfer, they provide almost all necessary information to calculate the cross section. The exclusive reaction is also optimal from an experimental perspective. The ground state of ^{12}N beta decays to the ground state of ^{12}C with a half-life of 11 ms; the emitted secondary electron providing a well-defined tag for event identification. The neutral-current channel has an

TABLE VI. Extraction of the isovector axial two-body current parameter $L_{1,A}$ from various experimental constraints.

Method	Extracted $L_{1,A}$(fm^3)
Reactor	3.6 ± 5.5
Solar	4.0 ± 6.3
Helioseismology	4.8 ± 6.7
$^3\text{H} \rightarrow {}^{3+}\text{He}\ e^- \bar{\nu}_e$	6.5 ± 2.4

TABLE VII. Experimentally measured (flux-averaged) cross sections on various nuclei at low energies (1–300 MeV). Experimental data gathered from the LAMPF (Willis *et al.*, 1980), KARMEN (Bodmann *et al.*, 1991; Zeitnitz *et al.*, 1994; Armbruster *et al.*, 1998; Maschuw, 1998; Ruf, 2005), E225 (Krakauer *et al.*, 1992), LSND (Athanassopoulos *et al.*, 1997; Auerbach *et al.*, 2001; Auerbach *et al.*, 2002; Distel *et al.*, 2003), GALLEX (Hampel *et al.*, 1998), and SAGE (Abdurashitov *et al.*, 1999; Abdurashitov *et al.*, 2006) experiments. Stopped π/μ beams can access neutrino energies below 53 MeV, while decay-in-flight measurements can extend up to 300 MeV. The ^{51}Cr sources have several monoenergetic lines around 430 and 750 keV, while the ^{37}Ar source has its main monoenergetic emission at $E_\nu = 811$ keV. Selected comparisons to theoretical predictions, using different approaches are also listed. The theoretical predictions are not meant to be exhaustive.

Isotope	Reaction Channel	Source	Experiment	Measurement (10^{-42} cm^2)	Theory (10^{-42} cm^2)
^{2}H	$^2\mathrm{H}(\nu_e, e^-)pp$	Stopped π/μ	LAMPF	52 ± 18(tot)	54 (IA) (Tatara, Kohyama, and Kubodera, 1990)
^{12}C	$^{12}\mathrm{C}(\nu_e, e^-)^{12}\mathrm{N}_{\mathrm{g.s.}}$	Stopped π/μ	KARMEN	9.1 ± 0.5(stat) ± 0.8(sys)	9.4 [Multipole](Donnelly and Peccei, 1979)
		Stopped π/μ	E225	10.5 ± 1.0(stat) ± 1.0(sys)	9.2 [EPT] (Fukugita, Kohyama, and Kubodera, 1988).
		Stopped π/μ	LSND	8.9 ± 0.3(stat) ± 0.9(sys)	8.9 [CRPA] (Kolbe, Langanke, and Vogel, 1999)
	$^{12}\mathrm{C}(\nu_e, e^-)^{12}\mathrm{N}^*$	Stopped π/μ	KARMEN	5.1 ± 0.6(stat) ± 0.5(sys)	5.4–5.6 [CRPA] (Kolbe, Langanke, and Vogel, 1999)
		Stopped π/μ	E225	3.6 ± 2.0(tot)	4.1 [Shell] (Hayes and Towner, 2000)
		Stopped π/μ	LSND	4.3 ± 0.4(stat) ± 0.6(sys)	
	$^{12}\mathrm{C}(\nu_\mu, \nu_\mu)^{12}\mathrm{C}^*$	Stopped π/μ	KARMEN	3.2 ± 0.5(stat) ± 0.4(sys)	2.8 [CRPA] (Kolbe, Langanke, and Vogel, 1999)
	$^{12}\mathrm{C}(\nu, \nu)^{12}\mathrm{C}^*$	Stopped π/μ	KARMEN	10.5 ± 1.0(stat) ± 0.9(sys)	10.5 [CRPA] (Kolbe, Langanke, and Vogel, 1999)
	$^{12}\mathrm{C}(\nu_\mu, \mu^-)X$	Decay in flight	LSND	1060 ± 30(stat) ± 180(sys)	1750–1780 [CRPA] (Kolbe, Langanke, and Vogel, 1999)
					1380 [Shell] (Hayes and Towner, 2000)
					1115 [Green's Function] (Meucci, Giusti, and Pacati, 2004)
	$^{12}\mathrm{C}(\nu_\mu, \mu^-)^{12}\mathrm{N}_{\mathrm{g.s.}}$	Decay in flight	LSND	56 ± 8(stat) ± 10(sys)	68–73 [CRPA] (Kolbe, Langanke, and Vogel, 1999)
					56 [Shell] (Hayes and Towner, 2000)
^{56}Fe	$^{56}\mathrm{Fe}(\nu_e, e^-)^{56}\mathrm{Co}$	Stopped π/μ	KARMEN	256 ± 108(stat) ± 43(sys)	264 [Shell] (Kolbe, Langanke, and Martínez-Pinedo, 1999)
^{71}Ga	$^{71}\mathrm{Ga}(\nu_e, e^-)^{71}\mathrm{Ge}$	^{51}Cr source	GALLEX, ave.	0.0054 ± 0.0009(tot)	0.0058 [Shell] (Haxton, 1998)
		^{51}Cr	SAGE	0.0055 ± 0.0007(tot)	
		^{37}Ar source	SAGE	0.0055 ± 0.0006(tot)	0.0070 [Shell] (Bahcall, 1997)
^{127}I	$^{127}\mathrm{I}(\nu_e, e^-)^{127}\mathrm{Xe}$	Stopped π/μ	LSND	284 ± 91(stat) ± 25(sys)	210–310 [Quasiparticle] (Engel, Pittel, and Vogel, 1994)

equally favorable channel, with the emission of a monoenergetic 15.11 MeV photon.

Studies of the above neutrino cross sections have been carried out at the LAMPF facility in the United States (Willis *et al.*, 1980) and the KArlsruhe Rutherford Medium Energy Neutrino Experiment (KARMEN) detector at ISIS at the Rutherford Laboratory in the United Kingdom. The neutrino beam in both experimental facilities is provided from proton beam stops. High-energy proton collisions on a fixed target produce a large π^+ flux which is subsequently stopped and allowed to decay. The majority of low-energy neutrinos are produced from the decay at rest from stopped μ^+ and π^+, providing a well-characterized neutrino beam with energies below 50 MeV.[8] The KARMEN experiment at the ISIS facility additionally benefited from a well-defined proton beam structure, which allowed efficient tagging of neutrino events against cosmic ray backgrounds. The main uncertainty affecting these cross section measurements stems primarily from the knowledge of the pion flux produced in the proton-target interactions.

Table VII summarizes the measurements to date on the inclusive and exclusive reactions on ^{12}C at low energies. Estimates of the cross sections using a variety of different techniques (shell model, RPA, QRPA, effective particle theory) demonstrate the robustness of the calculations. Some disagreement can be seen in the inclusive channels; this disagreement is to be expected since the final state is not as well defined as in the exclusive channels. More recent predictions employing extensive shell model calculations appear to show better agreement with the experimental data. A plot showing the collected data from the exclusive reaction $^{12}\mathrm{C}(\nu_e, e^-)^{12}\mathrm{N}$ and $^{12}\mathrm{C}(\nu_\mu, \mu^-)^{12}\mathrm{N}$ are shown in Figs. 6 and 7, respectively.

Table VII also lists other nuclei that have been under experimental study. Proton beam stops at the Los Alamos Meson Physics Facility have also been utilized to study low-energy neutrino cross sections on ^{127}I. Cross sections on iron targets have also been explored with low-energy beams at the KARMEN experiment (Ruf, 2005).

Perhaps the most remarkable of such measurements was the use of MCi radiological sources for low-energy electron cross section measurements. Both the Soviet-American Gallium Experiment (SAGE) (Abdurashitov *et al.*, 1999) and GALLium EXperiment (GALLEX) (Anselmann *et al.*, 1995) solar neutrino experiments have made use of a MCi ^{51}Cr source to study the reaction $^{71}\mathrm{Ga}(\nu_e, e^-)^{71}\mathrm{Ge}$ to both the ground and excited states of ^{71}Ge. The source strength of ^{51}Cr is typically determined using calorimetric techniques and the uncertainty on the final activity is constrained to about 1%–2%. The SAGE collaboration subsequently also made use of a gaseous ^{37}ArMCi source. Its activity, using a

[8]Neutrinos from decay-in-flight muons also allowed for cross section measurements for energies below 300 MeV.

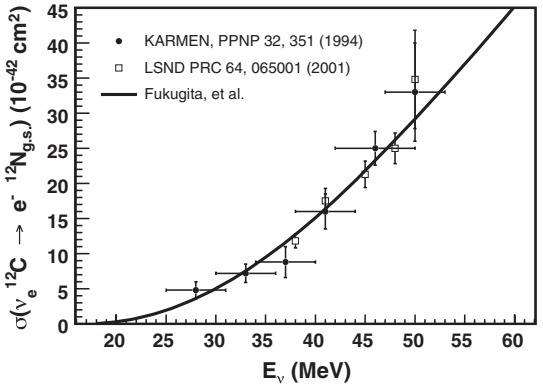

FIG. 6. Cross section as a function of neutrino energy for the exclusive reaction $^{12}C(\nu_e, e^-)^{12}N$ from μ^- decay-at-rest neutrinos. Experimental data measured by the KARMEN (Zeitnitz *et al.*, 1994) and LSND (Athanassopoulos *et al.*, 1997; Auerbach *et al.*, 2001) experiments. Theoretical prediction from Fukugita, Kohyama, and Kubodera, 1988.

variety of techniques, is constrained to better than 0.5% (Haxton, 1998; Barsanov *et al.*, 2007). Since ^{37}Ar provides a monoenergetic neutrino at slightly higher energies that its ^{51}Cr counterpart, it provides a much cleaner check on the knowledge of such low-energy cross sections (Barsanov *et al.*, 2007). Experimental measurements are in general in agreement with the theory, although the experimental values are typically lower than the corresponding theoretical predictions.

Finally, although the cross section was not measured explicitly using a terrestrial source, neutrino capture on chlorine constitutes an important channel used in experimental neutrino physics. The reaction $^{37}Cl(\nu_e, e^-)^{37}Ar$ was the first reaction used to detect solar neutrinos (Cleveland *et al.*, 1998).

In summary, the level at which low-energy cross sections are probed using nuclear targets is relatively few, making the ability to test the robustness of theoretical models and techniques somewhat limited. The importance of such low-energy cross sections is continually stressed by advances in astrophysics, particularly in the calculation of elemental abundances and

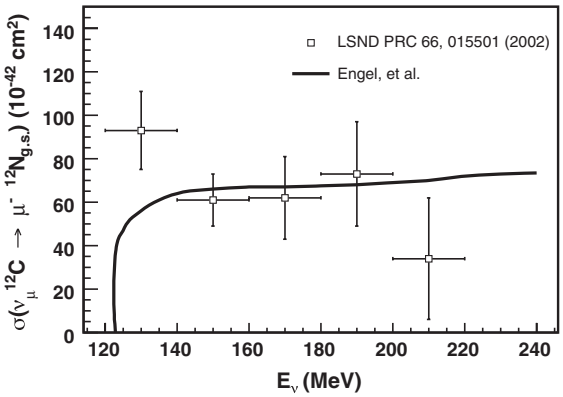

FIG. 7. Cross section as a function of neutrino energy for the exclusive reaction $^{12}C(\nu_\mu, \mu^-)^{12}N$ measured by the LSND (Auerbach *et al.*, 2002) experiment. Theoretical prediction from Engel *et al.*, 1996.

supernova physics (Langanke *et al.*, 2004; Heger *et al.*, 2005). Measurements of neutrino cross sections on nuclear targets is currently being revisited now that new high intensity stopped pion and muon sources are once again becoming available (Avignone *et al.*, 2000).

G. Transitioning to higher energy scales

As we transition from low-energy neutrino interactions to higher energies, the reader may notice that our approach is primarily focused on the scattering off a particular target, whether that target be a nucleus, a nucleon, or a parton. This approach is not accidental, as it is theoretically a much more well-defined problem when the target constituents are treated individually. With that said, we acknowledge that the approach is also limited, as it fails to incorporate the nucleus as a whole. Such departmentalization is part of the reason why the spheres of low-energy and high-energy physics appear so disjointed in both approach and terminology. Until a full, comprehensive model of the entire neutrino-target interaction is formulated, we are constrained to also follow this approach.

V. INTERMEDIATE ENERGY CROSS SECTIONS: $E_\nu \sim$ 0.1–20 GeV

As we move up farther still in energy, the description of neutrino scattering becomes increasingly more diverse and complicated. At these intermediate energies, several distinct neutrino scattering mechanisms start to play a role. The possibilities fall into three main categories:

- *Elastic and quasielastic scattering*: Neutrinos can elastically scatter off an entire nucleon liberating a nucleon (or multiple nucleons) from the target. In the case of charged current neutrino scattering, this process is referred to as "quasielastic scattering" and is a mechanism we first alluded to in Sec. IV.D, whereas for neutral-current scattering this is traditionally referred to as "elastic scattering."
- *Resonance production*: Neutrinos can excite the target nucleon to a resonance state. The resultant baryonic resonance (Δ, N^*) decays to a variety of possible mesonic final states producing combinations of nucleons and mesons.
- *Deep inelastic scattering*: Given enough energy, the neutrino can resolve the individual quark constituents of the nucleon. This is called deep inelastic scattering and manifests in the creation of a hadronic shower.

As a result of these competing processes, the products of neutrino interactions include a variety of final states ranging from the emission of nucleons to more complex final states including pions, kaons, and collections of mesons (Fig. 8). This energy regime is often referred to as the "transition region" because it corresponds to the boundary between quasielastic scattering (in which the target is a nucleon) on the one end and deep inelastic scattering (in which the target is the constituent parton inside the nucleon) on the other. Historically, adequate theoretical descriptions of quasielastic, resonance-mediated, and deep inelastic scattering have been formulated, however, there is no uniform description which

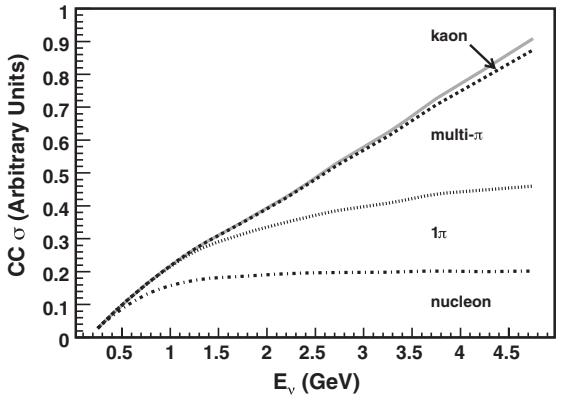

FIG. 8. Predicted processes to the total CC inclusive scattering cross section at intermediate energies. The underlying quasielastic, resonance, and deep inelastic scattering contributions can produce a variety of possible final states including the emission of nucleons, single pions, multipions, kaons, as well as other mesons (not shown). Combined, the inclusive cross section exhibits a linear dependence on neutrino energy as the neutrino energy increases.

globally describes the transition between these processes or how they should be combined. Moreover, the full extent to which nuclear effects impact this region is a topic that has only recently been appreciated. Therefore, in this section, we focus on what is currently known, both experimentally and theoretically, about each of the exclusive final-state processes that participate in this region.

To start, Fig. 9 summarizes the existing measurements of CC neutrino and antineutrino cross sections across this intermediate energy range

$$\nu_\mu N \to \mu^- X, \tag{54}$$

$$\bar{\nu}_\mu N \to \mu^+ X. \tag{55}$$

These results have been accumulated over many decades using a variety of neutrino targets and detector technologies. We immediately notice three things from this figure. First, the total cross sections approaches a linear dependence on neutrino energy. This scaling behavior is a prediction of the quark parton model (Feynman, 1969), a topic we return to later, and is expected if pointlike scattering off quarks dominates the scattering mechanism, for example, in the case of deep inelastic scattering. Such assumptions break down, of course, at lower neutrino energies (i.e., lower momentum transfers). Second, the neutrino cross sections at the lower energy end of this region are not typically as well measured as their high-energy counterparts. This is generally due to the lack of high statistics data historically available in this energy range and the challenges that arise when trying to describe all of the various underlying physical processes that can participate in this region. Third, antineutrino cross sections are typically less well measured than their neutrino counterparts. This is generally due to lower statistics and larger background contamination present in that case.

Most of our knowledge of neutrino cross sections in this intermediate energy range comes from early experiments that collected relatively small data samples (tens-to-a-few-thousand events). These measurements were conducted in

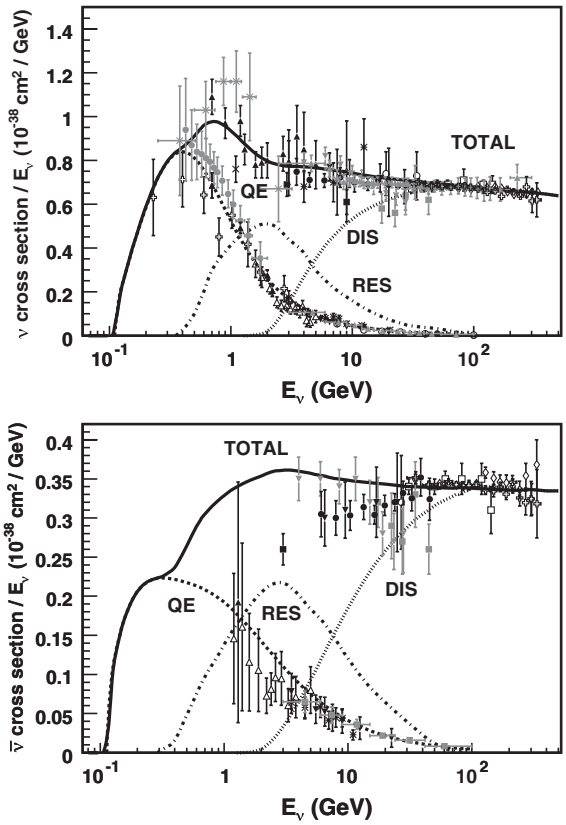

FIG. 9. Total neutrino and antineutrino per nucleon CC cross sections (for an isoscalar target) divided by neutrino energy and plotted as a function of energy. Data are the same as in Figs. 28, 11, and 12, with the inclusion of additional lower energy CC inclusive data from ▲ (Baker *et al.*, 1982), ∗ (Baranov *et al.*, 1979), ■ (Ciampolillo *et al.*, 1979), and ⋆ (Nakajima *et al.*, 2011). Also shown are the various contributing processes that will be investigated in the remaining sections of this review. These contributions include quasielastic scattering (dashed), resonance production (dot-dashed), and deep inelastic scattering (dotted). Example predictions for each are provided by the NUANCE generator (Casper, 2002). Note that the quasielastic scattering data and predictions have been averaged over neutron and proton targets and hence have been divided by a factor of 2 for the purposes of this plot.

the 1970s and 1980s using either bubble chamber or spark chamber detectors and represent a large fraction of the data presented in the summary plots we show. Over the years, interest in this energy region waned as efforts migrated to higher energies to yield larger event samples and the focus centered on measurement of electroweak parameters ($\sin^2\theta_W$) and structure functions in the deep inelastic scattering region. With the discovery of neutrino oscillations and the advent of higher intensity neutrino beams, however, this situation has been rapidly changing. The processes discussed here are important because they form some of the dominant signal and background channels for experiments searching for neutrino oscillations. This is especially true for experiments that use atmospheric or accelerator-based sources of neutrinos. With a view to better understanding these neutrino cross sections, new experiments such as Argon Neutrino Test (ArgoNeuT), KEK to Kamioka (K2K), Mini Booster Neutrino Experiment (MiniBooNE), Main INjector ExpeRiment: nu-A (MINERνA), Main Injector Neutrino Oscillation Search (MINOS), Neutrino

Oscillation MAgnetic Detector (NOMAD), SciBar Booster Neutrino Experiment (SciBooNE), and Tokai to Kamioka experiment (T2K) have started to study this intermediate energy region in greater detail. New theoretical approaches have also recently emerged.

We start by describing the key processes which can contribute to the total cross section at these intermediate neutrino energies. Here we focus on several key processes: quasielastic, NC elastic scattering, resonant single pion production, coherent pion production, multipion production, and kaon production before turning our discussion to deep inelastic scattering in the following section on high-energy neutrino interactions. For comparison, we also include predictions from the NUANCE event generator (Casper, 2002), chosen as a representative of the type of models used in modern neutrino experiments to describe this energy region. The bulk of our discussions center around measurements of ν_μ-nucleon scattering. Many of these arguments also carry over to ν_τ scattering, except for one key difference; the energy threshold for the reaction. Unlike for the muon case, the charged current ν_τ interaction cross section is severely altered because of the large τ lepton mass. Figure 10 reflects some of the large differences in the cross section that come about due to this threshold energy.

A. Quasielastic scattering

For neutrino energies less than ~2 GeV, neutrino-hadron interactions are predominantly quasielastic (QE), hence they provide a large source of signal events in many neutrino oscillation experiments operating in this energy range. In a QE interaction, the neutrino scatters off an entire nucleon rather than its constituent partons. In a charged current neutrino QE interaction, the target neutron is converted to a proton. In the case of an antineutrino scattering, the target proton is converted into a neutron,

$$\nu_\mu n \rightarrow \mu^- p, \qquad \bar{\nu}_\mu p \rightarrow \mu^+ n. \tag{56}$$

Such simple interactions were extensively studied in the 1970s–1990s primarily using deuterium-filled bubbble chambers. The main interest at the time was in testing the vector-axial vector (V-A) nature of the weak interaction and in measuring the axial-vector form factor of the nucleon, topics that were considered particularly important in providing an anchor for the study of NC interactions (Sec. V.B). As examples, Singh and Oset (1992) and Lyubushkin *et al.* (2009) provided valuable summaries of some of these early QE investigations.

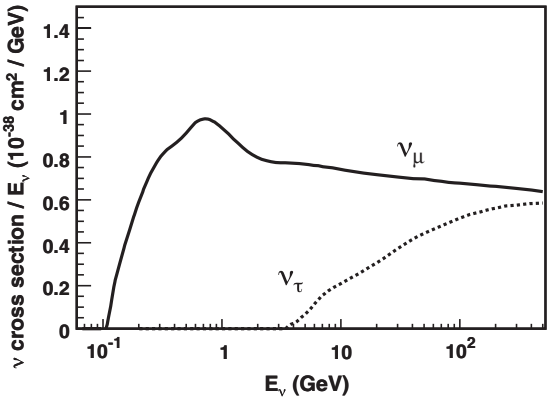

FIG. 10. Plot comparing the total charged current ν_μ (solid) and ν_τ (dashed) per nucleon cross sections divided by neutrino energy and plotted as a function of neutrino energy.

In predicting the QE scattering cross section, early experiments relied heavily on the formalism first written down in Llewellyn-Smith (1972). In the case of QE scattering off free nucleons, the QE differential cross section can be expressed as

$$\frac{d\sigma}{dQ^2} = \frac{G_F^2 M^2}{8\pi E_\nu^2}\left[A \pm \frac{s-u}{M^2}B + \frac{(s-u)^2}{M^4}C\right], \tag{57}$$

where $(-)+$ refers to (anti)neutrino scattering, G_F is the Fermi coupling constant, Q^2 is the squared four-momentum transfer ($Q^2 = -q^2 > 0$), M is the nucleon mass, m is the lepton mass, E_ν is the incident neutrino energy, and $s - u = 4ME_\nu - Q^2 - m^2$. The factors A, B, and C are functions of the familiar vector (F_1 and F_2), axial-vector (F_A), and pseudoscalar (F_P) form factors of the nucleon

$$A = \frac{m^2 + Q^2}{M^2}\left[(1+\eta)F_A^2 - (1-\eta)F_1^2 + \eta(1-\eta)F_2^2 + 4\eta F_1 F_2 - \frac{m^2}{4M^2}\left((F_1+F_2)^2 + (F_A+2F_P)^2 - \left(\frac{Q^2}{M^2}+4\right)F_P^2\right)\right], \tag{58}$$

$$B = \frac{Q^2}{M^2}F_A(F_1+F_2), \tag{59}$$

$$C = \frac{1}{4}(F_A^2 + F_1^2 + \eta F_2^2), \tag{60}$$

where $\eta = Q^2/4M^2$. Much of these equations should be familiar from Sec. IV. Historically, this formalism was used to analyze neutrino QE scattering data on deuterium, subject to minor modifications for nuclear effects. In this way, experiments studying neutrino QE scattering could in principle measure the vector, axial-vector, and pseudoscalar form factors given that the weak hadronic current contains all three of these components. In practice, the pseudoscalar contribution was typically neglected in the analysis of ν_μ QE scattering as it enters the cross section multiplied by m^2/M^2. Using CVC, the vector form factors could be obtained from electron scattering, thus leaving the neutrino experiments to measure the axial-vector form factor of the nucleon. For the axial-vector form factor, it was (and still is) customary to assume a dipole form

$$F_A(Q^2) = \frac{g_A}{(1 + Q^2/M_A^2)^2}, \tag{61}$$

which depends on two empirical parameters: the value of the axial-vector form factor at $Q^2 = 0$, $g_A = F_A(0) = 1.2694 \pm 0.0028$ (Nakamura, K. *et al.*, 2010), and an "axial mass" M_A. With the vector form factors under control from electron scattering and g_A determined with high precision from nuclear beta decay, measurement of the axial-vector form factor (and hence M_A) became the focus of the earliest

measurements of neutrino QE scattering. Values of M_A ranging from 0.65 to 1.09 GeV were obtained in the period from the late 1960s to early 1990s resulting from fits to both the total rate of observed events and the shape of their measured Q^2 dependence [for a recent review, see Lyubushkin *et al.* (2009)]. In addition to providing the first measurements of M_A and the QE cross section, many of these experiments also performed checks of CVC, fit for the presence of second-class currents, and experimented with different forms for the axial-vector form factor. By the end of this period, the neutrino QE cross section could be accurately and consistently described by V-A theory assuming a dipole axial-vector form factor with $M_A = 1.026 \pm 0.021$ GeV (Bernard *et al.*, 2002). These conclusions were largely driven by experimental measurements on deuterium, but less-precise data on other heavier targets also contributed. More recently, some attention has been given to reanalyzing these same data using modern vector form factors as input. The use of updated vector form factors slightly shifts the best-fit axial mass values obtained from these data; however, the conclusion is still that $M_A \sim 1.0$ GeV.[9]

Modern day neutrino experiments no longer include deuterium but use complex nuclei as their neutrino targets. As a result, nuclear effects become much more important and produce sizable modifications to the QE differential cross section from Eq. (57). With QE events forming the largest contribution to signal samples in many neutrino oscillation experiments, there has been renewed interest in the measurement and modeling of QE scattering on nuclear targets. In such situations, the nucleus is typically described in terms of individual quasifree nucleons that participate in the scattering process (the so-called "impulse approximation" approach) (Frullani and Mougey, 1984). Most neutrino experiments use a relativistic Fermi-gas model (Smith and Moniz, 1972) when simulating their QE scattering events, although many other independent particle approaches have been developed in recent years that incorporate more sophisticated treatments. These include spectral function (Nakamura and Seki, 2002; Benhar *et al.*, 2005; Ankowski and Sobczyk, 2006; Benhar and Meloni, 2007; Juszczak, Sobczyk, and Zmuda, 2010), superscaling (Amaro *et al.*, 2005), RPA (Nieves, Amaro, and Valverde, 2004; Nieves, Valverde, and Vicente Vacas, 2006; Leitner and Mosel, 2009; Sajjad Athar, Chauhan, and Singh, 2010), and plane-wave impulse approximation-based calculations (Butkevich, 2010). In concert, the added nuclear effects from these improved calculations tend to reduce the predicted neutrino QE cross section beyond the Fermi-gas model-based predictions. These reductions are typically on the order of 10%–20% (Alvarez-Ruso, 2010).

Using Fermi-gas model-based simulations and analyzing higher statistics QE data on a variety of nuclear targets, new experiments have begun to repeat the axial-vector measurements that fueled much of the early investigations of QE scattering. Axial mass values ranging from 1.05 to 1.35 GeV have been recently obtained (Gran *et al.*, 2006; Espinal and Sanchez, 2007; Aguilar-Arevalo, 2008, 2010a; Dorman, 2009; Lyubushkin *et al.*, 2009), with most of the experiments systematically measuring higher M_A values than those found in the deuterium fits. This has recently sparked some debate, especially given that higher M_A values naturally imply higher cross sections and hence larger event yields for neutrino experiments.[10] We return to this point later.

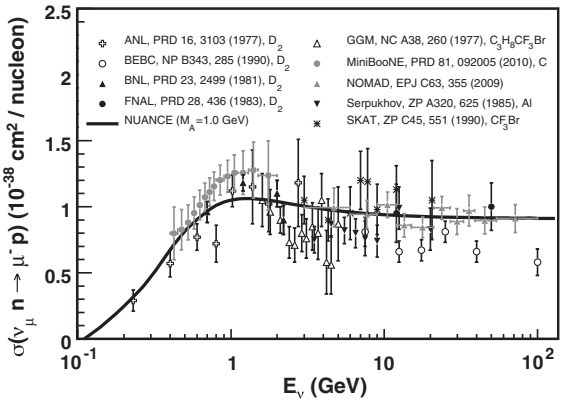

FIG. 11. Existing measurements of the ν_μ quasielastic scattering cross section, $\nu_\mu n \to \mu^- p$, as a function of neutrino energy on a variety of nuclear targets. The free nucleon scattering prediction assuming $M_A = 1.0$ GeV is shown for comparison. From Casper (2002). This prediction is altered by nuclear effects in the case of neutrino-nucleus scattering. Care should be taken when interpreting measurements on targets heavier than hydrogen and deuterium.

Neutrino experiments have also begun to remeasure the absolute QE scattering cross section making use of more reliable incoming neutrino fluxes made available in modern experimental setups. Figure 11 summarizes the existing measurements of ν_μ QE scattering cross sections as a function of neutrino energy from both historical and recent measurements. As expected, we observe a linearly rising cross section that is damped by the form factors at higher neutrino energies. What is not expected is the disparity observed between recent measurements. High statistics measurements of the QE scattering cross section by the MiniBooNE (Aguilar-Arevalo *et al.*, 2010a) and NOMAD (Lyubushkin *et al.*, 2009) experiments, both on carbon, appear to differ in normalization by about 30%. The low-energy MiniBooNE results are higher than expected from the Fermi-gas model (Smith and Moniz, 1972) and more sophisticated impulse approximation calculations (Frullani and Mougey, 1984; Maieron *et al.*, 2003; Nieves, Amaro, and Valverde, 2004; Leitner *et al.*, 2006; Martinez *et al.*, 2006; Nieves *et al.*, 2006; Benhar and Meloni, 2007; Ankowski and Sobczyk, 2008; Butkevich, 2009; Leitner *et al.*, 2009; Athar *et al.*, 2010) assuming an axial mass, $M_A = 1.0$ GeV, from deuterium-based measurements as input.

How can it be that new, high statistics measurements of this simple process are not coming out as expected? The fact that modern measurements of QE scattering have seemingly

[9]A value of $M_A = 1.014 \pm 0.014$ GeV was obtained from a recent global fit to the deuterium data in Bodek *et al.* (2007), while a consistent value of $M_A = 0.999 \pm 0.011$ GeV was obtained in Kuzmin *et al.* (2008) from a fit that additionally includes some of the early heavy target data.

[10]Note that modern determinations of M_A have largely been obtained from fits to the shape of the observed Q^2 distribution of QE events and not their normalization.

raised more questions than they have answered has been recently noted (Gallagher, Garvey, and Zeller, 2011; Sobczyk, 2011). It is currently believed that nuclear effects beyond the impulse approximation approach are responsible for the discrepancies noted in the experimental data. In particular, it is now being recognized that nucleon-nucleon correlations and two-body exchange currents must be included in order to provide a more accurate description of neutrino-nucleus QE scattering. These effects yield significantly enhanced cross sections (larger than the free scattering case) which, in some cases, appear to better match the experimental data (Aguilar-Arevalo *et al.*, 2010a) at low neutrino energies (Amaro *et al.*, 2011b; Barbaro *et al.*, 2011; Bodek and Budd, 2011; Giusti and Meucci, 2011; Martini, Ericson, and Chanfray, 2011; Nieves, Ruiz-Simo, and Vicente-Vacas, 2011; Sobczyk, 2012). They also produce final states that include multiple nucleons, especially when it comes to scattering off of nuclei. The final state need not just include a single nucleon, hence why one needs to be careful in defining a "quasielastic" event especially when it comes to scattering off nuclei.

In hindsight, the increased neutrino QE cross sections and harder Q^2 distributions (high M_A) observed in much of the experimental data should probably have not come as a surprise. Such effects were also measured in transverse electron-nucleus quasielastic scattering many years prior (Carlson, 2002). The possible connection between electron and neutrino QE scattering observations has only been recently appreciated. Today, the role that additional nuclear effects may play in neutrino-nucleus QE scattering remains the subject of much theoretical and experimental scrutiny. Improved theoretical calculations and experimental measurements are already underway. As an example, the first double differential cross section distributions for ν_μ QE scattering were recently reported by the MiniBooNE experiment (Aguilar-Arevalo *et al.*, 2010a). It is generally recognized that such model-independent measurements are more useful than comparing M_A values. Such differential cross section data are also providing an important new testing ground for improved nuclear model calculations (Amaro *et al.*, 2011a; Giusti and Meucci, 2011; Martini, Ericson, and Chanfray, 2011; Nieves, Simo, and Vacas, 2012; Sobczyk, 2012). Moving forward, additional differential cross section measurements, detailed measurements of nucleon emission, and studies of antineutrino QE scattering are needed before a solid description can be secured.

So far we have focused on neutrino QE scattering. Figure 12 shows the status of measurements of the corresponding antineutrino QE scattering cross section. Recent results from the NOMAD experiment have expanded the reach out to higher neutrino energies, however, there are currently no existing measurements of the antineutrino QE scattering cross section below 1 GeV. Given that the newly appreciated effects of nucleon-nucleon correlations are expected to be different for neutrinos and antineutrinos, a high priority has been recently given to the study of antineutrino QE scattering at these energies. A precise handle on neutrino and antineutrino QE interaction cross sections will be particularly important in the quest for the detection of *CP* violation in the leptonic sector going into the future.

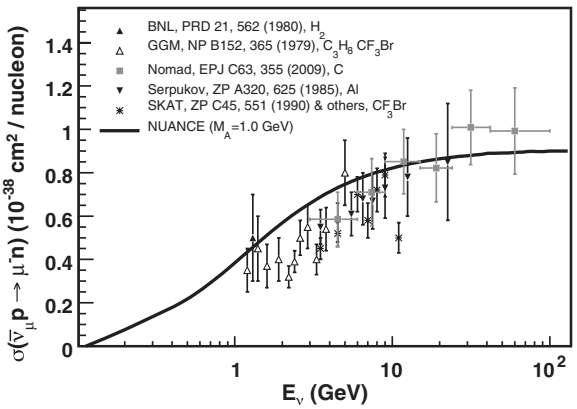

FIG. 12. Same as Fig. 11 except for antineutrino QE scattering, $\bar{\nu}_\mu p \to \mu^+ n$.

Up to now, we discussed the case where nucleons can be ejected in the elastic scattering of neutrinos from a given target. The final state is traditionally a single nucleon, but can also include multiple nucleons, especially in the case of neutrino-nucleus scattering. For antineutrino QE scattering, it should be noted that the Cabibbo-suppressed production of hyperons is also possible, for example,

$$\bar{\nu}_\mu p \to \mu^+ \Lambda^0, \tag{62}$$

$$\bar{\nu}_\mu n \to \mu^+ \Sigma^-, \tag{63}$$

$$\bar{\nu}_\mu p \to \mu^+ \Sigma^0. \tag{64}$$

Cross sections for QE hyperon production by neutrinos were calculated very early on (Cabibbo and Chilton, 1965; Llewellyn-Smith, 1972) and verified in low statistics measurements by a variety of bubble chamber experiments (Eichten *et al.*, 1972; Erriques *et al.*, 1977; Ammosov *et al.*, 1987; Brunner *et al.*, 1990). New calculations have also recently surfaced (Singh and Vacas, 2006; Mintz and Wen, 2007; Kuzmin and Naumov, 2009). We will say more about strange particle production later when we discuss kaon production (Sec. V.F).

Combined, all experimental measurements of QE scattering cross sections have been conducted using beams of muon neutrinos and antineutrinos. No direct measurements of ν_e or $\bar{\nu}_e$ QE scattering cross sections have yet been performed at these energies.

B. NC elastic scattering

Neutrinos can also elastically scatter from nucleons via neutral-current (NC) interactions

$$\nu p \to \nu p, \qquad \bar{\nu} p \to \bar{\nu} p, \tag{65}$$

$$\nu n \to \nu n, \qquad \bar{\nu} p \to \bar{\nu} p. \tag{66}$$

Equations (57)–(60) still apply in describing NC elastic scattering from free nucleons with the exception that, in this case, the form factors include additional coupling factors and a contribution from strange quarks

$$F_1(Q^2) = \left(\frac{1}{2} - \sin^2\theta_W\right)\left[\frac{\tau_3[1+\eta(1+\mu_p-\mu_n)]}{(1+\eta)(1+Q^2/M_V^2)^2}\right] - \sin^2\theta_W\left[\frac{1+\eta(1+\mu_p+\mu_n)}{(1+\eta)(1+Q^2/M_V^2)^2}\right] - \frac{F_1^s(Q^2)}{2}F_2(Q^2)$$
$$= \left(\frac{1}{2} - \sin^2\theta_W\right)\frac{\tau_3(\mu_p-\mu_n)}{(1+\eta)(1+Q^2/M_V^2)^2} - \sin^2\theta_W\frac{\mu_p+\mu_n}{(1+\eta)(1+Q^2/M_V^2)^2} - \frac{F_2^s(Q^2)}{2}F_A(Q^2)$$
$$= \frac{g_A\tau_3}{2(1+Q^2/M_A^2)^2} - \frac{F_A^s(Q^2)}{2}.$$

Here $\tau_3 = +1(-1)$ for proton (neutron) scattering, $\sin^2\theta_W$ is the weak mixing angle, and $F_{1,2}^s(Q^2)$ are the strange vector form factors, assuming a dipole form. The strange axial-vector form factor is commonly denoted as

$$F_A^s(Q^2) = \frac{\Delta s}{(1+Q^2/M_A^2)^2}, \tag{67}$$

where Δs is the strange quark contribution to the nucleon spin and M_A is the same axial mass appearing in the expression for CC QE scattering [Eq. (61)].

Over the years, experiments typically measured NC elastic cross section ratios with respect to QE scattering to help minimize systematics. Table VIII lists a collection of historical measurements of the NC elastic and QE cross section ratio $\nu_\mu p \to \nu_\mu p/\nu_\mu n \to \mu^- p$. These ratios have been integrated over the kinematic range of the experiment. More recently, the MiniBooNE experiment measured the NC elastic and QE ratio on carbon in bins of Q^2 (Aguilar-Arevalo *et al.*, 2010b).

Experiments such as BNL E734 and MiniBooNE have additionally reported measurements of flux-averaged absolute differential cross sections $d\sigma/dQ^2$ for NC elastic scattering on carbon. From these distributions, measurements of parameters appearing in the cross section for this process, M_A and Δs, can be directly obtained. Table IX summarizes those findings. As with QE scattering, a new appreciation for the presence of nuclear effects in such neutral-current interactions has also recently arisen with many new calculations of this cross section on nuclear targets (Amaro *et al.*, 2006; Benhar and Veneziano, 2011; Butkevich and Perevalov, 2011; Meucci, Giusti, and Pacati, 2011). Just as in the charged current case, nuclear corrections can be on the order of 20% or more.

TABLE VIII. Measurements of the ratio $\nu_\mu p \to \nu_\mu p/\nu_\mu n \to \mu^- p$ taken from BNL E734 (Faissner *et al.*, 1980; Coteus *et al.*, 1981; Ahrens *et al.*, 1988), BNL E613 (Entenberg *et al.*, 1979), and Gargamelle (Pohl *et al.*, 1978). Also indicated is the Q^2 interval over which the ratio was measured.

Experiment	Target	Ratio	Q^2(GeV^2)
BNL E734	CH_2	0.153 ± 0.018	0.5–1.0
BNL CIB	Al	0.11 ± 0.03	0.3–0.9
Aachen	Al	0.10 ± 0.03	0.2–1.0
BNL E613	CH_2	0.11 ± 0.02	0.4–0.9
Gargamelle	CF_3Br	0.12 ± 0.06	0.3–1.0

C. Resonant single pion production

Now that we discussed quasielastic and elastic scattering mechanisms, we consider another interaction possibility: this time an inelastic interaction. Given enough energy, neutrinos can excite the struck nucleon to an excited state. In this case, the neutrino interaction produces a baryon resonance (N^*). The baryon resonance quickly decays, most often to a nucleon and single pion final state

$$\nu_\mu N \to \mu^- N^*, \tag{68}$$

$$N^* \to \pi N', \tag{69}$$

where N, $N' = n$, p. Other higher multiplicity decay modes are also possible and will be discussed later.

The most common means of single pion production in intermediate energy neutrino scattering arises through this mechanism. In scattering off of free nucleons, there are seven possible resonant single pion reaction channels (seven each for neutrino and antineutrino scattering), three charged current:

$$\nu_\mu p \to \mu^- p\pi^+, \qquad \bar\nu_\mu p \to \mu^+ p\pi^-, \tag{70}$$

$$\nu_\mu n \to \mu^- p\pi^0, \qquad \bar\nu_\mu p \to \mu^+ n\pi^0, \tag{71}$$

$$\nu_\mu n \to \mu^- n\pi^+, \qquad \bar\nu_\mu n \to \mu^+ n\pi^- \tag{72}$$

and four neutral current:

$$\nu_\mu p \to \nu_\mu p\pi^0, \qquad \bar\nu_\mu p \to \bar\nu_\mu p\pi^0, \tag{73}$$

$$\nu_\mu p \to \nu_\mu n\pi^+, \qquad \bar\nu_\mu p \to \bar\nu_\mu p\pi^0, \tag{74}$$

$$\nu_\mu n \to \nu_\mu n\pi^0, \qquad \bar\nu_\mu n \to \bar\nu_\mu n\pi^0, \tag{75}$$

$$\nu_\mu n \to \nu_\mu p\pi^-, \qquad \bar\nu_\mu n \to \bar\nu_\mu p\pi^-. \tag{76}$$

TABLE IX. Measurements of the axial mass and strange quark content to the nucleon spin from neutrino NC elastic scattering data from BNL E734 (Ahrens *et al.*, 1988) and MiniBooNE (Aguilar-Arevalo *et al.*, 2010b). BNL-E734 reported a measurement of $\eta = 0.12 \pm 0.07$ which implies $\Delta s = -g_A\eta = -0.15 \pm 0.09$. Note that updated fits to the BNL-E734 data were also later performed by several groups (Garvey *et al.*, 1993; Alberico *et al.*, 1999).

Experiment	M_A (GeV)	Δs
BNL E734	1.06 ± 0.05	-0.15 ± 0.09
MiniBooNE	1.39 ± 0.11	0.08 ± 0.26

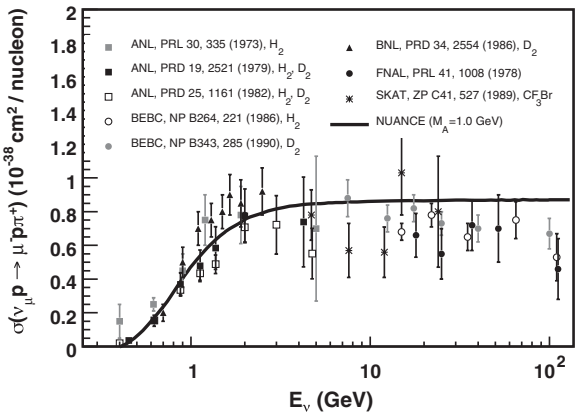

FIG. 13. Existing measurements of the cross section for the CC process, $\nu_\mu p \to \mu^- p\pi^+$, as a function of neutrino energy. Also shown is the prediction from Casper (2002) assuming $M_A = 1.1$ GeV. Modern measurements (Table XII) exist but cannot be directly compared with this historical data.

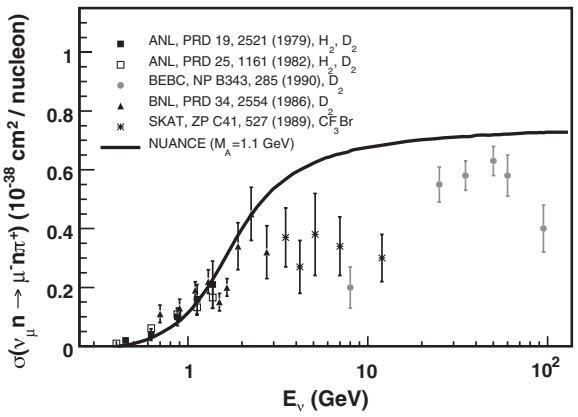

FIG. 15. Existing measurements of the cross section for the CC process, $\nu_\mu n \to \mu^- n\pi^+$, as a function of neutrino energy. Also shown is the prediction from Casper (2002) assuming $M_A = 1.1$ GeV. Modern measurements (Table XII) exist but cannot be directly compared with this historical data.

To describe such resonance production processes, neutrino experiments most commonly use calculations from the Rein and Sehgal model (Feynman, Kislinger, and Ravndal, 1971; Rein and Sehgal, 1981; Rein, 1987) with the additional inclusion of lepton mass terms. This model gives predictions for both CC and NC resonance production and a prescription for handling interferences between overlapping resonances. The cross sections for the production of numerous different resonances are typically evaluated, though at the lowest energies the process is dominated by production of the $\Delta(1232)$.

Figures 13–15 summarize the historical measurements of CC neutrino single pion production cross sections as a function of neutrino energy. Table X lists corresponding measurements in antineutrino scattering. Many of these measurements were conducted on light (hydrogen or deuterium) targets and served as a crucial verification of cross section predictions at the time. Measurements of the axial mass were often repeated using these samples. Experiments also performed tests of resonance production models by measuring invariant mass and angular distributions. However, many of these tests were often limited in statistics.

Compared to their charged current counterparts, measurements of neutral-current single pion cross sections tend to be much more sparse. Most of these data exist in the form of NC and CC cross section ratios (Table XI); however, a limited number of absolute cross section measurements were also performed over the years (Figs. 16–21).

Today, improved measurements and predictions of neutrino-induced single pion production have become increasingly important because of the role such processes play in the interpretation of neutrino oscillation data (Walter, 2007). In this case, both NC and CC processes contribute. NC π^0 production is often the largest ν_μ-induced background in experiments searching for $\nu_\mu \to \nu_e$ oscillations. In addition, CC π production processes can present a non-negligible complication in the determination of neutrino energy in experiments measuring parameters associated with ν_μ and $\bar{\nu}_\mu$ disappearance. Since such neutrino oscillation experiments use heavy materials as their neutrino

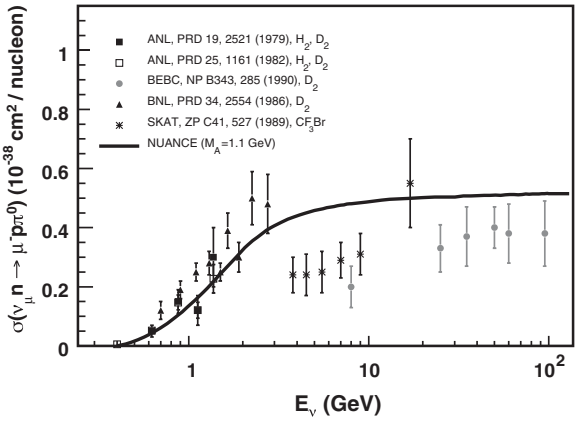

FIG. 14. Existing measurements of the cross section for the CC process, $\nu_\mu n \to \mu^- p\pi^0$, as a function of neutrino energy. Also shown is the prediction from Casper (2002) assuming $M_A = 1.1$ GeV. Modern measurements (Table XII) exist but cannot be directly compared with this historical data.

TABLE X. Measurements of antineutrino CC single pion production from BEBC (Allasia *et al.*, 1983; Allen *et al.*, 1986; Jones *et al.*, 1989), FNAL (Barish *et al.*, 1980), Gargamelle (Bolognese *et al.*, 1979), and Sepukhov heavy liquid chamber (SKAT) (Grabosch *et al.*, 1989).

Channel	Experiment	Target	No. Events
$\bar{\nu}_\mu p \to \mu^+ p\pi^-$:			
	BEBC	D_2	300
	BEBC	H_2	609
	GGM	CF_3Br	282
	FNAL	H_2	175
	SKAT	CF_3Br	145
$\bar{\nu}_\mu p \to \mu^+ n\pi^0$:			
	GGM	CF_3Br	179
	SKAT	CF_3Br	83
$\bar{\nu}_\mu n \to \mu^+ n\pi^-$:			
	BEBC	D_2	545
	GGM	CF_3Br	266
	SKAT	CF_3Br	178

TABLE XI. Measurements of NC and CC single pion cross section ratios ($N = n, p$). The Gargamelle data have been corrected to a free nucleon ratio (Krenz *et al.*, 1978a).

Experiment	Target	NC/CC ratio	Value	Reference
ANL	H_2	$\sigma(\nu_\mu p \to \nu_\mu p\pi^0)/\sigma(\nu_\mu p \to \mu^- p\pi^+)$	0.51 ± 0.25	(Barish *et al.*, 1974)
ANL	H_2	$\sigma(\nu_\mu p \to \nu_\mu p\pi^0)/\sigma(\nu_\mu p \to \mu^- p\pi^+)$	0.09 ± 0.05[a]	(Derrick *et al.*, 1981)
ANL	H_2	$\sigma(\nu_\mu p \to \nu_\mu n\pi^+)/\sigma(\nu_\mu p \to \mu^- p\pi^+)$	0.17 ± 0.08	(Barish *et al.*, 1974)
ANL	H_2	$\sigma(\nu_\mu p \to \nu_\mu n\pi^+)/\sigma(\nu_\mu p \to \mu^- p\pi^+)$	0.12 ± 0.04	(Derrick *et al.*, 1981)
ANL	D_2	$\sigma(\nu_\mu n \to \nu_\mu p\pi^-)/\sigma(\nu_\mu n \to \mu^- n\pi^+)$	0.38 ± 0.11	(Fogli and Nardulli, 1980)
GGM	$C_3H_8CF_3Br$	$\sigma(\nu_\mu N \to \nu_\mu N\pi^0)/2\sigma(\nu_\mu n \to \mu^- p\pi^0)$	0.45 ± 0.08	(Krenz *et al.*, 1978a)
CERN PS	Al	$\sigma(\nu_\mu N \to \nu_\mu N\pi^0)/2\sigma(\nu_\mu n \to \mu^- p\pi^0)$	0.40 ± 0.06	(Fogli and Nardulli, 1980)
BNL	Al	$\sigma(\nu_\mu N \to \nu_\mu N\pi^0)/2\sigma(\nu_\mu n \to \mu^- p\pi^0)$	0.17 ± 0.04	(Lee *et al.*, 1977)
BNL	Al	$\sigma(\nu_\mu N \to \nu_\mu N\pi^0)/2\sigma(\nu_\mu n \to \mu^- p\pi^0)$	0.25 ± 0.09[b]	(Nienaber, 1988)
ANL	D_2	$\sigma(\nu_\mu n \to \nu_\mu p\pi^-)/\sigma(\nu_\mu p \to \mu^- p\pi^+)$	0.11 ± 0.022	(Derrick *et al.*, 1981)

[a]In their later paper (Derrick *et al.*, 1981), Derrick *et al.* remark that while this result is 1.6σ smaller than their previous result (Barish *et al.*, 1974), the neutron background was later better understood.
[b]The BNL NC π^0 data (Lee *et al.*, 1977) were later reanalyzed after properly taking into account multipion backgrounds and found to have a larger fractional cross section (Nienaber, 1988).

targets, measuring and modeling nuclear effects in pion production processes has become paramount. Such effects are sizable, not well known, and ultimately complicate the description of neutrino interactions. Once created in the initial neutrino interaction, the pion must escape the nucleus before it can be detected. Along its journey, the pion can rescatter, get absorbed, or charge exchange thus altering its identity and kinematics. Improved calculations of such "final-state interactions" have been undertaken by a number of groups (Paschos *et al.*, 2007; Antonello *et al.*, 2009; Dytman, 2009; Leitner and Mosel, 2009; Leitner and Mosel, 2010a, 2010b). The impact of in-medium effects on the Δ width and the possibility for intranuclear Δ reinteractions ($\Delta N \to NN$) also play a role. The combined result are sizable distortions to the interaction cross section and kinematics of final-state hadrons that are produced in a nuclear environment.

While new calculations of pion production have proliferated, new approaches to the experimental measurement of these processes have also surfaced in recent years. Modern experiments have realized the importance of final-state effects, often directly reporting the distributions of final-state particles they observe. Such "observable" cross sections are more useful in that they measure the combined effects of nuclear processes and are much less model dependent. Table XII lists the collection of some of these most recent pion production cross section reportings. Measurements have been produced in the form of both ratios and absolute cross sections, all on carbon-based targets. Similar measurements on additional nuclear targets are clearly needed to help round out our understanding of nuclear effects in pion production interactions.

Before we move on, it should be noted that many of the same baryon resonances that decay to single pion final states can also decay to photons (e.g., $\Delta \to N\gamma$ and $N^* \to N\gamma$). Such radiative decay processes have small branching fractions ($<1\%$) yet, like NC π^0 production, they still pose non-negligible sources of background to $\nu_\mu \to \nu_e$ oscillation searches. There have been no direct experimental measurements of neutrino-induced resonance radiative decay to date; however, studies of photon production in deep inelastic neutrino interactions have been performed at higher energies

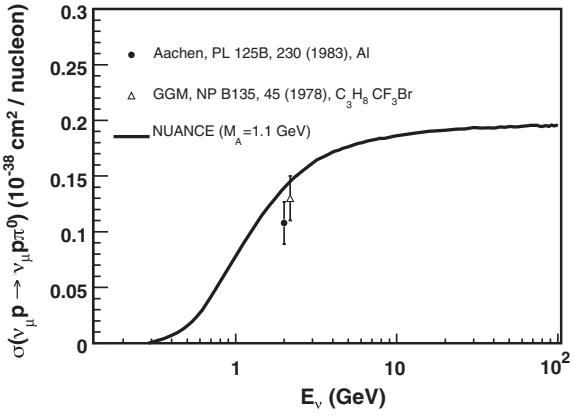

FIG. 16. Existing measurements of the cross section for the NC process, $\nu_\mu p \to \nu_\mu p\pi^0$, as a function of neutrino energy. Also shown is the prediction from Casper (2002) assuming $M_A = 1.1$ GeV. The Gargamelle measurement comes from a more recent reanalysis of these data. Modern measurements (Table XII) exist but cannot be directly compared with this historical data. From Hawker, 2002.

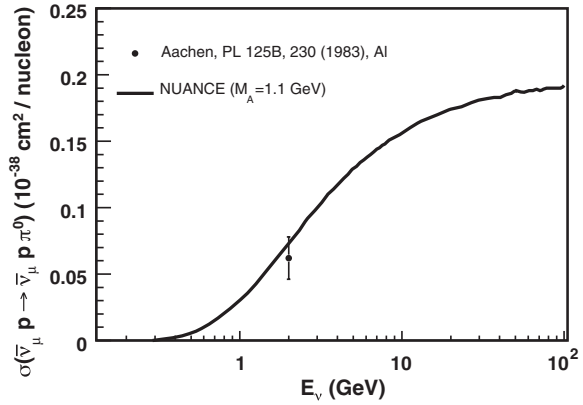

FIG. 17. Existing measurements of the cross section for the NC process, $\bar{\nu}_\mu p \to \bar{\nu}_\mu p\pi^0$, as a function of neutrino energy. Also shown is the prediction from Casper (2002) assuming $M_A = 1.1$ GeV. Modern measurements (Table XII) exist but cannot be directly compared with this historical data.

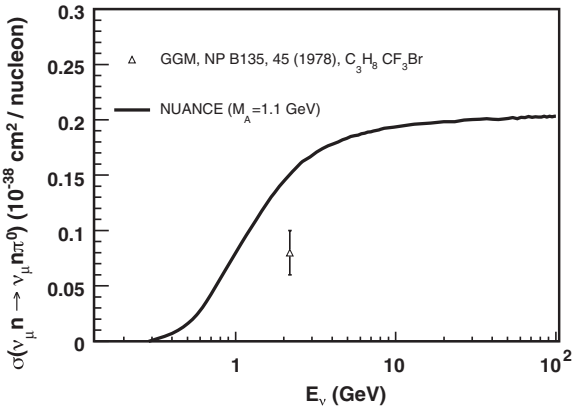

FIG. 18. Existing measurements of the cross section for the NC process, $\nu_\mu n \to \nu_\mu n \pi^0$, as a function of neutrino energy. Also shown is the prediction from Casper (2002) assuming $M_A = 1.1$ GeV. The Gargamelle measurement comes from a more recent reanalysis of these data. Modern measurements (Table XII) exist but cannot be directly compared with this historical data. From Hawker, 2002.

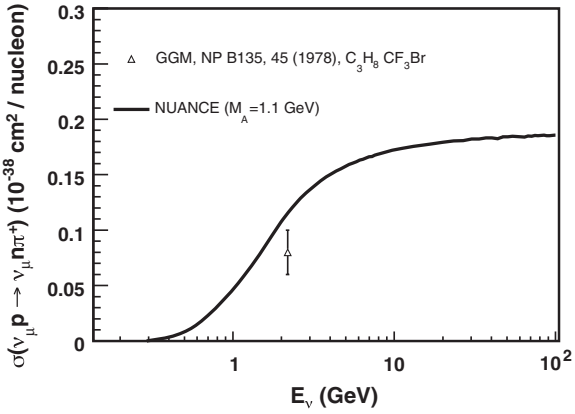

FIG. 19. Existing measurements of the cross section for the NC process, $\nu_\mu p \to \nu_\mu n \pi^+$, as a function of neutrino energy. Also shown is the prediction from Casper (2002) assuming $M_A = 1.1$ GeV.

(Ballagh *et al.*, 1983). New experimental investigations are clearly needed. As an example, such a photon search was recently reported by the NOMAD collaboration (Kullenberg *et al.*, 2012). New calculations have already begun to explore

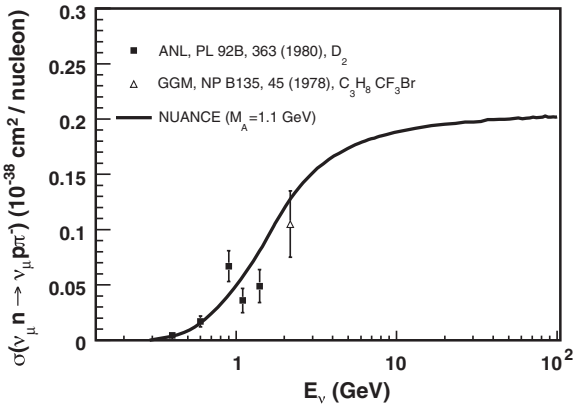

FIG. 20. Existing measurements of the cross section for the NC process, $\nu_\mu n \to \nu_\mu p \pi^-$, as a function of neutrino energy. Also shown is the prediction from Casper (2002) assuming $M_A = 1.1$ GeV.

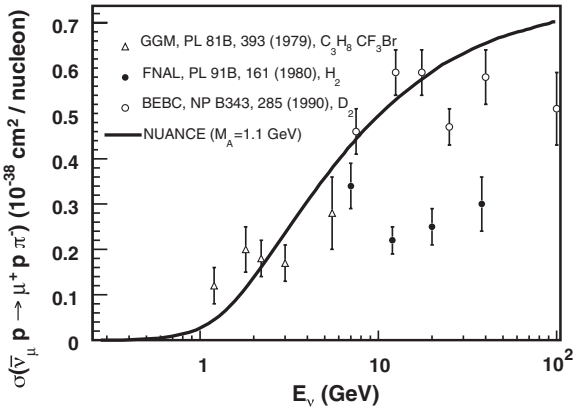

FIG. 21. Existing measurements of the cross section for the NC process, $\bar{\nu}_\mu n \to \bar{\nu}_\mu p \pi^-$, as a function of neutrino energy. Also shown is the prediction from Casper (2002) assuming $M_A = 1.1$ GeV.

the possibility for standard model–based sources of photon production in neutrino scattering (Harvey, Hill, and Hill, 2007; Efrosinin, Kudenko, and Khotjantsev, 2009; Jenkins and Goldman, 2009; Hill, 2011; Ankowski *et al.*, 2012).

In addition to photon decay, baryon resonances can also decay in a variety of other modes. This includes multipion and kaon final states which we return to later in this section.

TABLE XII. Current measurements of single pion production by neutrinos. In the last column, σ refers to a measurement of the total flux-integrated cross section. Measurements are listed from K2K (Nakayama *et al.*, 2005; Rodriguez *et al.*, 2008; Mariani *et al.*, 2011), MiniBooNE (Aguilar-Arevalo *et al.*, 2009; 2010; 2011a; 2011b), and SciBooNE (Kurimoto *et al.*, 2010a).

Experiment	Target	Process	Cross section measurements
K2K	C_8H_8	ν_μ CC π^+/QE	σ, $\sigma(E_\nu)$
K2K	C_8H_8	ν_μ CC π^0/QE	σ
K2K		ν_μ NC π^0/CC	σ
MiniBooNE	CH_2	ν_μ CC π^+/QE	$\sigma(E_\nu)$
MiniBooNE	CH_2	ν_μ CC π^+	σ, $\sigma(E_\nu)$, $\frac{d\sigma}{dQ^2}$, $\frac{d\sigma}{dT_\mu}$, $\frac{d\sigma}{dT_\pi}$, $\frac{d^2\sigma}{dT_\mu d\cos\theta_\mu}$, $\frac{d^2\sigma}{dT_\pi d\cos\theta_\pi}$
MiniBooNE	CH_2	ν_μ CC π^0	σ, $\sigma(E_\nu)$, $\frac{d\sigma}{dQ^2}$, $\frac{d\sigma}{dE_\mu}$, $\frac{d\sigma}{d\cos\theta_\mu}$, $\frac{d\sigma}{dp_\pi}$, $\frac{d\sigma}{d\cos\theta_\pi}$
MiniBooNE	CH_2	ν_μ NC π^0	σ, $\frac{d\sigma}{dp_\pi}$, $\frac{d\sigma}{d\cos\theta_\pi}$
MiniBooNE	CH_2	$\bar{\nu}_\mu$ NC π^0	σ, $\frac{d\sigma}{dp_\pi}$, $\frac{d\sigma}{d\cos\theta_\pi}$
SciBooNE	C_8H_8	ν_μ NC π^0/CC	σ

D. Coherent pion production

In addition to resonance production, neutrinos can also coherently produce single pion final states. In this case, the neutrino coherently scatters from the entire nucleus, transferring negligible energy to the target (A). These low-Q^2 interactions produce no nuclear recoil and a distinctly forward-scattered pion, compared to their resonance-mediated counterparts. Both NC and CC coherent pion production processes are possible,

$$\nu_\mu A \to \nu_\mu A \pi^0, \qquad \bar{\nu}_\mu A \to \bar{\nu}_\mu A \pi^0, \tag{77}$$

$$\nu_\mu A \to \mu^- A \pi^+, \qquad \bar{\nu}_\mu A \to \mu^+ A \pi^-. \tag{78}$$

While the cross sections for these processes are predicted to be comparatively small, coherent pion production has been observed across a broad energy range in both NC and CC interactions of neutrinos and antineutrinos. Figure 22 shows a collection of existing measurements of coherent pion production cross sections for a variety of nuclei. A valuable compilation of the same is also available in Vilain *et al.*, 1993. Most of these historical measurements were performed at higher energies ($E_\nu > 2$ GeV). Table XIII provides a listing of more recent measurements of coherent pion production, most in the form of cross section ratios that were measured at low energy ($E_\nu < \sim 2$ GeV). Experiments measuring coherent pion production at these very low neutrino energies have typically observed less coherent pion production than predicted by models which well describe the high-energy data. In addition, the production of CC coherent pion events at low energy has been seemingly absent from much of the experimental data (Hasegawa *et al.*, 2005; Hiraide *et al.*, 2008), although refined searches have indicated some evidence for their existence (Hiraide, 2009).

To date, it has been a challenge to develop a single description that can successfully describe existing coherent pion production measurements across all energies. The most common theoretical approach for describing coherent pion production is typically based on Adler's partially conserved axial current (PCAC) theorem (Adler, 1964) which relates neutrino-induced coherent pion production to pion-nucleus elastic scattering in the limit $Q^2 = 0$. A nuclear form factor is then invoked to extrapolate to nonzero values of Q^2. Such PCAC-based models (Rein and Sehgal, 1983) have existed for many years and have been rather successful in describing coherent pion production at high energy (the prediction shown in Fig. 22 is such a model). With the accumulation of increasingly large amounts of low-energy neutrino data, revised

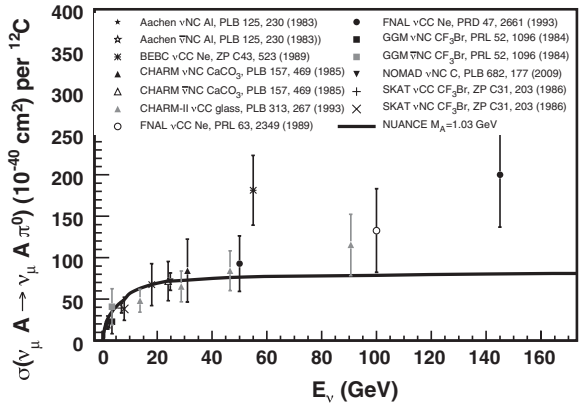

FIG. 22. Measurements of absolute coherent pion production cross sections from a variety of nuclear targets and samples, as indicated in the legend. Both NC and CC data are displayed on the same plot after rescaling the CC data using the prediction that $\sigma_{\mathrm{NC}} = \frac{1}{2}\sigma_{\mathrm{CC}}$ (Rein and Sehgal, 1983). In addition, data from various targets have been corrected to carbon cross sections assuming $A^{1/3}$ scaling (Rein and Sehgal, 1983). Also shown is the prediction from Casper (2002).

approaches have been applied to describe the reduced level of coherent pion production observed by low-energy experiments. Two such approaches have been developed. The first class of models are again based on PCAC (Rein and Sehgal, 1983; Belkov and Kopeliovich, 1987; Paschos and Kartavtsev, 2003; Kopeliovich, 2005; Paschos *et al.*, 2006; Berger and Sehgal, 2009; Hernandez *et al.*, 2009; Paschos *et al.*, 2009). The other class is microscopic models involving Δ resonance production Kelkar *et al.* (1997), Singh *et al.* (2006), Alvarez-Ruso *et al.* (2007), Amaro *et al.* (2009), T. Leitner *et al.* (2009), Hernandez *et al.* (2010), Nakamura, S. X. *et al.* (2010), and Martini, Ericson, and Chanfray (2011). Because this latter class involves Δ formation, their validity is limited to the low-energy region. An excellent review of the current experimental and theoretical situation is available in Alvarez-Ruso (2011a). The study and prediction of coherent pion production is important as it provides another source of potential background for neutrino oscillation experiments.

E. Multipion production

As mentioned, the baryonic resonances created in neutrino-nucleon interactions can potentially decay to multipion final states. Other inelastic processes, such as deep inelastic scattering, can also contribute a copious source

TABLE XIII. Modern measurements of CC (top) and NC (bottom) coherent pion production by neutrinos, at the time of this writing. Measurements are listed from K2K (Hasegawa *et al.*, 2005), MiniBooNE (Aguilar-Arevalo *et al.*, 2008), NOMAD (Kullenberg *et al.*, 2009), and SciBooNE (Hiraide *et al.*, 2008; Kurimoto *et al.*, 2010a, 2010b). All are ratio measurements performed at low energy, with the exception of the absolute coherent pion production cross section measurement recently reported by NOMAD. Higher energy coherent pion production results have also been recently reported by the MINOS experiment (Cherdack, 2011).

Experiment	Target	E_ν	Measurement
K2K	C_8H_8	1.3 GeV	σ(CC coherent π^+/CC)
SciBooNE	C_8H_8	1.1 GeV	σ(CC coherent π^+/CC)
SciBooNE	C_8H_8	1.1, 2.2 GeV	σ(CC coherent π^+/NC coherent π^0)
MiniBooNE	CH_2	1.1 GeV	σ(NC coherent π^0/NC π^0)
NOMAD	C-based	24.8 GeV	σ(NC coherent π^0)
SciBooNE	C_8H_8	1.1 GeV	σ(NC coherent π^0/CC)

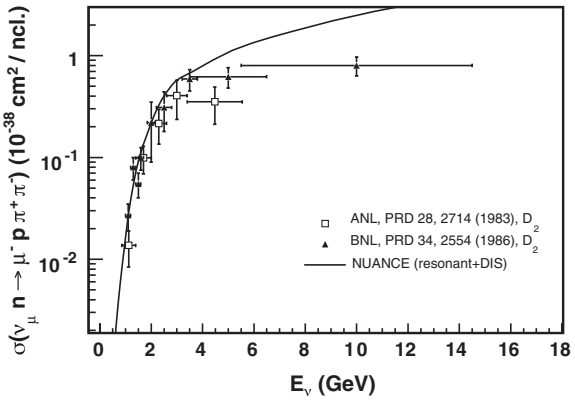

FIG. 23. Existing measurements of the $\nu_\mu n \to \mu^- p \pi^+ \pi^-$ scattering cross section as a function of neutrino energy. Also shown is the prediction from Casper (2002) including both resonant and DIS contributions to this reaction channel.

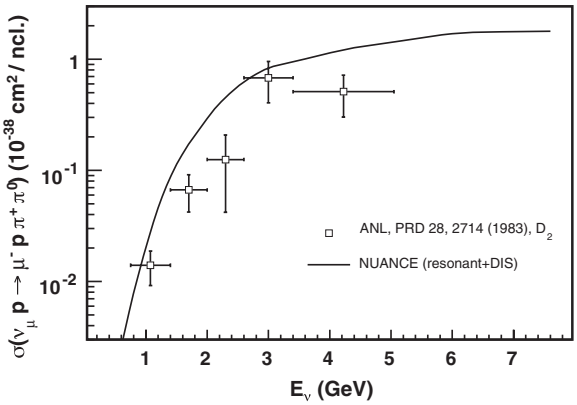

FIG. 24. Existing measurements of the $\nu_\mu p \to \mu^- p \pi^+ \pi^0$ scattering cross section as a function of neutrino energy. Also shown is the prediction from Casper (2002) including both resonant and DIS contributions to this reaction channel.

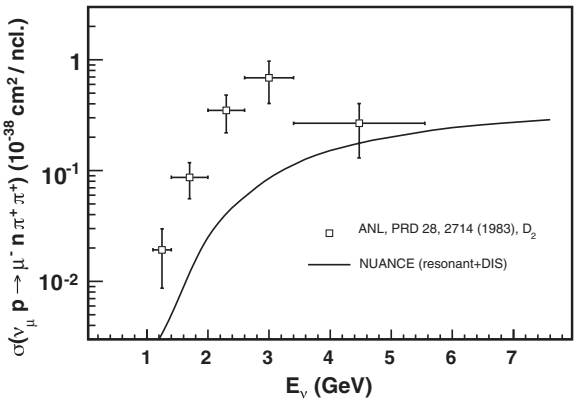

FIG. 25. Existing measurements of the $\nu_\mu p \to \mu^- n \pi^+ \pi^+$ scattering cross section as a function of neutrino energy. Also shown is the prediction from Casper (2002) including both resonant and DIS contributions to this reaction channel.

of multipion final states depending on the neutrino energy. Figures 23–25 show existing measurements of neutrino-induced di-pion production cross sections compared to an example prediction including contributions from both resonant and deep inelastic scattering mechanisms. Because of the inherent complexity of reconstructing multiple pions final states, there are not many existing experimental measurements of this process. All of the existing measurements have been performed strictly using deuterium-filled bubble chambers. Improved measurements will be important because they test our understanding of the transition region and will provide a constraint on potential backgrounds for neutrino oscillation experiments operating in higher energy beams.

F. Kaon production

Neutrino interactions in this energy range can also produce final states involving strange quarks. Some of the contributing strange production channels at intermediate energies include the following processes:

$$\begin{array}{ll} \text{CC:} & \text{NC:} \\ \nu_\mu n \to \mu^- K^+ \Lambda^0 & \nu_\mu p \to \nu_\mu K^+ \Lambda^0 \\ \nu_\mu p \to \mu^- K^+ p & \nu_\mu n \to \nu_\mu K^0 \Lambda^0 \\ \nu_\mu n \to \mu^- K^0 p & \nu_\mu p \to \nu_\mu K^+ \Sigma^0 \\ \nu_\mu n \to \mu^- K^+ n & \nu_\mu p \to \nu_\mu K^0 \Sigma^+ \\ \nu_\mu p \to \mu^- K^+ \Sigma^+ & \nu_\mu n \to \nu_\mu K^0 \Sigma^0 \\ \nu_\mu n \to \mu^- K^+ \Sigma^0 & \nu_\mu n \to \nu_\mu K^+ \Sigma^- \\ \nu_\mu n \to \mu^- K^0 \Sigma^+ & \nu_\mu n \to \nu_\mu K^- \Sigma^+. \end{array} \tag{79}$$

These reactions typically have small cross sections due in part to the kaon mass and because the kaon channels are not enhanced by any dominant resonance. Measuring neutrino-induced kaon production is of interest primarily as a source of potential background for proton decay searches. Proton decay modes containing a final-state kaon, $p \to K^+ \bar{\nu}$, have large branching ratios in many supersymmetry grand unified theory models. Because there is a nonzero probability that an atmospheric neutrino interaction can mimic such a proton decay signature, estimating these background rates has become an increasingly important component to such searches.

Figure 26 shows the only two experiments which have published cross sections on the dominant associated production channel, $\nu_\mu n \to \mu^- K^+ \Lambda^0$. Both bubble chamber measurements were performed on a deuterium target and are based on less than 30 events combined. Many other measurements of strange particle production yields have been performed throughout the years, most using bubble chambers (Barish *et al.*, 1974; Deden *et al.*, 1975; Berge *et al.*, 1976, 1978; Blietschau *et al.*, 1976; Bell *et al.*, 1978; Hasert *et al.*, 1978; Krenz *et al.*, 1978b; Baker *et al.*, 1981, 1986; Bosetti *et al.*, 1982; Brock *et al.*, 1982; Grassler *et al.*, 1982; Son *et al.*, 1983; Aderholz *et al.*, 1992; Willocq *et al.*, 1992; Jones *et al.*, 1993; DeProspo *et al.*, 1994; Agababyan *et al.*, 2006). More recently, NOMAD has reported NC and CC strange particle production yields and multiplicities for a variety of reaction kinematics (Astier *et al.*, 2002; Naumov *et al.*, 2004; Chukanov *et al.*, 2006).

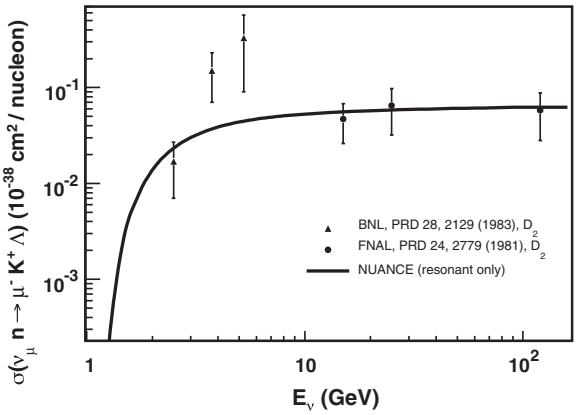

FIG. 26. Measurements of the associated production cross section, $\nu_\mu n \to \mu^- K^+ \Lambda^0$, as a function of neutrino energy. Also shown is the prediction from Casper (2002) which includes both resonant and DIS contributions.

As far as theoretical calculations go, predictions for these neutrino-induced kaon production processes have existed for several decades (Albright, 1975; Ezawa *et al.*, 1975; Shrock, 1975; Amer, 1978; Dewan, 1981), although there have been several revised calculations in recent years (Adera *et al.*, 2010; Alam *et al.*, 2010, 2012).

G. Outlook

In summary, neutrino scattering at intermediate energies is notoriously complex and the level to which these contributing processes have been studied remains incomplete (Benhar, 2010; Alvarez-Ruso, 2011b). Improved experimental measurements and theoretical calculations will be especially important for reducing systematics in future precision neutrino oscillation experiments. Luckily, such studies are already underway making use of new intense accelerator-based sources of neutrinos. However, for such updated cross section measurements to be robust, they must be accompanied by an equally precise knowledge of the incoming neutrino flux. Improved hadro-production measurements are key to providing the level of precision necessary. In addition, further scrutiny of nuclear effects in intermediate energy neutrino and antineutrino interactions is absolutely essential. Analysis of data from the MINERνA experiment will soon enable the first detailed look at nuclear effects in neutrino interactions. Together, theoretical advances and new data taken on a variety of nuclear targets from the ArgoNeuT, K2K, MicroBooNE, MINERνA, MiniBooNE, MINOS, NOMAD, NOvA, and SciBooNE experiments should provide both a necessary and broad foundation going into the future. In order to make progress in our understanding of this energy regime and provide the most clarity, experiments should strive to report what they directly detect in the final state, for example, in the form of model-independent differential cross sections.

VI. HIGH-ENERGY CROSS SECTIONS: $E_\nu \sim$ 20–500 GeV

Up to now, we have largely discussed neutrino scattering from composite entities such as nucleons or nuclei. Given enough energy, the neutrino can actually begin to resolve the internal structure of the target. In the most common high-energy interaction, the neutrino can scatter off an individual quark inside the nucleon, a process called deep inelastic scattering (DIS). An excellent review of this subject has been previously published in this journal (Conrad, Shaevitz, and Bolton, 1998), therefore we provide only a brief summary of the DIS cross section, relevant kinematics, and most recent experimental measurements here.

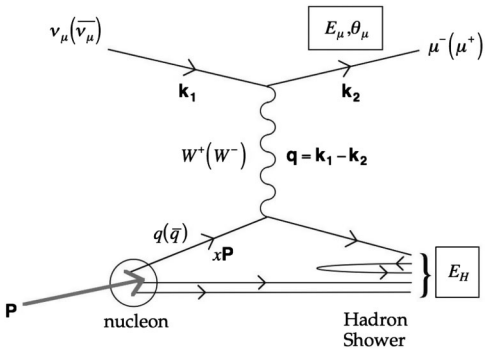

FIG. 27. Feynman diagram for a CC neutrino DIS process. In the case of NC DIS, the outgoing lepton is instead a neutrino and the exchange particle is a Z boson. From Conrad, Shaevitz, and Bolton, 1998.

A. Deep inelastic scattering

Neutrino deep inelastic scattering has long been used to validate the standard model and probe nucleon structure. Over the years, experiments have measured cross sections, electroweak parameters, coupling constants, nucleon structure functions, and scaling variables using such processes. In deep inelastic scattering (Fig. 27), the neutrino scatters off a quark in the nucleon via the exchange of a virtual W or Z boson producing a lepton and a hadronic system in the final state.[11] Both CC and NC processes are possible

$$\nu_\mu N \to \mu^- X, \qquad \bar{\nu}_\mu N \to \mu^+ X, \tag{80}$$

$$\nu_\mu N \to \nu_\mu X, \qquad \bar{\nu}_\mu N \to \bar{\nu}_\mu X. \tag{81}$$

Here we restrict ourselves to the case of ν_μ scattering, as an example, though ν_e and ν_τ DIS interactions are also possible.

Following the formalism introduced in Sec. II, DIS processes can be completely described in terms of three dimensionless kinematic invariants. The first two, the inelasticity (y) and the four-momentum transfer ($Q^2 = -q^2$), have already been defined. We now define the Bjorken scaling variable x,

$$x = \frac{Q^2}{2p_e \cdot q} \qquad \text{(Bjorken scaling variable)}. \tag{82}$$

The Bjorken scaling variable plays a prominent role in deep inelastic neutrino scattering, where the target can carry a portion of the incoming energy momentum of the struck nucleus.

[11] Quarks cannot be individually detected; they quickly recombine and thus appear as a hadronic shower.

On a practical level, these Lorentz-invariant parameters cannot be readily determined from four-vectors, but they can be reconstructed using readily measured observables in a given experiment,

$$x = \frac{Q^2}{2M\nu} = \frac{Q^2}{2ME_\nu y}, \tag{83}$$

$$y = E_{\rm had}/E_\nu, \tag{84}$$

$$Q^2 = -m_\mu^2 + 2E_\nu(E_\mu - p_\mu \cos\theta_\mu), \tag{85}$$

where E_ν is the incident neutrino energy, M_N is the nucleon mass, $\nu = E_{\rm had}$ is the energy of the hadronic system, and E_μ, p_μ, and $\cos\theta_\mu$ are the energy, momentum, and scattering angle of the outgoing muon in the laboratory frame. In the case of NC scattering, the outgoing neutrino is not reconstructed. Thus, experimentally, all of the event information must be inferred from the hadronic shower in that case.

Using these variables, the inclusive cross section for DIS scattering of neutrinos and antineutrinos can be written as

$$\frac{d^2\sigma^{\nu,\bar\nu}}{dxdy} = \frac{G_F^2 M E_\nu}{\pi(1+Q^2/M_{W,Z}^2)^2}\left[\frac{y^2}{2}2xF_1(x,Q^2) + \left(1-y-\frac{Mxy}{2E}\right)F_2(x,Q^2) \pm y\left(1-\frac{y}{2}\right)xF_3(x,Q^2)\right], \tag{86}$$

where G_F is again the Fermi weak coupling constant, $M_{W,Z}$ is the mass of the $W^\pm$ (Z^0 boson) in the case of CC (NC) scattering, and the $+(-)$ sign in the last term refers to neutrino (antineutrino) interactions. In Eq. (86), $F_i(x, Q^2)$ are the dimensionless nucleon structure functions that encompass the underlying structure of the target. For electron scattering, there are two structure functions while for neutrino scattering there is additionally a third structure function, $xF_3(x, Q^2)$, which represents the V, A interference term.

Assuming the quark parton model, in which the nucleon consists of partons (quarks and gluons), $F_i(x, Q^2)$ can be expressed in terms of the quark composition of the target. They depend on the target and type of scattering interaction and are functions of x and Q^2. In the simplest case, the nucleon structure functions can then be expressed as the sum of the probabilities,

$$F_2(x,Q^2) = 2\sum_{i=u,d,\ldots}[xq(x,Q^2) + x\bar q(x,Q^2)], \tag{87}$$

$$xF_3(x,Q^2) = 2\sum_{i=u,d,\ldots}[xq(x,Q^2) - x\bar q(x,Q^2)], \tag{88}$$

where the sum is over all quark species. The struck quark carries a fraction x of the nucleon's momentum, such that xq ($x\bar q$) is the probability of finding the quark (antiquark) with a given momentum fraction. These probabilities are known as parton distribution functions (PDFs). In this way, $F_2(x, Q^2)$ measures the sum of the quark and antiquark PDFs in the nucleon, while $xF_3(x, Q^2)$ measures their difference and is therefore sensitive to the valence quark PDFs. The third structure function $2xF_1(x, Q^2)$ is commonly related to $F_2(x, Q^2)$ via a longitudinal structure function, $R_L(x, Q^2)$,

$$F_2(x,Q^2) = \frac{1+R_L(x,Q^2)}{1+4M^2x^2/Q^2}2xF_1(x,Q^2), \tag{89}$$

where $R_L(x, Q^2)$ is the ratio of cross sections for scattering off longitudinally and transversely polarized exchange bosons.

Measurement of these structure functions has been the focus of many charged lepton and neutrino DIS experiments, which together have probed $F_2(x, Q^2)$, $R_L(x, Q^2)$, and xF_3 (in the case of neutrino scattering) over a wide range of x and Q^2 values (Nakamura, K. *et al.*, 2010). Neutrino scattering is unique, however, in that it measures the valence quark distributions through measurement of xF_3 and the strange quark distribution through detection of neutrino-induced dimuon production. These provide important constraints that cannot be obtained from either electron or muon scattering experiments.

While Eq. (86) provides a tidy picture of neutrino DIS, additional effects must be included in any realistic description of these processes. The inclusion of lepton masses (Albright and Jarlskog, 1975; Kretzer and Reno, 2002), higher order QCD processes (Moch and Vermaseren, 2000; McFarland and Moch, 2003; Dobrescu and Ellis, 2004), nuclear effects, radiative corrections (Sirlin and Marciano, 1981; Arbuzov *et al.*, 2005; De Rujula, Petronzio, and Savoy-Navarro, 1979; Bardin and Dokuchaeva, 1986; Diener *et al.*, 2004), target mass effects (Schienbein *et al.*, 2008), heavy quark production (Barnett, 1976; Georgi and Politzer, 1976; Gottschalk, 1981), and nonperturbative higher twist effects (Buras, 1980) further modify the scattering kinematics and cross sections. In general, these contributions are typically well known and do not add large uncertainties to the predicted cross sections.

Having completed a brief description of DIS, we next turn to some of the experimental measurements. Table XIV lists the most recent experiments that have probed such high-energy neutrino scattering. To isolate DIS events, neutrino experiments typically apply kinematic cuts to remove quasielastic scattering (Sec. V.A) and resonance-mediated (Sec. V.C) contributions from their data. Using high statistics samples of DIS events, these experiments have provided measurements of the weak mixing angle $\sin^2\theta_W$ from NC

TABLE XIV. Attributes of neutrino experiments that have recently studied DIS, including CHORUS (Onegut *et al.*, 2006; Kayis-Topaksu *et al.*, 2008a), MINOS (Adamson *et al.*, 2010), NOMAD (Wu *et al.*, 2008), and NuTeV (Zeller *et al.*, 2002; Tzanov *et al.*, 2006; Mason *et al.*, 2007a).

Experiment	Target	E_ν (GeV)	Statistics	Year	Results
CHORUS	Pb	10–200	$8.7\times10^5\,\nu$, $1.5\times10^5\,\bar\nu$	1995–1998	$F_2(x,Q^2)$, $xF_3(x,Q^2)$
MINOS	Fe	3–50	$19.4\times10^5\,\nu$, $1.6\times10^5\,\bar\nu$	2005–present	$\sigma(E_\nu)$
NOMAD	C	3–300	$10.4\times10^5\,\nu$	1995–1998	$\sigma(E_\nu)$
NuTeV	Fe	30–360	$8.6\times10^5\,\nu$, $2.3\times10^5\,\bar\nu$	1996–1997	$F_2(x,Q^2)$, $xF_3(x,Q^2)$, $\sigma(E_\nu)$, $\frac{d^2\sigma}{dxdy}$, $\sin^2\theta_W$

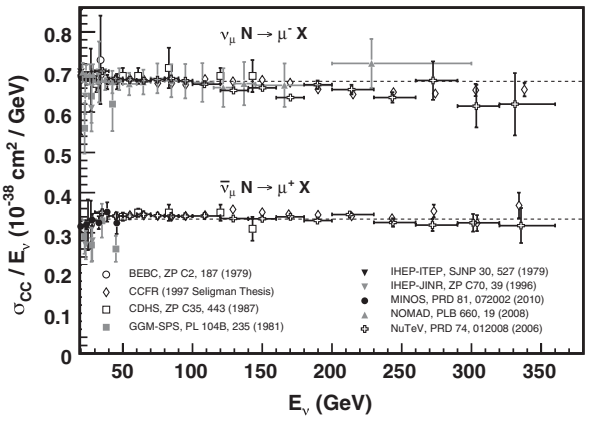

FIG. 28. Measurements of the inclusive neutrino and antineutrino CC cross sections ($\nu_\mu N \to \mu^- X$ and $\bar{\nu}_\mu N \to \mu^+ X$) divided by neutrino energy plotted as a function of neutrino energy. Here N refers to an isoscalar nucleon within the target. The dotted lines indicate the world-averaged cross sections, $\sigma^\nu/E_\nu = (0.677 \pm 0.014) \times 10^{-38}$ cm^2/GeV and $\sigma^{\bar{\nu}}/E_\nu = (0.334 \pm 0.008) \times 10^{-38}$ cm^2/GeV, for neutrinos and antineutrinos, respectively, (Nakamura, K. *et al.*, 2010). For an extension to lower neutrino energies, see the complete compilation in Fig. 9.

DIS samples as well as measurements of structure functions, inclusive cross sections, and double differential cross sections for CC single muon and dimuon production. Figure 28 specifically shows measurements of the inclusive CC cross section from the NOMAD, NuTeV, and MINOS experiments compared to historical data. As can be seen, the CC cross section is measured to a few percent in this region. A linear dependence of the cross section on neutrino energy is also exhibited at these energies, a confirmation of the quark parton model predictions.

In addition to such inclusive measurements as a function of neutrino energy, experiments have reported differential cross sections, for example, most recently Tzanov *et al.* (2006). Also, over the years, exclusive processes such as opposite-sign dimuon production have been measured (Dore, 2011). Such dimuon investigations have been performed in counter experiments like CCFR (Foudas *et al.*, 1990; Rabinowitz *et al.*, 1993; Bazarko *et al.*, 1995), CDHS (Abramowicz *et al.*, 1982), CHARM-II (Vilain *et al.*, 1999), E616 (Lang *et al.*, 1987), Harvard-Penn-Wisconsin-Fermilab (HPWF) (Aubert *et al.*, 1974; Benvenuti *et al.*, 1978), NOMAD (Astier *et al.*, 2000), and NuTeV (Goncharov *et al.*, 2001; Mason *et al.*, 2007b), in bubble chambers like Big European Bubble Chamber (BEBC) (Gerbier, 1985), Fermi National Accelerator Laboratory (FNAL) (Ballagh *et al.*, 1981; Baker *et al.*, 1985) and Gargamelle (Haatuft *et al.*, 1983) as well as in nuclear emulsion detectors such as E531 (Ushida *et al.*, 1983) and CERN Hybrid Oscillation Research apparatUS (CHORUS) (Onengut *et al.*, 2004; Kayis-Topaksu *et al.*, 2005, 2008b, 2011; Onengut *et al.*, 2005). This latter class of measurements is particularly important for constraining the strange and antistrange quark content of the nucleon and their momentum dependence.

In the near future, high statistics measurements of neutrino and antineutrino DIS are expected from the MINERνA experiment (Drakoulakos *et al.*, 2004). With multiple nuclear targets, MINERνA will also be able to complete the first detailed examination of nuclear effects in neutrino DIS.

VII. ULTRA-HIGH-ENERGY NEUTRINOS: 0.5 TEV–1 EEV

In reaching the ultra-high-energy scale, we find ourselves, remarkably, back to the beginning of our journey at extremely low energies. Neutrinos at this energy scale have yet to manifest themselves as confirmed observations, though our present technology is remarkably close to dispelling that fact. To date, the highest energy neutrino recorded is several hundred TeV (DeYoung, 2011). However, experimentalists and theorists have their aspirations set much higher, to energies above 10^{15} eV. On the theoretical side, this opens the door for what could be called "neutrino astrophysics." A variety of astrophysical objects and mechanisms become accessible at these energies, providing information that is complementary to that already obtained from electromagnetic or hadronic observations.

In response to the call, the experimental community has forged ahead with a number of observational programs and techniques geared toward the observation of ultra-high-energy neutrinos from astrophysical sources. The range of these techniques include detectors scanning for ultra-high-energy cosmic neutrino-induced events in large volumes of water [Baikal (Antipin *et al.*, 2007; Aynutdinov *et al.*, 2009), Antares (Aslanides *et al.*, 1999)], ice [Antarctic Muon And Neutrino Detector Array (AMANDA) (Achterberg *et al.*, 2007), IceCube (de los Heros, 2011), Radio Ice Cerenkov Experiment (RICE) (Kravchenko *et al.*, 2003), Fast On-orbit Recording of Transient Events (FORTE) (Lehtinen *et al.*, 2004), ANITA (Barwick *et al.*, 2006)], the Earth's atmosphere [Pierre Auger (Abraham *et al.*, 2008), HiRes (Abbasi *et al.*, 2004)], and the lunar regolith [Goldstone Lunar Ultra-High Energy experiment (GLUE) (Gorham *et al.*, 2004)]. Even more future programs are in the planning stages. As such, the knowledge of neutrino cross section in this high-energy region is becoming ever increasing in importance. Once first detection is firmly established, the emphasis is likely to shift toward obtaining more detailed information about the observed astrophysical objects, and thus the neutrino fluxes will need to be examined in much greater detail.

The neutrino cross sections in this energy range[12] are essentially extensions of the high-energy parton model discussed in Sec. VI. However, at these energies, the propagation term from the interaction vertex is no longer dominated by the W-Z boson mass. As a result, the cross section no longer grows linearly with neutrino energy. The propagator term in fact suppresses the cross sections for energies above 10 TeV. Likewise, the $(1-y)^2$ suppression that typically allows distinction between neutrino and antineutrino interactions is much less pronounced, making the two cross sections (νN and $\bar{\nu} N$) nearly identical.

For a rough estimate of the neutrino cross section at these high energies ($10^{16} \leq E_\nu \leq 10^{21}$ eV), the following power

[12]Typically, the high-energy region is demarcated by $E_\nu \geq 10^6$ GeV.

law dependence provides a reasonable approximation (Gandhi *et al.*, 1996):

$$\sigma_{\nu N}^{\mathrm{CC}} = 5.53 \times 10^{-36}\ \mathrm{cm}^2 \left(\frac{E_\nu}{1\ \mathrm{GeV}}\right)^{\alpha}, \tag{90}$$

$$\sigma_{\nu N}^{\mathrm{NC}} = 2.31 \times 10^{-36}\ \mathrm{cm}^2 \left(\frac{E_\nu}{1\ \mathrm{GeV}}\right)^{\alpha}, \tag{91}$$

where $\alpha \simeq 0.363$.

There is one peculiar oddity that is worth highlighting for neutrino cross sections at such high energies. Neutrino-electron scattering is usually subdominant to any neutrino-nucleus interaction because of its small target mass. There is one notable exception, however when the neutrino undergoes a resonant enhancement from the formation of an intermediate W boson in $\bar{\nu}_e e^-$ interactions. This resonance formation takes place at $E_{\mathrm{res}} = M_W^2/2m_e = 6.3$ PeV and is by far more prominent than any νN interaction up to 10^{21} eV (see Fig. 29). The mechanism was first suggested by Glashow in 1960 as a means to directly detect the W boson (Glashow, 1960). The cross section was later generalized by Berezinsky and Gazizov (1977) to other possible channels:

$$\frac{d\sigma(\bar{\nu}_e e^- \to \bar{\nu}_e e^-)}{dy} = \frac{2G_F^2 m_e E_\nu}{\pi}\left[\frac{g_R^2}{(1+2m_e E_\nu y/M_Z^2)^2} + \left|\frac{g_L}{1+2m_e E_\nu y/M_Z^2} + \frac{1}{1-2m_e E_\nu/M_W^2 + i\Gamma_W/M_W}\right|^2\right], \tag{92}$$

where $g_{L,R}$ are the left- and right-handed fermion couplings, M_W is the W-boson mass, and Γ_W is the W-decay width (~ 2.08 GeV). This resonance occurs only for s-channel processes mediated by W exchange,

$$\frac{d\sigma(\nu_l e \to \nu_l e)}{dy} = \frac{2m_e G_F^2 E_\nu}{\pi}\frac{1}{(1+2m_e E_\nu y/M_Z^2)^2} \times [g_L^2 + g_R^2(1-y)^2],$$

$$\frac{d\sigma(\bar{\nu}_l e \to \bar{\nu}_l e)}{dy} = \frac{2m_e G_F^2 E_\nu}{\pi}\frac{1}{(1+2m_e E_\nu y/M_Z^2)^2} \times [g_R^2 + g_L^2(1-y)^2].$$

When compared to that of neutrino-nucleon scattering or even nonresonant neutrino-lepton scattering, $\bar{\nu}_e$ scattering dominates. Such high cross sections can often cause the Earth to be opaque to neutrinos in certain energy regimes and depart substantially from standard model predictions if new physics is present (Gandhi *et al.*, 1996).

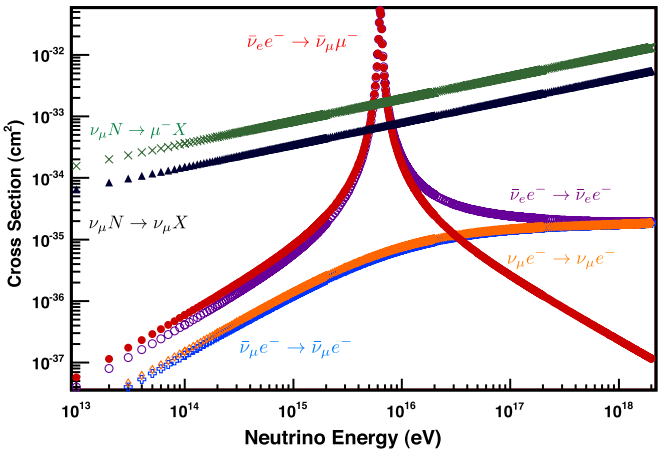

FIG. 29 (color online). Neutrino electron and nucleon scattering in the ultra-high-energy regime ($E_\nu \geq 10^4$ GeV). Shown are the electron interactions $\bar{\nu}_\mu e^- \to \bar{\nu}_\mu e^-$ (crosses), $\nu_\mu e^- \to \nu_\mu e^-$ (diamonds), $\bar{\nu}_e e^- \to \bar{\nu}_e e^-$ (hollow circles), $\bar{\nu}_e e^- \to \bar{\nu}_\mu e^-$ (filled circles), and the nucleon charged current (cross markers) and neutral-current (filled triangles) interactions. The leptonic W resonance channel is clearly evident (Butkevich *et al.*, 1988; Gandhi *et al.*, 1996).

A. Uncertainties and projections

For a more accurate prediction of the cross section, a well-formulated model of the relevant quark structure functions is needed. This predictive power is especially important in the search for new physics. At such high energies, the neutrino cross section can depart substantially from the standard model prediction if new physics is at play. Study of such high-energy neutrinos can be a possible probe into new physics.

Direct neutrino scattering measurements at such extreme energies are, of course, unavailable. Therefore, predictions rely heavily on the existing knowledge of parton distribution functions and, as the reader can imagine, extrapolation can introduce substantial uncertainties to these predictions. The best constraints on the relevant parton distribution functions stem from data collected from high-energy ep scattering experiments such as Hadron-Electron Ring Accelerator (HERA) (Chekanov *et al.*, 2003). The challenge rests on the ability to fit existing data to as low values of x as possible. At high energies, the propagator term limits the maximum Q^2 to the $M_{W,Z}$ mass. The relevant range for x then falls inversely with neutrino energy,

$$x \sim \frac{M_W}{E_\nu} \tag{93}$$

which, for EeV scales, implies x down to 10^{-8} or lower. The ZEUS Collaboration has recently extended their analysis of parton distribution function data down to $x \simeq 10^{-5}$, allowing a more robust extrapolation of the neutrino cross section to higher energies (Cooper-Sarkar and Sarkar, 2008). Uncertainties in their parton distribution function translate into $\pm 4\%$ uncertainties for the neutrino cross section for center-of-mass energy of 10^4 GeV and $\pm 14\%$ uncertainties at $\sqrt{s} = 10^6$ GeV.

An equal factor in the precise evaluation of these cross sections is the selection of an adequate PDF itself. The conventional PDF makes use of the Dokshitzer-Gribov-Lipatov-Altarelli-Parisi formalism (Altarelli and Parisi, 1977; Dokshitzer, 1977), which is a next-to-leading order

QCD calculation. As one pushes further down in x, the PDFs introduce greater uncertainties, whereby other approaches can be used, such as the formalism adopted by the Balitsky-Fadin-Kuraev-Lipatov group (Kuraev, Lipatov, and Fadin, 1977; Ciafaloni *et al.*, 2006). In reality, the approaches of both Dokshitzer-Gribov-Lipatov-Altarelli-Parisi and Balitsky-Fadin-Kuraev-Lipatov need to be combined in order to properly account for the Q^2 and x evolution of these PDFs.

One of the more difficult effects to account for in these parametrization schemes is that of gluon recombination ($gg \rightarrow g$). Such a saturation must take place at the very highest energies in order to preserve unitarity. Groups have made use of nonlinear color glass condensate models as a way to model these effects (Iancu and Venugopalan, 2003). Such techniques have been successfully applied to Relativistic Heavy Ion Collider (RHIC) data (Jalilian-Marian and Kovchegov, 2006).

VIII. SUMMARY

In this work, we presented a comprehensive review of neutrino interaction cross sections. Our discussion ranged from eV to EeV energy scales and therefore spanned a broad range of underlying physics processes, theoretical calculations, and experimental measurements.

While our knowledge of neutrino scattering may not be equally precise at all energies, one cannot help but marvel at how far our theoretical frameworks extend. From literally zero-point energy to unfathomable reaches, it appears that our models can shed some light in the darkness. Equally remarkable is the effort by which we seek to ground our theories. Where data do not exist, we seek other anchors by which we can assess their validity. When even that approach fails, we pile model against model in the hopes of finding weaknesses that ultimately will strengthen our foundations.

As the journey continues into the current millennium, we find that more and more direct data are being collected to guide our theoretical understanding. Currently, new experiments are coming online to shed more light on neutrino interactions. Therefore, we believe that, as comprehensive as we have tried to make this review, it is certainly an incomplete story whose chapters continue to be written.

ACKNOWLEDGMENTS

The authors thank S. Brice, S. Dytman, D. Naples, J. P. Krane, G. Mention, and R. Tayloe for help in gathering experimental data used in this review. The authors also thank W. Haxton, W. Donnelly, and R. G. H. Robertson for their comments and suggestions pertaining to this work. J. A. Formaggio is supported by the United States Department of Energy under Grant No. DE-FG02-06ER-41420. G. P. Zeller is supported via the Fermi Research Alliance, LLC under Contract No. DE-AC02-07CH11359 with the United States Department of Energy.

REFERENCES

Abbasi, R. U., *et al.* (High Resolution Flys Eye Collaboration), 2004, Phys. Rev. Lett. **92**, 151101.
Abdurashitov, J. N., *et al.*, 2006, Phys. Rev. C **73**, 045805.
Abdurashitov, J. N., *et al.* (The SAGE Collaboration), 1999, Phys. Rev. C **59**, 2246.
Abe, K., *et al.*, 1989, Phys. Rev. Lett. **62**, 1709.
Abraham, J., *et al.* (Pierre Auger Collaboration), 2008, Phys. Rev. Lett. **100**, 211101.
Abramowicz, H., *et al.*, 1982, Z. Phys. C **15**, 19.
Achkar, B., *et al.*, 1995, Nucl. Phys. **B434**, 503.
Achterberg, A., *et al.* (IceCube), 2007, Phys. Rev. D **75**, 102001.
Adams, T., *et al.* (NuSOnG), 2009, Int. J. Mod. Phys. A **24**, 671.
Adamson, P., *et al.*, 2010, Phys. Rev. D **81**, 072002.
Adelberger, E., *et al.*, 2010, arXiv:1004.2318.
Adera, G. B., *et al.*, 2010, Phys. Rev. C **82**, 025501.
Aderholz, M., *et al.*, 1992, Phys. Rev. D **45**, 2232.
Adler, S. L., 1964, Phys. Rev. **135**, B963.
Agababyan, N. M., *et al.*, 2006, Phys. At. Nucl. **69**, 35.
Aguilar-Arevalo, A., *et al.*, 2010a, Phys. Rev. D **81**, 092005.
Aguilar-Arevalo, A., *et al.*, 2010b, Phys. Rev. D **82**, 092005.
Aguilar-Arevalo, A. A., 2008, Phys. Rev. Lett. **100**, 032301.
Aguilar-Arevalo, A. A., *et al.*, 2008, Phys. Lett. B **664**, 41.
Aguilar-Arevalo, A. A., *et al.*, 2009, Phys. Rev. Lett. **103**, 081801.
Aguilar-Arevalo, A. A., *et al.*, 2010, Phys. Rev. D **81**, 013005.
Aguilar-Arevalo, A. A., *et al.*, 2011a, Phys. Rev. D **83**, 052007.
Aguilar-Arevalo, A. A., *et al.*, 2011b, Phys. Rev. D **83**, 052009.
Aharmin, B., *et al.*, 2005, Phys. Rev. C **72**, 055502.
Aharmin, B., *et al.*, 2007, Phys. Rev. C **75**, 045502.
Aharmin, B., *et al.*, 2008, Phys. Rev. Lett. **101**, 111301.
Ahmad, Q., *et al.*, 2001, Phys. Rev. Lett. **87**, 071301.
Ahmad, Q., *et al.*, 2002a, Phys. Rev. Lett. **89**, 011301.
Ahmad, Q., *et al.*, 2002b, Phys. Rev. Lett. **89**, 011302.
Ahmed, S., *et al.*, 2004, Phys. Rev. Lett. **92**, 181301.
Ahrens, L., *et al.*, 1983, Phys. Rev. Lett. **51**, 1514.
Ahrens, L., *et al.*, 1990, Phys. Rev. D **41**, 3297.
Ahrens, L. A., *et al.*, 1988, Phys. Lett. B **202**, 284.
Alam, M., I. Simo, M. Athar, and M. Vicente Vacas, 2012, Phys. Rev. D **85**, 013014, 15 pp. and 6 figures.
Alam, R., *et al.*, 2010, Phys. Rev. D **82**, 033001.
Alberico, W. M., *et al.*, 1999, Nucl. Phys. A **651**, 277.
Albright, C., 1975, Phys. Rev. D **12**, 1329.
Albright, C. H., and C. Jarlskog, 1975, Nucl. Phys. **B84**, 467.
Alimonti, G., *et al.* (Borexino), 2002, Astropart. Phys. **16**, 205.
Allasia, D., *et al.* (Amsterdam-Bologna-Padua-Pisa-Saclay-Turin Collaboration), 1983, Z. Phys. C **20**, 95.
Allen, P., *et al.* (Aachen-Birmingham-Bonn-CERN-London-Munich-Oxford Collaboration), 1986, Nucl. Phys. **B264**, 221.
Allen, R., *et al.*, 1993, Phys. Rev. D **47**, 11.
Altarelli, G., and G. Parisi, 1977, Nucl. Phys. **B126**, 298.
Alvarez-Ruso, L., 2010, arXiv:1012.3871.
Alvarez-Ruso, L., 2011a, AIP Conf. Proc. **1405**, 140.
Alvarez-Ruso, L., 2011b, AIP Conf. Proc. **1382**, 161.
Alvarez-Ruso, L., *et al.*, 2007, Phys. Rev. C **75**, 055501.
Amaro, J., M. Barbaro, J. Caballero, and T. Donnelly, 2011a, arXiv:1112.2123.
Amaro, J., M. Barbaro, J. Caballero, T. Donnelly, and J. Udias, 2011b, Phys. Rev. D **84**, 033004.
Amaro, J. E., M. Barbaro, J. Caballero, and T. Donnelly, 2006, Phys. Rev. C **73**, 035503.
Amaro, J. E., M. Barbaro, J. Caballero, T. Donnelly, and J. Udias, 2007, Phys. Rev. C **75**, 034613.
Amaro, J. E., M. B. Barbaro, J. A. Caballero, T. W. Donnelly, A. Molinari, and I. Sick, 2005, Phys. Rev. C **71**, 015501.
Amaro, J. E., *et al.*, 2009, Phys. Rev. D **79**, 013002.
Amer, A. A., 1978, Phys. Rev. D **18**, 2290.
Ammosov, V. V., *et al.*, 1987, Z. Phys. C **36**, 377.

Ankowski, A. M., O. Benhar, T. Mori, R. Yamaguchi, and M. Sakuda, 2012, Phys. Rev. Lett. **108**, 052505, 5 pp., 4 figures.
Ankowski, A. M., and J. T. Sobczyk, 2006, Phys. Rev. C **74**, 054316.
Ankowski, A. M., and J. T. Sobczyk, 2008, Phys. Rev. C **77**, 044311.
Anselmann, P., *et al.*, 1995, Phys. Lett. B **342**, 440.
Antipin, K., *et al.*, 2007, Nucl. Phys. B, Proc. Suppl. **168**, 296.
Antonello, M., *et al.*, 2009, Acta Phys. Pol. B **40**, 2519 [http://arXiv.org/abs/arXiv:0912.0538].
Apollonio, M., *et al.*, 2003, The European Physical Journal C-Particles and Fields **27**, 331.
Arbuzov, A. B., *et al.*, 2005, J. High Energy Phys. 06, 078.
Armbruster, B., *et al.*, 1998, Phys. Lett. B **423**, 15.
Arpesella, C., *et al.* (The Borexino Collaboration), 2008, Phys. Rev. Lett. **101**, 091302.
Aslanides, E., *et al.* (ANTARES), 1999, arXiv:astro-ph/9907432.
Astier, P., *et al.*, 2002, Nucl. Phys. **B621**, 3.
Astier, P., *et al.* (NOMAD Collaboration), 2000, Phys. Lett. B **486**, 35.
Athanassopoulos, C., *et al.*, 1997, Phys. Rev. C **55**, 2078.
Athar, M. S., *et al.*, 2010, Eur. Phys. J. A **43**, 209.
Aubert, B., *et al.*, 1974, AIP Conf. Proc. **22**, 201 [http://lss.fnal.gov/archive/preprint/fermilab-conf-74-120-e.shtml].
Auerbach, L. B., *et al.* (LSND Collaboration), 2001, Phys. Rev. D **63**, 112001.
Auerbach, L. B., *et al.* (LSND Collaboration), 2002, Phys. Rev. C **66**, 015501.
Auerbach, L. B., *et al.*, 2001, Phys. Rev. C **64**, 065501.
Auerbach, N., and A. Klein, 1983, Nucl. Phys. **A395**, 77.
Aufderheide, M. B., S. D. Bloom, D. A. Resler, and C. D. Goodman, 1994, Phys. Rev. C **49**, 678.
Avignone, F. T., *et al.*, 2000, Phys. At. Nucl. **63**, 1007.
Aynutdinov, V., *et al.*, 2009, Nucl. Instrum. Methods Phys. Res. A **602**, 14, proceedings of the 3rd International Workshop on a Very Large Volume Neutrino Telescope for the Mediterranean Sea.
Bahcall, J. N., 1997, Phys. Rev. C **56**, 3391.
Baker, N., *et al.*, 1985, Phys. Rev. D **32**, 531.
Baker, N., *et al.*, 1982, Phys. Rev. D **25**, 617.
Baker, N. J., *et al.*, 1981, Phys. Rev. D **24**, 2779.
Baker, N. J., *et al.*, 1986, Phys. Rev. D **34**, 1251.
Ballagh, H., *et al.*, 1981, Phys. Rev. D **24**, 7.
Ballagh, H. C., *et al.*, 1983, Phys. Rev. Lett. **50**, 1963.
Baranov, D., *et al.*, 1979, Phys. Lett. B **81**, 255.
Barbaro, M., *et al.*, 2011, arXiv:1110.4739.
Bardin, D. Y., and V. A. Dokuchaeva, 1986, Report No. JINR-E-26; 2.
Barish, S., *et al.*, 1980, Phys. Lett. B **91**, 161.
Barish, S., *et al.*, 1974, Phys. Rev. Lett. **33**, 1446.
Barish, S. J., *et al.*, 1974, Phys. Rev. Lett. **33**, 448.
Barnett, R. M., 1976, Phys. Rev. D **14**, 70.
Barsanov, V. I., *et al.*, 2007, Phys. At. Nucl. **70**, 300.
Barwick, S. W., *et al.* (ANITA), 2006, Phys. Rev. Lett. **96**, 171101.
Bazarko, A., *et al.* (CCFR Collaboration), 1995, Z. Phys. C **65**, 189.
Beacom, J., W. Farr, and P. Vogel, 2002, Phys. Rev. D **66**, 033001.
Beacom, J., and P. Vogel, 1999, Phys. Rev. D **60**, 053003.
Beacom, J. F., and S. J. Parke, 2001, Phys. Rev. D **64**, 091302.
Belkov, A. A., and B. Z. Kopeliovich, 1987, Sov. J. Nucl. Phys. **46**, 499.
Bell, J., *et al.*, 1978, Phys. Rev. Lett. **41**, 1008.
Benhar, O., 2010, arXiv:1012.2032.
Benhar, O., N. Farina, H. Nakamura, M. Sakuda, and R. Seki, 2005, Phys. Rev. D **72**, 053005.
Benhar, O., and D. Meloni, 2007, Nucl. Phys. A **789**, 379.
Benhar, O., and G. Veneziano, 2011, Phys. Lett. B **702**, 433.
Benvenuti, A., *et al.*, 1978, Phys. Rev. Lett. **41**, 1204.
Benvenuti, A., *et al.*, 1974, Phys. Rev. Lett. **32**, 800.
Berestetskii, V. B., E. M. Lifshitz, and L. Pitaevski, 1974, *Relativistic quantum theory, Part I* (Pergamon Press, New York).
Berezinsky, V. S., and A. Z. Gazizov, 1977, JETP Lett. **25**, 254.
Berge, J., *et al.*, 1976, Phys. Rev. Lett. **36**, 127.
Berge, J. P., *et al.*, 1978, Phys. Rev. D **18**, 1359.
Berger, C., and L. M. Sehgal, 2009, Phys. Rev. D **79**, 053003.
Bernard, V., *et al.*, 2002, J. Phys. G **28**, R1.
Bethe, H. A., and R. E. Peierls, 1934, Nature (London) **133**, 532.
Blietschau, J., *et al.*, 1976, Phys. Lett. B **60**, 207.
Bodek, A., and H. Budd, 2011, Eur. Phys. J. C **71**, 1726.
Bodek, A., *et al.*, 2007, arXiv:0709.3538.
Bodmann, B., *et al.*, 1991, Phys. Lett. B **267**, 321.
Boehm, F., *et al.*, 2001, Phys. Rev. D **64**, 112001.
Bolognese, T., J. Engel, J. Guyonnet, and J. Riester, 1979, Phys. Lett. B **81**, 393.
Bosetti, P., *et al.*, 1982, Nucl. Phys. **B209**, 29.
Brock, R., *et al.*, 1982, Phys. Rev. D **25**, 1753.
Brunner, J., *et al.* (SKAT Collaboration), 1990, Z. Phys. C **45**, 551.
Buras, A. J., 1980, Rev. Mod. Phys. **52**, 199, academic Training Lectures presented at Fermilab, Batavia, Ill., 1979.
Butkevich, A., 2010, Phys. Rev. C **82**, 055501.
Butkevich, A., P. Krastev, A. Leonov-Vendrovsky, I. Zheleznykh, and A. Kaidalov, 1988, Z. Phys. C **39**, 241.
Butkevich, A., and D. Perevalov, 2011, Phys. Rev. C **84**, 015501.
Butkevich, A. V., 2009, Phys. Rev. C **80**, 014610.
Butler, M., and J.-W. Chen, 2000, Nucl. Phys. A **675**, 575.
Butler, M., J.-W. Chen, and X. Kong, 2001, Phys. Rev. C **63**, 035501.
Butler, M., J.-W. Chen, and P. Vogel, 2002, Phys. Lett. B **549**, 26.
Cabibbo, N., and F. Chilton, 1965, Phys. Rev. **137**, B1628.
Carlson, J., *et al.*, 2002, Phys. Rev. C **65**, 024002.
Casper, D., 2002, Nucl. Phys. B, Proc. Suppl. **112**, 161.
Caurier, E., G. Martínez-Pinedo, F. Nowacki, A. Poves, and A. P. Zuker, 2005, Rev. Mod. Phys. **77**, 427.
Chekanov, S., *et al.* (ZEUS), 2003, Phys. Rev. D **67**, 012007.
Cherdack, D., 2011, AIP Conf. Proc. **1405**, 115.
Chukanov, A., *et al.*, 2006, Eur. Phys. J. C **46**, 69.
Ciafaloni, M., D. Colferai, G. P. Salam, and A. M. Stasto, 2006, Phys. Lett. B **635**, 320.
Ciampolillo, S., *et al.* (Gargamelle Neutrino Propane Collaboration, Aachen-Brussels-CERN-Ecole Poly-Orsay-Padua Collaboration), 1979, Phys. Lett. B **84**, 281.
Cleveland, B. T., T. Daily, J. Raymond Davis, J. R. Distel, K. Lande, C. K. Lee, P. S. Wildenhain, and J. Ullman, 1998, Astrophys. J. **496**, 505.
Cocco, A., G. Mangano, and M. Messina, 2007, arXiv:hep-ph/0703075.
Conrad, J. M., M. S. Shaevitz, and T. Bolton, 1998, Rev. Mod. Phys. **70**, 1341.
Cooper-Sarkar, A., and S. Sarkar, 2008, J. High Energy Phys. 01, 075.
Coteus, P., *et al.*, 1981, Phys. Rev. D **24**, 1420.
Cowan, C. L., F. Reines, F. B. Harrison, H. W. Kruse, and A. D. McGuire, 1956, Science **124**, 103.
Declais, Y., *et al.*, 1994, Phys. Lett. B **338**, 383.
Deden, H., *et al.*, 1975, Phys. Lett. B **58**, 361.
de Forest Jr., T., and D. Walecka, 1966, Adv. Phys. **15**, 1.
de los Heros, C. P. (IceCube Collaboration), 2011, Nucl. Instrum. Methods Phys. Res., Sect. A **630**, 119.
Deniz, M., and H. T. Wong (TEXONO Collaboration), 2008, arXiv:0810.0809.

Deniz, M., *et al.* (TEXONO Collaboration), 2010, Phys. Rev. D **81**, 072001.
DeProspo, D., *et al.*, 1994, Phys. Rev. D **50**, 6691.
Derrick, M., *et al.*, 1981, Phys. Rev. D **23**, 569.
De Rujula, A., R. Petronzio, and A. Savoy-Navarro, 1979, Nucl. Phys. **B154**, 394.
Dewan, H. K., 1981, Phys. Rev. D **24**, 2369.
DeYoung, T., 2011 (private communication).
Diener, K.-P. O., *et al.*, 2004, Phys. Rev. D **69**, 073005.
Distel, J. R., B. T. Cleveland, K. Lande, C. K. Lee, P. S. Wildenhain, G. E. Allen, and R. L. Burman, 2003, Phys. Rev. C **68**, 054613.
Dobrescu, B. A., and R. Ellis, 2004, Phys. Rev. D **69**, 114014.
Dokshitzer, Y. L., 1977, Sov. Phys. JETP **46**, 641.
Donnelly, T., D. Hitlin, M. Schwartz, J. Walecka, and S. Wiesner, 1974, Phys. Lett. B **49**, 8.
Donnelly, T., and R. Peccei, 1979, Phys. Rep. **50**, 1.
Donnelly, T., and J. Walecka, 1975, Annu. Rev. Nucl. Sci. **25**, 329.
Dore, U., 2011, arXiv:1103.4572.
Dorman, M., 2009, AIP Conf. Proc. **1189**, 133.
Drakoulakos, D., *et al.*, 2004, arXiv:hep-ex/0405002.
Drell, S. D., and J. D. Walecka, 1964, Ann. Phys. (N.Y.) **28**, 18.
Dytman, S., 2009, Acta Phys. Pol. B **40**, 2445.
Efrosinin, V., Y. Kudenko, and A. Khotjantsev, 2009, Phys. At. Nucl. **72**, 459.
Eichten, T., *et al.*, 1972, Phys. Lett. B **40**, 593.
Engel, J., E. Kolbe, K. Langanke, and P. Vogel, 1996, Phys. Rev. C **54**, 2740.
Engel, J., S. Pittel, and P. Vogel, 1994, Phys. Rev. C **50**, 1702.
Entenberg, A., *et al.*, 1979, Phys. Rev. Lett. **42**, 1198.
Erriques, O., *et al.*, 1977, Phys. Lett. B **70**, 383.
Espinal, X., and F. Sanchez, 2007, AIP Conf. Proc. **967**, 117.
Ezawa, Y., *et al.*, 1975, Prog. Theor. Phys. **53**, 1455.
Faissner, H., *et al.*, 1980, Phys. Rev. D **21**, 555.
Feynman, R., 1969, Phys. Rev. Lett. **23**, 1415.
Feynman, R. P., and M. Gell-Mann, 1958, Phys. Rev. **109**, 193.
R. P. Feynman, M. Kislinger, and F. Ravndal , 1971, Phys. Rev. D **3**, 2706.
Fogli, G. L., and G. Nardulli, 1980, Nucl. Phys. **B165**, 162.
Formaggio, J., *et al.* (NuTeV Collaboration), 2001, Phys. Rev. Lett. **87**, 071803.
Formaggio, J. A., E. Figueroa-Feliciano, and A. J. Anderson, 2012, Phys. Rev. D **85**, 013009.
Foudas, C., *et al.*, 1990, Phys. Rev. Lett. **64**, 1207.
Freedman, D. Z., D. N. Schramm, and D. L. Tubbs, 1977, Annu. Rev. Nucl. Sci. **27**, 167.
Frullani, S., and J. Mougey, 1984, Adv. Nucl. Phys. **14**, 1.
Fujii, A., and Y. Yamaguchi, 1964, Prog. Theor. Phys. **31**, 107.
Fukuda, Y., *et al.*, 1998, Phys. Rev. Lett. **81**, 1158.
Fukugita, M., Y. Kohyama, and K. Kubodera, 1988, Phys. Lett. B **212**, 139.
Gallagher, H., G. Garvey, and G. P. Zeller, 2011, Annu. Rev. Nucl. Part. Sci. **61**, 355.
Gandhi, R., C. Quigg, M. H. Reno, and I. Sarcevic, 1996, Astropart. Phys. **5**, 81.
Gando, A., *et al.* (The KamLAND Collaboration), 2011, Phys. Rev. D **83**, 052002.
Garvey, G. T., *et al.*, 1993, Phys. Rev. C **48**, 761.
Georgi, H., and D. Politzer, 1976, Phys. Rev. D **14**, 1829.
Gerbier, G., *et al.*, 1985, Z. Phys. C **29**, 15.
Gerstein, S., and Y. B. Zeldovich, 1956, Sov. Phys. JETP **2**, 576.
Giunti, C., and C. W. Kim, 2007, *Fundamentals of Neutrino Physics and Astrophysics* (Oxford University Press), ISBN 9780198508717.
Giusti, C., and A. Meucci, 2011, arXiv:1110.4005.
Glashow, S. L., 1960, Phys. Rev. **118**, 316.
Goncharov, M., *et al.* (NuTeV Collaboration), 2001, Phys. Rev. D **64**, 112006.
Goodman, C. D., C. A. Goulding, M. B. Greenfield, J. Rapaport, D. E. Bainum, C. C. Foster, W. G. Love, and F. Petrovich, 1980, Phys. Rev. Lett. **44**, 1755.
Gorham, P. W., C. L. Hebert, K. M. Liewer, C. J. Naudet, D. Saltzberg, and D. Williams, 2004, Phys. Rev. Lett. **93**, 041101.
Gottschalk, T., 1981, Phys. Rev. D **23**, 56.
Grabosch, H., *et al.* (SKAT Collaboration), 1989, Z. Phys. C **41**, 527.
Gran, R., *et al.*, 2006, Phys. Rev. D **74**, 052002.
Grassler, H., *et al.*, 1982, Nucl. Phys. **B194**, 1.
Haatuft, A., K. Myklebost, J. Olsen, M. Willutzky, and P. Petitjean (Bergen-CERN-Strasbourg Collaboration), 1983, Nucl. Phys. **B222**, 365.
Hampel, W., *et al.*, 1998, Phys. Lett. B **420**, 114.
Hardy, J. C., and I. S. Towner, 1999, AIP Conf. Proc. **481**, 129.
Harvey, J. A., C. T. Hill, and R. J. Hill, 2007, Phys. Rev. Lett. **99**, 261601.
Hasegawa, M., *et al.*, 2005, Phys. Rev. Lett. **95**, 252301.
Hasert, F., *et al.*, 1973, Phys. Lett. B **46**, 121.
Hasert, F., *et al.* (Gargamelle Neutrino Collaboration), 1973, Phys. Lett. B **46**, 138.
Hasert, F. J., *et al.*, 1978, Phys. Lett. B **73**, 487.
Hawker, E., 2002, Proceedings of the Second International Workshop on Neutrino-Nucleus Interactions in the Few-GeV Region, Irvine, CA, unpublished [http://www.ps.uci.edu/~nuint/proceedings/hawker.pdf].
Haxton, W. C., 1998, Phys. Lett. B **431**, 110.
Hayes, A. C., and I. S. Towner, 2000, Phys. Rev. C **61**, 044603.
Heger, A., E. Kolbe, W. Haxton, K. Langanke, G. Martinezpinedo, and S. Woosley, 2005, Phys. Lett. B **606**, 258.
Hernandez, E., *et al.*, 2009, Phys. Rev. D **80**, 013003.
Hernandez, E., *et al.*, 2010, Phys. Rev. D **82**, 077303.
Hill, R. J., 2011, Phys. Rev. D **84**, 017501.
Hiraide, K., 2009, AIP Conf. Proc. **1189**, 249.
Hiraide, K., *et al.*, 2008, Phys. Rev. D **78**, 112004.
Hoummada, A., S. L. Mikou, M. Avenier, G. Bagieu, J. F. Cavaignac, and D. H. Koang, 1995, Appl. Radiat. Isot. **46**, 449.
Iancu, E., and R. Venugopalan, 2003, arXiv:hep-ph/0303204.
Ikeda, K., 1964, Prog. Theor. Phys. **31**, 434.
Jalilian-Marian, J., and Y. V. Kovchegov, 2006, Prog. Part. Nucl. Phys. **56**, 104.
Jenkins, J., and T. Goldman, 2009, Phys. Rev. D **80**, 053005.
Jones, G., *et al.* (WA21 Collaboration, Birmingham-CERN-Imperial-Coll-Munich-Oxford-University Coll Collaboration), 1989, Z. Phys. C **43**, 527.
Jones, G. T., *et al.*, 1993, Z. Phys. C **57**, 197.
Juszczak, C., J. T. Sobczyk, and J. Zmuda, 2010, Phys. Rev. C **82**, 045502.
Kayis-Topaksu, A., *et al.*, 2011, New J. Phys. **13**, 093002.
Kayis-Topaksu, A., *et al.*, 2008a, Nucl. Phys. B **798**, 1.
Kayis-Topaksu, A., *et al.* (CHORUS Collaboration), 2005, Phys. Lett. B **626**, 24.
Kayis-Topaksu, A., *et al.* (CHORUS Collaboration), 2008b, Nucl. Phys. **B798**, 1.
Kelkar, N. G., *et al.*, 1997, Phys. Rev. C **55**, 1964.
Kim, C. W., and H. Primakoff, 1965, Phys. Rev. **140**, B566.
Kolbe, E., K. Langanke, and G. Martínez-Pinedo, 1999, Phys. Rev. C **60**, 052801.
Kolbe, E., K. Langanke, and P. Vogel, 1999, Nucl. Phys. **A652**, 91.
Kopeliovich, B. Z., 2005, Nucl. Phys. B, Proc. Suppl. **139**, 219.

Kozlov, Y., *et al.*, 2000, Phys. At. Nucl. **63**, 1016.
Krakauer, D. A., *et al.*, 1992, Phys. Rev. C **45**, 2450.
Kravchenko, I., *et al.*, 2003, Astropart. Phys. **20**, 195.
Krenz, W., *et al.*, 1978a, Nucl. Phys. **B135**, 45.
Krenz, W., *et al.*, 1978b, Phys. Lett. B **73**, 493.
Kretzer, S., and M. Reno, 2002, Phys. Rev. D **66**, 113007.
Kullenberg, C., *et al.* (NOMAD Collaboration), 2012, Phys. Lett. B **706**, 268.
Kullenberg, C. T., *et al.*, 2009, Phys. Lett. B **682**, 177.
Kuraev, E. A., L. N. Lipatov, and V. S. Fadin, 1977, Sov. Phys. JETP **45**, 199.
Kuramoto, T., M. Fukugita, Y. Kohyama, and K. Kubodera, 1990, Nucl. Phys. **A512**, 711.
Kurimoto, Y., *et al.*, 2010a, Phys. Rev. D **81**, 033004.
Kurimoto, Y., *et al.*, 2010b, Phys. Rev. D **81**, 111102(R).
Kurylov, A., M. J. Ramsey-Musolf, and P. Vogel, 2002, Phys. Rev. C **65**, 055501.
Kuvshinnikov, A. A., *et al.*, 1991, JETP Lett. **54**, 253.
Kuzmin, K., and V. Naumov, 2009, Phys. At. Nucl. **72**, 1501.
Kuzmin, K. S., *et al.*, 2008, Eur. Phys. J. C **54**, 517.
Kwon, H., F. Boehm, A. A. Hahn, H. E. Henrikson, J. L. Vuilleumier, J. F. Cavaignac, D. H. Koang, B. Vignon, F. v. Feilitzsch, and R. L. Mössbauer, 1981, Phys. Rev. D **24**, 1097.
Lang, K., *et al.*, 1987, Z. Phys. C **33**, 483.
Langanke, K., G. Martínez-Pinedo, P. von Neumann-Cosel, and A. Richter, 2004, Phys. Rev. Lett. **93**, 202501.
Lee, W., *et al.*, 1977, Phys. Rev. Lett. **38**, 202.
Lehtinen, N. G., P. W. Gorham, A. R. Jacobson, and R. A. Roussel-Dupré, 2004, Phys. Rev. D **69**, 013008.
Leitner, T., O. Buss, L. Alvarez-Ruso, and U. Mosel, 2009, Phys. Rev. C **79**, 034601.
Leitner, T., and U. Mosel, 2009, Phys. Rev. C **79**, 038501.
Leitner, T., and U. Mosel, 2010a, Phys. Rev. C **82**, 035503.
Leitner, T., and U. Mosel, 2010b, Phys. Rev. C **81**, 064614.
Leitner, T., *et al.*, 2006, Phys. Rev. C **73**, 065502.
Leitner, T., *et al.*, 2009, Phys. Rev. C **79**, 057601.
Llewellyn-Smith, C. H., 1972, Phys. Rep. **C3**, 261.
Luyten, J. R., H. P. C. Rood, and H. A. Tolhoek, 1963, Nucl. Phys. **41**, 236.
Lyubushkin, V., *et al.*, 2009, Eur. Phys. J. C **63**, 355.
Maieron, C., *et al.*, 2003, Phys. Rev. C **68**, 048501.
Marciano, W. J., and Z. Parsa, 2003, J. Phys. G **29**, 2629.
Marciano, W. J., and A. Sirlin, 1981, Phys. Rev. Lett. **46**, 163.
Mariani, C., *et al.*, 2011, Phys. Rev. D **83**, 054023.
Martinez, M. C., *et al.*, 2006, Phys. Rev. C **73**, 024607.
Martini, M., 2011, arXiv:1110.5895.
Martini, M., M. Ericson, and G. Chanfray, 2011, Phys. Rev. C **84**, 055502.
Maschuw, R., 1998, Prog. Part. Nucl. Phys. **40**, 183.
Mason, D., *et al.*, 2007a, Phys. Rev. Lett. **99**, 192001.
Mason, D., *et al.* (NuTeV Collaboration), 2007b, Phys. Rev. Lett. **99**, 192001.
McFarland, K. S., and S.-O. Moch, 2003, *Proceedings for the Mini-Workshop on Electroweak Precision Data and the Higgs Mass, Zeuthen, Germany, DESY-PROC-2003-01* [http://www-library.desy.de/preparch/desy/proc/proc03-01.html].
Mention, G., *et al.*, 2011, Phys. Rev. D **83**, 073006.
Meucci, A., C. Giusti, and F. D. Pacati, 2004, Nucl. Phys. **A739**, 277.
Meucci, A., C. Giusti, and F. D. Pacati, 2011, Phys. Rev. D **84**, 113003.
Mikheyev, S. P., and A. Y. Smirnov, 1989, Prog. Part. Nucl. Phys. **23**, 41.
Mintz, S., and L. Wen, 2007, Eur. Phys. J. A **33**, 299.
Mishra, S., *et al.*, 1990, Phys. Lett. B **252**, 170.
Moch, S., and J. Vermaseren, 2000, Nucl. Phys. **B573**, 853.
Mosconi, B., P. Ricci, and E. Truhlik, 2006, Nucl. Phys. **A772**, 81.
Mosconi, B., P. Ricci, E. Truhlik, and P. Vogel, 2007, Phys. Rev. C **75**.
Mueller, T. A., *et al.*, 2011, arXiv:1101.2663.
Nakajima, Y., *et al.* (SciBooNE Collaboration), 2011, Phys. Rev. D **83**, 012005.
Nakamura, H., and R. Seki, 2002, Nucl. Phys. B, Proc. Suppl. **112**, 197.
Nakamura, K., *et al.*, 2010, J. Phys. G **37**, 075021.
Nakamura, S., T. Sato, V. Gudkov, and K. Kubodera, 2001, Phys. Rev. C **63**, 034617.
Nakamura, S. X., *et al.*, 2010, Phys. Rev. C **81**, 035502.
Nakayama, S., *et al.*, 2005, Phys. Lett. B **619**, 255.
Naumov, D., *et al.*, 2004, Nucl. Phys. **B700**, 51.
Navarro, J., 2006, Physics in Perspective **8**, 64.
Nguyen, N. T., 1975, Nucl. Phys. **A254**, 485.
Nico, J. S., and W. M. Snow, 2005, Annu. Rev. Nucl. Part. Sci. **55**, 27.
Nienaber, P., 1988, Ph.D. thesis, (Univerity of Illinois at Urbana-Champaign).
Nieves, J., J. E. Amaro, and M. Valverde, 2004, Phys. Rev. C **70**, 055503.
Nieves, J., I. Ruiz-Simo, and M. Vicente-Vacas, 2011, arXiv:1110.1200.
Nieves, J., I. Simo, and M. Vacas, 2012, Phys. Lett. B **707**, 72.
Nieves, J., M. Valverde, and M. Vicente Vacas, 2006, Phys. Rev. C **73**, 025504.
Nieves, J., *et al.*, 2006, Phys. Rev. C **73**, 025501.
Onegut, G., *et al.*, 2006, Phys. Lett. B **632**, 65.
Onengut, G., *et al.* (CHORUS Collaboration), 2004, Phys. Lett. B **604**, 145.
Onengut, G., *et al.* (CHORUS Collaboration), 2005, Phys. Lett. B **613**, 105.
Paschos, E. A., A. V. Kartavtsev, 2003, arXiv:hep-ph0309148.
Paschos, E. A., *et al.*, 2006, Phys. Rev. D **74**, 054007.
Paschos, E. A., *et al.*, 2007, arXiv:0704.1991.
Paschos, E. A., *et al.*, 2009, Phys. Rev. D **80**, 033005.
Pasierb, E., H. S. Gurr, J. Lathrop, F. Reines, and H. W. Sobel, 1979, Phys. Rev. Lett. **43**, 96.
Peccei, R. D., and T. Donnelly, 1979, Phys. Rep. **50**, 1.
Pohl, M., *et al.*, 1978, Phys. Lett. B **72**, 489.
Rabinowitz, S., *et al.*, 1993, Phys. Rev. Lett. **70**, 134.
Rein, D., 1987, Z. Phys. C **35**, 43.
Rein, D., and L. M. Sehgal, 1981, Ann. Phys. (N.Y.) **133**, 79.
Rein, D., and L. M. Sehgal, 1983, Nucl. Phys. **B223**, 29.
Reines, F., H. S. Gurr, and H. W. Sobel, 1976, Phys. Rev. Lett. **37**, 315.
Ricci, P., and E. Truhlik, 2010, arXiv:1012.2216.
Riley, S., *et al.*, 1999, Phys. Rev. C **59**, 1780.
Rodriguez, A., *et al.*, 2008, Phys. Rev. D **78**, 032003.
Ruf, G., 2005, Master's thesis, University of Bonn, Germany.
Sajjad Athar, M., S. Chauhan, and S. Singh, 2010, Eur. Phys. J. A **43**, 209.
Schienbein, I., *et al.*, 2008, J. Phys. G **35**, 053101.
Scholberg, K., 2006, Phys. Rev. D **73**, 033005.
Schreckenbach, K., G. Colvin, W. Gelletly, and F. Von Feilitzsch, 1985, Phys. Lett. B **160**, 325.
Serebrov, A., *et al.*, 2005, Phys. Lett. B **605**, 72.
Shrock, R., 1975, Phys. Rev. D **12**, 2049.
Singh, S. K., and E. Oset, 1992, Nucl. Phys. **A542**, 587.
Singh, S. K., and M. J. V. Vacas, 2006, Phys. Rev. D **74**, 053009.
Singh, S. K., *et al.*, 2006, Phys. Rev. Lett. **96**, 241801.
Sirlin, A., 1980, Phys. Rev. D **22**, 971.

Sirlin, A., and W. Marciano, 1981, Nucl. Phys. **B189**, 442.
Smith, R. A., and E. J. Moniz, 1972, Nucl. Phys. **B43**, 605.
Sobczyk, J. T., 2011, AIP Conf. Proc. **1405**, 59.
Sobczyk, J. T., 2012, arXiv:1109.1081.
Son, D., *et al.*, 1983, Phys. Rev. D **28**, 2129.
Taddeucci, T. N., C. A. Goulding, T. A. Carey, R. C. Byrd, C. D. Goodman, C. Gaarde, J. Larsen, D. Horen, J. Rapaport, and E. Sugarbaker, 1987, Nucl. Phys. **A469**, 125.
Tatara, N., Y. Kohyama, and K. Kubodera, 1990, Phys. Rev. C **42**, 1694.
't Hooft, G., 1971, Phys. Lett. B **37**, 195.
Towner, I. S., 1998, Phys. Rev. C **58**, 1288.
Tzanov, M., *et al.*, 2006a, Phys. Rev. D **74**, 012008.
Ushida, N., *et al.* (Canada-Japan-Korea-USA Hybrid Emulsion Spectrometer Collaboration), 1983, Phys. Lett. **121B**, 292.
Vershinsky, A. G., *et al.*, 1991, JETP Lett. **53**, 513.
Vidyakin, G. S., *et al.*, 1987, JETP **93**, 424.
Vilain, P., *et al.*, 1993, Phys. Lett. B **313**, 267.
Vilain, P., *et al.* (CHARM II Collaboration), 1999, Eur. Phys. J. C **11**, 19.
Vilain, P., *et al.* (CHARM-II Collaboration), 1995a, Phys. Lett. B **364**, 121.
Vilain, P., *et al.* (CHARM-II Collaboration), 1995b, Phys. Lett. B **345**, 115.
Volpe, C., N. Auerbach, G. Colò, T. Suzuki, and N. Van Giai, 2000, Phys. Rev. C **62**, 015501.
Walter, C., 2007, AIP Conf. Proc. **967**, 3.
Watson, J. W., W. Pairsuwan, B. D. Anderson, A. R. Baldwin, B. S. Flanders, R. Madey, R. J. McCarthy, B. A. Brown, B. H. Wildenthal, and C. C. Foster, 1985, Phys. Rev. Lett. **55**, 1369.
Webber, D. M., *et al.* (MuLan), 2011, Phys. Rev. Lett. **106**, 041803.
Weinberg, S., 1962, Phys. Rev. **128**, 1457.
Weinberg, S., 1967, Phys. Rev. Lett. **19**, 1264.
Willis, S. E., *et al.*, 1980, Phys. Rev. Lett. **44**, 522.
Willocq, S., *et al.*, 1992, Z. Phys. C **53**, 207.
Wolfenstein, L., 1978, Phys. Rev. D **17**, 2369.
Wu, Q., *et al.*, 2008, Phys. Lett. B **660**, 19.
Zacek, G., *et al.*, 1986, Phys. Rev. D **34**, 2621.
Zeitnitz, B., *et al.*, 1994, Prog. Part. Nucl. Phys. **32**, 351.
Zeller, G. P., *et al.*, 2002, Phys. Rev. Lett. **88**, 091802.